

**Innovative Masking of Ferrous Inserts in Magnesium
Aerospace Components Prior to Tagnite Anodization
(v.1, Unlimited Release)**

by William C. Gorman, Jr.

ARL-CR-716

July 2013

prepared by

**Technology Applications Group, Inc.
810 S. 48th St.
Grand Forks, ND 58201**

under contract

SP4701-10-C-0021

NOTICES

Disclaimers

The findings in this report are not to be construed as an official Department of the Army position unless so designated by other authorized documents.

Citation of manufacturer's or trade names does not constitute an official endorsement or approval of the use thereof.

Destroy this report when it is no longer needed. Do not return it to the originator.

Army Research Laboratory

Aberdeen Proving Ground, MD 21005-5069

ARL-CR-716**July 2013**

Innovative Masking of Ferrous Inserts in Magnesium Aerospace Components Prior to Tagnite Anodization (v.1, Unlimited Release)

**William C. Gorman, Jr.
Technology Applications Group, Inc.**

prepared by

**Technology Applications Group, Inc.
810 S. 48th St.
Grand Forks, ND 58201**

under contract

SP4701-10-C-0021

REPORT DOCUMENTATION PAGE			Form Approved OMB No. 0704-0188	
<p>Public reporting burden for this collection of information is estimated to average 1 hour per response, including the time for reviewing instructions, searching existing data sources, gathering and maintaining the data needed, and completing and reviewing the collection information. Send comments regarding this burden estimate or any other aspect of this collection of information, including suggestions for reducing the burden, to Department of Defense, Washington Headquarters Services, Directorate for Information Operations and Reports (0704-0188), 1215 Jefferson Davis Highway, Suite 1204, Arlington, VA 22202-4302. Respondents should be aware that notwithstanding any other provision of law, no person shall be subject to any penalty for failing to comply with a collection of information if it does not display a currently valid OMB control number.</p> <p>PLEASE DO NOT RETURN YOUR FORM TO THE ABOVE ADDRESS.</p>				
1. REPORT DATE (DD-MM-YYYY) July 2013		2. REPORT TYPE Final		3. DATES COVERED (From - To) 11 September 2011–11 September 2012
4. TITLE AND SUBTITLE Innovative Masking of Ferrous Inserts in Magnesium Aerospace Components Prior to Tagnite Anodization (v.1, Unlimited Release)		5a. CONTRACT NUMBER SP4701-10-C-0021 (BIF III)		
		5b. GRANT NUMBER		
		5c. PROGRAM ELEMENT NUMBER		
6. AUTHOR(S) William C. Gorman, Jr.		5d. PROJECT NUMBER		
		5e. TASK NUMBER		
		5f. WORK UNIT NUMBER		
7. PERFORMING ORGANIZATION NAME(S) AND ADDRESS(ES) Technology Applications Group, Inc. 810 S. 48th St. Grand Forks, ND 58201		8. PERFORMING ORGANIZATION REPORT NUMBER		
9. SPONSORING/MONITORING AGENCY NAME(S) AND ADDRESS(ES) U.S. Army Research Laboratory ATTN: RDRL-WMM-D Aberdeen Proving Ground, MD 21005-5069		10. SPONSOR/MONITOR'S ACRONYM(S)		
		11. SPONSOR/MONITOR'S REPORT NUMBER(S) ARL-CR-716		
12. DISTRIBUTION/AVAILABILITY STATEMENT Approved for public release; distribution is unlimited.				
13. SUPPLEMENTARY NOTES				
14. ABSTRACT <p>In the past, it has not been possible to apply an anodized coating to a magnesium aviation component containing mixed metals—in particular, ferrous inserts. The presence of the mixed metals inserts during anodization will lead to the rapid oxidation of the inserts, which results in metal loss and damage to the magnesium substrate. Technology Applications Group has developed masking technology that overcomes this limitation and allows magnesium aviation components to be anodized in the presence of mixed metals. This technology was developed to show that magnesium DOD aviation components coming out of overhaul cycle can be successfully Tagnite anodized without damaging the mixed metal components. Applying a Tagnite coating to overhaul components in this manner gives these components a corrosion-resistance coating that is better than the original coatings applied on new build magnesium aviation components, leading to a longer component lifetime. In addition, the use of the Tagnite coating after overhaul will eliminate or minimize the need for chromate conversion coatings for touchup.</p> <p>This Industrial Base Innovation Fund effort focused on the development and testing of masking tools for three magnesium components on the AH-64, two components on the UH-60, and one component on the UH-47. This masking technology was successfully demonstrated in front of representatives of the Army Aviation community in February 2012.</p>				
15. SUBJECT TERMS magnesium, anodization, ferrous inserts, mixed metals, masking				
16. SECURITY CLASSIFICATION OF:			17. LIMITATION OF ABSTRACT UU	18. NUMBER OF PAGES 116
a. REPORT Unclassified	b. ABSTRACT Unclassified	c. THIS PAGE Unclassified		
				19b. TELEPHONE NUMBER (Include area code) 410-306-0820

Contents

List of Figures	v
List of Tables	ix
Executive Summary	xi
1. Introduction	1
2. Task I: Identification of High-Priority Magnesium Components	2
3. Task II: Manufacturing and Testing of Potential Masking Solutions	4
3.1 Task IIa: Evaluation of Dymax UV Curable Maskant	7
3.2 Task IIb: Masking of UH-60 Magnesium Components	13
3.3 Task IIc: Masking of AH-64 Magnesium Components	19
3.3.1 H-64 Tail Rotor Gearbox Housing: Masking Tool Development	22
3.3.2 H-64 Tail Rotor Gearbox Housing: Tagnite Application on Masked Parts	25
3.3.3 H-64 Tail Rotor Cover: Masking Tool Development	26
3.3.4 H-64 Tail Rotor Cover: Tagnite Application on Masked Parts	29
3.3.5 H-64 Mechanical Drive Housing (a.k.a. Intermediate Gearbox): Masking Tool Development	31
3.4 Task IId: Masking of CH-47 Magnesium Components	39
3.4.1 H-47 Accessory Cover: Masking Tool Development	40
3.4.2 H-47 Accessory Cover: Tagnite Application on Masked Parts	43
3.4.3 H-47 Accessory Cover: Masking Tool Development – Cover No. 2	44
3.4.4 H-47 Accessory Cover: Cold Spray Repair of Corrosion Damage	46
3.5 Task IIe: IBIF Demonstration at TAG (February 2012)	48
4. Task III: Develop Precleaning Protocol	49
5. Task IV: Early Warning Electrolyte Leakage Mitigation	50
5.1 Masking Tool Costing and Manpower Requirements	50
5.2 Conclusion	53
6. Task V: Evaluation of Flight Critical Components	53

7. Task VI: Parts Washer After Brush Tagnite	53
8. Conclusions	54
9. Galvanic Corrosion Study	55
Appendix. Performance of Corrosion Protective Coatings on Magnesium Alloy ZE41	57
Distribution List	101

List of Figures

Figure 1. Original magnesium components to be masked (as received). From left to right: AH-64 tail rotor cover, UH-60 gearbox center housing assembly, UH-60 gearbox housing, AH-64 mechanical drive housing, and AH-64 tail rotor gearbox.	3
Figure 2. UH-47 magnesium component (as received). Upper left: front side of UH-47 accessory cover. Lower left: back side of UH-47 fan impeller.	3
Figure 3. Tagnite process flow diagram.	4
Figure 4. H-47 gearbox with aluminum masking installed. Left: aluminum stud covers with silicon O-rings. Right: aluminum press-in plugs with silicon O-rings, held in place with aluminum “bridges.”	5
Figure 5. Typical problems encountered when masking typical steel liner-type inserts.	5
Figure 6. New magnesium component for the F-35 Joint Strike Fighter with pressed-in steel liner. Left: (top view) steel liner raised about the magnesium casting. Right: (bottom view) steel liner flush with the magnesium casting.	6
Figure 7. After installation of aluminum covers on F-35 part. Top: installed top cover. Bottom: installed bottom cover with bolts.	7
Figure 8. Dymax 728-G Maskant (left) and 730-BT Maskant (right).	8
Figure 9. (a) Use plater’s tape to partition panel, (b) brush on maskant, (c) remove plater’s tape and cure maskant, and (d) evaluate pretreatment and Tagnite coat panel.	9
Figure 10. Two coats of 730-BT maskant after various cure times.	10
Figure 11. Panel with one coat of 728-G. Red shows area where maskant lost adhesion during Tagnite process. Yellow shows lifting of maskant after Tagnite.	11
Figure 12. Both panels were placed in fluoride activator for 1 h and were Tagnite coated for 12 min at 9A/ft ² . Left: 730-BT maskant had significant lifting (yellow arrows) during the Tagnite process. Right: 728-G maskant remained intact throughout the entire process, leading to well-defined masked areas.	11
Figure 13. The as-received condition of the H-60 center housing.	14
Figure 14. H-60 gearbox housing shown in as-received condition.	14
Figure 15. H-60 center housing after media blast cleaning.	14
Figure 16. H-60 gearbox housing after media blast cleaning.	15
Figure 17. Mixed metal types on H-60 magnesium components. Left: threaded studs with black caps and machine face buttons (green). Upper right: mounting pad bushings. Lower right: bottom of studs penetrated through the as-cast surface (green).	15
Figure 18. Masked H-60 components. Left: aluminum stud covers on center housing, right: stud covers and helicoil covers (red) on gearbox housing.	16
Figure 19. Example of masking tool failure around mounting pad.	17

Figure 20. Masking of machine face buttons on H-60. Left: bridges (green) that support machine face button covers. Upper right: machine face button cover (yellow). Lower right: damage to button after Tagnite (red).....	17
Figure 21. Masking for stud bottoms on H-60 components. Left: masking for stud bottoms using linkage to bridge. Right: close-up of stud bottoms after Tagnite (no damage).	18
Figure 22. UV curable maskant on H-60 component. Left: UV maskant covering buttons on machine face. Right: UV maskant covering stud buttons on inside lip of component.	18
Figure 23. Tail rotor gearbox housing.	20
Figure 24. Tail rotor gearbox cover.	20
Figure 25. Mechanical drive housing.....	20
Figure 26. H-64 tail rotor gearbox housing after media blast.....	21
Figure 27. H-64 tail rotor gearbox cover after media blast.....	21
Figure 28. H-64 mechanical drive housing after media blast.	21
Figure 29. Tail rotor gearbox housing. Large machine face contains 18 studs (black caps), 3 helicoil inserts (yellow), and steel liner in housing body (green).....	22
Figure 30. Tail rotor gearbox housing. Small machine face contains six studs (black caps), three helicoil inserts (yellow), and steel liner in housing body (green).....	22
Figure 31. Tail rotor gearbox housing; profile contains two inserts (green).	23
Figure 32. Tail rotor gearbox housing; profile contains four studs (yellow) and one insert (green).	23
Figure 33. Masking of studs, helicoils, and inserts on tail rotor gearbox housing: stud covers (red), helicoil covers (yellow), and insert cover (green).....	24
Figure 34. Tail rotor gearbox housing steel liners.	24
Figure 35. Masking of steel liners on H-64 tail rotor gearbox housing.....	25
Figure 36. H-64 tail rotor gearbox housing after Tagnite 8500.....	26
Figure 37. H-64 tail rotor gearbox housing after Brush Tagnite touchup around mixed metal inserts.	26
Figure 38. Tail rotor cover contains 12 studs on machine face (left), 7 extended studs (center and right), 2 alignment pins (right), and 2 inserts (left and center).	27
Figure 39. H-64 tail rotor cover contains three helicoil inserts (blue), and 1 pressed-in bearing liner (red).	27
Figure 40. Two types of aluminum bridge designs used to cover alignment pins on H-64 tail rotor cover.	28
Figure 41. Examples of aluminum insert and helicoil covers.....	28
Figure 42. Left: location of stud bottoms that are exposed on bottom of the flange. Right: stud bottoms after filling with Dymax UV maskant.....	29
Figure 43. H-64 tail rotor cover after Immersion Tagnite 8500. Lower left: close-up of steel liner bottom after masking removal. Lower right: close-up of helicoil after masking removal.	30

Figure 44. Damage to interior of H-64 tail rotor cover during masking removal.	30
Figure 45. H-64 tail rotor cover – steel liner masking. Left: original cover had a raised steel lip that the cover could rest on (green arrow). Second cover did not have the raised lip and cover was installed on lip in the as-cast section of the interior diameter (red arrow). Center and right: second cover after Tagnite showing the large uncovered area after the masking removal.	31
Figure 46. H-64 intermediate gearbox – top of housing contains 10 studs, 3 helicoil inserts, and steel liner in housing body.	31
Figure 47. H-64 intermediate gearbox – front of housing contains 8 studs, 3 helicoil inserts, and steel liner in housing body.	32
Figure 48. Location of two inserts on backside of H-64 intermediate gearbox.....	32
Figure 49. Location of two steel liners in the interior of H-64 intermediate gearbox looking from the top.....	33
Figure 50. Close up view of two steel liners looking from the top. Steel liners are mounted at a 90° angle.....	33
Figure 51. Threaded aluminum stud covers (blue) and helicoil covers (green) installed on the H-64 intermediate gearbox.	34
Figure 52. Threaded aluminum insert covers installed on the H-64 intermediate gearbox.....	34
Figure 53. Top steel liner of H-64 intermediate gearbox. Blue shaded area represents primary leakage areas.	36
Figure 54. H-64 intermediate gearbox after Immersion Tagnite 8200 and removal of masking tools. Bottom left: top steel liner after Tagnite. Bottom right: bottom steel liner after Tagnite.....	37
Figure 55. Installation of Acme masking tools on steel liners of H-64 intermediate gearbox. Left: masking on bottom steel liner. Right: masking on top steel liner.....	37
Figure 56. View of UV maskant around the bottom of the steel liners after Tagnite.....	38
Figure 57. Extensive damage to the steel liners after removal of Acme masking tools. Left: top steel liner. Right: bottom steel liner.....	38
Figure 58. As-received pictures of two H-47 accessory covers from CCAD/SAFR.....	39
Figure 59. H-47 accessory cover after media blast cleaning.	40
Figure 60. H-47 accessory cover – bottom contains 15 threaded studs, 5 bearing races with through holes, 5 bearing races (enclosed), 13 stud bottoms for UV maskant, and 4 inserts. ..	40
Figure 61. H-47 accessory cover – top contains 41 threaded studs, 5 bearing races with through holes, 2 inserts, and 5 stud bottoms for UV maskant.	41
Figure 62. Drainage holes for bearing races on H-47 accessory cover. Drainage holes for recessed bearing races (left) and drainage holes for bearing races with through passageways (right).....	42
Figure 63. Typical masking on threaded studs.	42
Figure 64. Example of UV curable maskant on stud bottoms of H-47 accessory cover.	43
Figure 65. H-47 accessory cover after Tagnite and removal of masking tools.	43

Figure 66. Various mixed metal inserts on H-47 accessory cover after Immersion Tagnite process. Left: perimeter inserts. Center: recessed and through bearing races (no damage). Right: through bearing races with light rust damage.	44
Figure 67. Additional inserts on top of second H-47 accessory cover (view 1): nonmagnetic (green) and magnetic (red).	44
Figure 68. Additional inserts on bottom of second H-47 accessory cover (view 2): nonmagnetic (green) and magnetic (red).	45
Figure 69. Additional inserts on bottom of second H-47 accessory cover (view 3): nonmagnetic (green) and magnetic (red).	45
Figure 70. Location of snap ring grooves with corrosion damage. Insert shows location with greatest corrosion damage in snap ring groove.	46
Figure 71. H-47 accessory cover – snap ring groove cold spray repair. Left: after cold spray and remachining. Right: after Immersion Tagnite.	47
Figure 72. Location of porosity on as-cast surface to be cold spray repaired.	47
Figure 73. Cold spray repair of as-cast surface on H-47 accessory cover. Left: after cold spray repair. Right: after blending of repair and Immersion Tagnite.	48
Figure 74. H-60 center housings and H-64 tail rotor gearbox housings for IBIF demonstration (as-received condition).	49

List of Tables

Table 1. Original magnesium components to be evaluated.	2
Table 2. Supplemental magnesium component to be evaluated.	3
Table 3. Summary of operating conditions for pretreatment baths used in the Tagnite process.....	8
Table 4. Summary of operating parameters used during the Tagnite anodization step.....	8
Table 5. Masking time and tooling costs for H-60 components.....	51
Table 6. Masking time and tooling costs for H-64 components.....	51
Table 7. Masking time and tooling costs for H-47 components.....	52
Table 8. Estimated cost of masking components and applying Tagnite and Brush Tagnite as a percentage of the replacement cost.	53

INTENTIONALLY LEFT BLANK.

Executive Summary

Technology Applications Group has developed masking technology that allows magnesium aviation components to be anodized in the presence of mixed metals. This technology was developed to show that magnesium aviation components coming in for overhaul can have the old coatings removed and Tagnite anodize coating applied without damaging any of the mixed metal components installed in the magnesium. The masking tools need to be installed by skilled artisans—a process that increases the man-hours needed to properly coat the components. However, applying a Tagnite coating to overhaul components in this manner gives these overhauled components a corrosion-resistance coating that is better than the original coatings applied on new build magnesium aviation components. Tagnite coatings will extend the lifetime of the components and eliminate or reduce the use of chromate conversion coatings.

The masking technology was developed specifically for each component evaluated. This Industrial Base Innovation Fund (IBIF) effort focused on the development and testing of masking tools for three magnesium components on the AH-64 Apache, two components on the UH-60 Black Hawk, and one component on the UH-47 Chinook. This masking technology was successfully demonstrated in front of representatives of the Army Aviation community in February 2012.

INTENTIONALLY LEFT BLANK.

1. Introduction

New magnesium aerospace castings are semi-machined at the job shop then sent to a metal finishing shop for a magnesium anodize finish such as Tagnite, DOW 17, or HAE. Anodized coatings not only provide a barrier layer against corrosion and wear resistance but also serve as an excellent base for primers, paints, and top coats. After anodizing the magnesium casting, the casting is then sent back to the machine shop for installation of the ferrous studs, helicoils, liners, bushings, and/or bearing races. This process is followed by final machining, assembly, primer, and topcoat paint. The anodizing step must be done prior to the installation of the ferrous and other dissimilar metals because these materials are incompatible with the anodize process. After final machining, bare magnesium is exposed and must be treated in some manner to promote paint adhesion. Because mixed metals have now been installed, anodization of these newly exposed bare areas cannot be done. The only available option at this point is to dip the magnesium castings in a chemical conversion coating, such as DOW 7, DOW 9, or DOW 19. These chemical coatings are immeasurably thin, have very little corrosion resistance, and contain toxic hexavalent chromium. These chemical conversion coatings are still in use because they provide a surface finish for paint adhesion on magnesium while being compatible with the ferrous inserts. As a consequence, the areas with the chromate conversion coatings are typically found next to mixed metals. Because of the lack of corrosion protection, these areas are prone to galvanic corrosion.

During the overhaul phase of the magnesium component, the primer and topcoat paint are stripped off to allow for visual and penetrant inspection of the casting. After passing the inspection, the entire magnesium castings are dipped in a chemical conversion coating, such as DOW 7, DOW 9, or DOW 19. Once the overhauled magnesium castings are placed back into service, their expected lifetimes are shortened dramatically because of the lack of corrosion protection on all external surfaces. This project proposes that Tagnite be used as a superior alternative to the chemical conversion coatings currently applied to used or overhauled magnesium components.

The Tagnite anodized system is an immersion process in which the magnesium casting is placed in a large tank containing the Tagnite electrolyte. First, in order to repair a finished magnesium component by the Tagnite process, the component must be removed from the rotorcraft and extensively degreased. Second, all finished magnesium components have been primed and/or sealed and painted. The Tagnite process does not tolerate the presence of organic finishes. The high voltages used in the Tagnite process will actually undermine the paint, causing it to peel or flake off. The underlying magnesium metal is exposed and will be aggressively attacked by the anodizing process, resulting in “burning” or metal loss; therefore, all organic finishes must be stripped from magnesium prior to the Tagnite process. Last, most finished magnesium castings

have ferrous materials such as studs, liners, and threaded inserts. The Tagnite process is known as anodization and involves high-voltage/high-current density in an alkaline environment. In an anodization process, the magnesium component is made the anode or positively charged end of an electrical circuit. To complete the circuit, a cathode is needed. In the Tagnite process, the electrolyte is placed in a stainless steel tank, and during the coating process, this stainless steel tank is used as the cathode. Anodization involves the formation of an oxide layer on the surface of the magnesium component; in this case, magnesium oxide (MgO) is formed. Steel, iron, stainless steel, brass, cadmium plating, and other metals cannot be anodized. If any of these dissimilar metals are in contact with the Tagnite electrolyte during the anodization process, they will react violently with the charged electrolyte bath, which will lead to the rapid oxidation (i.e., rust formation) of the ferrous material. The highly conductive nature of these dissimilar metals and the high-voltage/high-current density conditions of the Tagnite anodization process will cause all of the power to concentrate on the dissimilar metals. As a result, the dissimilar metals will literally burn away and damage the surrounding magnesium. Therefore, in order for an anodized coating to be applied to a housing with mixed metals, all the mixed metal material must be “masked off” or sealed off from electrolyte contact to prevent the selective oxidation of ferrous material.

This Industrial Base Innovation Fund (IBIF) effort investigates the use of masking technology for the protection of mixed metal components on magnesium housings in order to apply the Tagnite coating on used or overhauled magnesium aviation components.

2. Task I: Identification of High-Priority Magnesium Components

The original proposal called for the IBIF efforts to be focused strictly on the UH-60 platform. However, discussions with U.S. Army Aviation and Missile Research, Development, and Engineering Center (AMRDEC) engineers determined that there were severe corrosion issues with several magnesium components on the AH-64 platform as well, so these components should be included in the IBIF effort. The AMRDEC engineers initially focused on two UH-60 components and three AH-64 components. The parts are summarized in table 1. These components are seen in figure 1.

Table 1. Original magnesium components to be evaluated.

Army Aviation Platform	Part Description	Part No.
UH-60	Gearbox center housing assembly	70357-06305-042
UH-60	Gearbox housing	70358-26607-042
AH-64	Mechanical drive housing (a.k.a. intermediate gearbox)	7-311330011
AH-64	Tail rotor gearbox housing	7-311340011-9
AH-64	Tail rotor gearbox cover	7-311340012-5



Figure 1. Original magnesium components to be masked (as received).
From left to right: AH-64 tail rotor cover, UH-60 gearbox center housing assembly, UH-60 gearbox housing, AH-64 mechanical drive housing, and AH-64 tail rotor gearbox.

Later during this IBIF effort, one component from the UH-47 platform was added for evaluation. This component is listed in table 2 and displayed in figure 2.

Table 2. Supplemental magnesium component to be evaluated.

Army Aviation Platform	Part Description	Part No.
UH-47	Accessory cover	145D2309-3

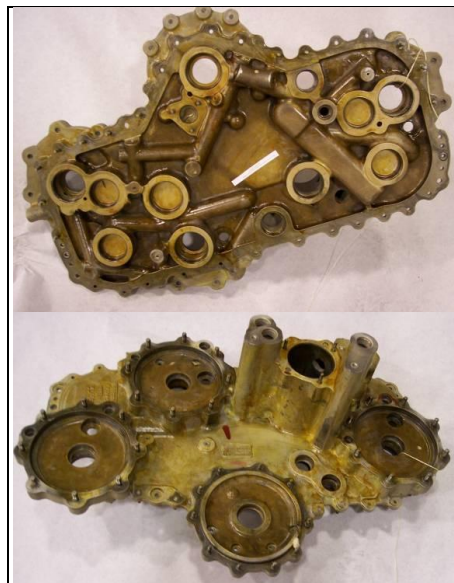


Figure 2. UH-47 magnesium component (as received). Upper left: front side of UH-47 accessory cover. Lower left: back side of UH-47 fan impeller.

3. Task II: Manufacturing and Testing of Potential Masking Solutions

There are several factors that influence the choice of masking material for use in the Tagnite process. The masking material must possess the following characteristics:

- Chemically compatible with the Tagnite process (pretreatment and anodize steps).
- Able to handle large temperature extremes (36 to 180 °F) seen in the Tagnite process (figure 3 is a flow diagram detailing the Tagnite processing steps and conditions).
- Easily removed after the Tagnite process and leave a residue-free surface.

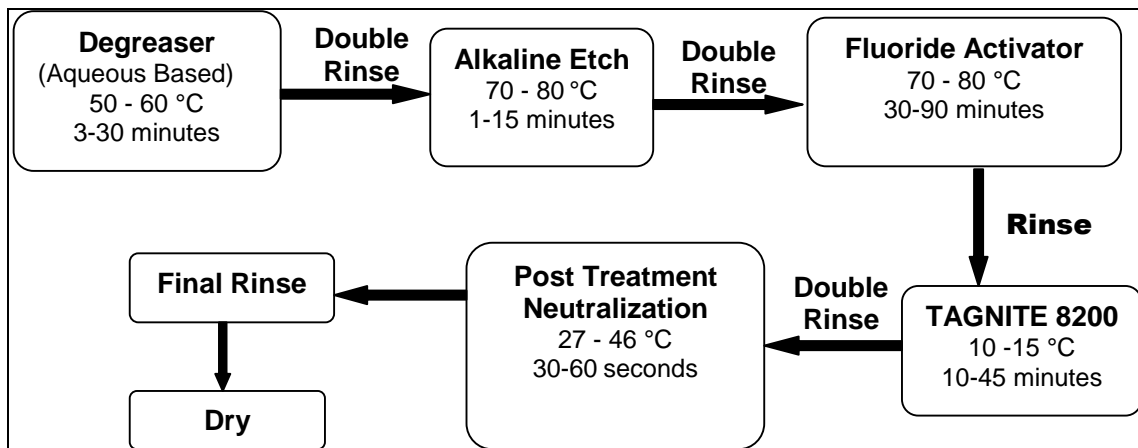


Figure 3. Tagnite process flow diagram.

Technology Applications Group (TAG) has investigated the application of Tagnite anodize coating onto used magnesium components that have ferrous materials installed. Initial investigations focused on aerospace components that contained only studs or inserts, such as helicoils. One of the first parts investigated was an engine gearbox for the CH-47 Chinook helicopter.

The masking approach for this part was to manufacture threaded caps made from aluminum to be installed over the studs. An O-ring was installed at the bottom of the stud to prevent leakage on Tagnite electrolyte around the stud. The inserts or alignment pins were masked using press-in aluminum plugs with O-rings. The press-in plugs were held in place using a “bridge” between two threaded studs. Once all the masking was installed, the gearbox (figure 4) was run through all the pretreatment, Tagnite, and post-treatment process without a single failure.

However, the primary technical challenge of applying Tagnite to used magnesium casting is that most of these housings contain steel liners, inserts, or bearing races. These types of steel inserts have nonthreaded surfaces with overhangs or lips on the magnesium casing. The profile of these types of inserts has proven to be technically difficult to mask off or isolate.

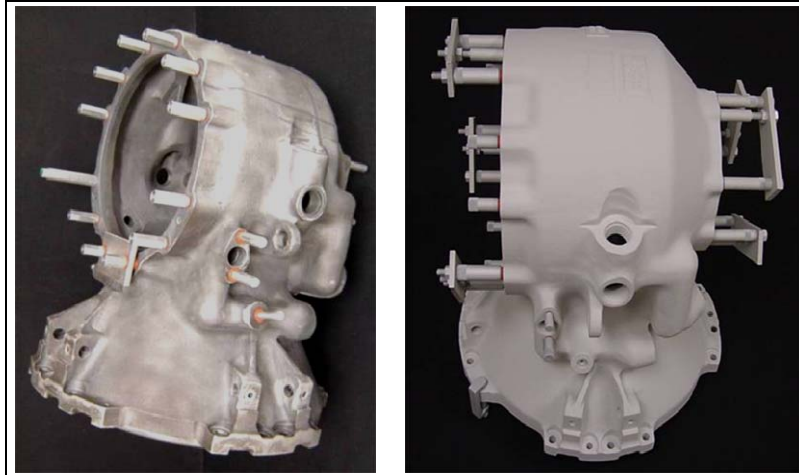


Figure 4. H-47 gearbox with aluminum masking installed. Left: aluminum stud covers with silicon O-rings. Right: aluminum press-in plugs with silicon O-rings, held in place with aluminum "bridges."

Figure 5 (an accessory cover) illustrates the problem with developing masking tools. The steel bushings are smooth with large through holes, therefore there is no convenient place to attach masking tools. In addition, a small steel lip that overhangs the magnesium poses another masking dilemma.

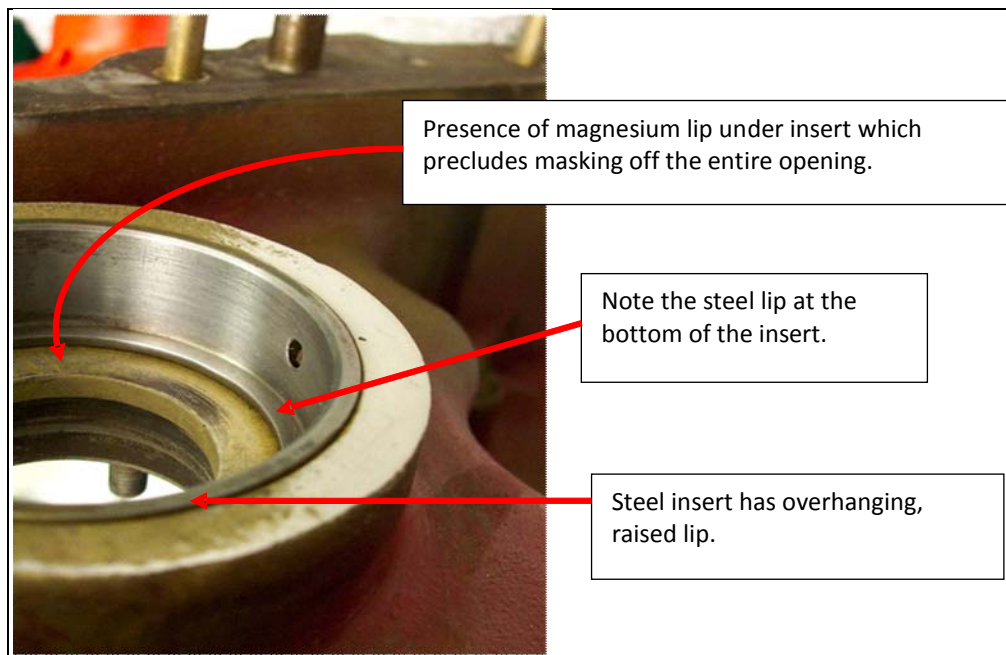


Figure 5. Typical problems encountered when masking typical steel liner-type inserts.

These steel liners and bushings present significant challenges from a masking standpoint. The following operational issues need to be considered:

- How to cover the liners and bushings to prevent contact with the Tagnite electrolyte.
- How to keep the masking or covers in place during processing.
- How to prevent leakage under the masking material during processing.
- Operator notification when leakage occurs around the masking.
- Time and expense to install and disassemble masking material.

TAG's first experience masking steel liners occurred with two magnesium components from the F-35 program (figure 6). These new magnesium castings have the steel liners pressed into the magnesium castings prior to the Tagnite anodization process. TAG was successfully able to mask this steel liner by using aluminum covers for the top and bottom part of the liner. O-rings were placed on the outside perimeter of the steel liner, and the covers were placed on both sides of the liner and bolted together using aluminum bolts and O-rings.

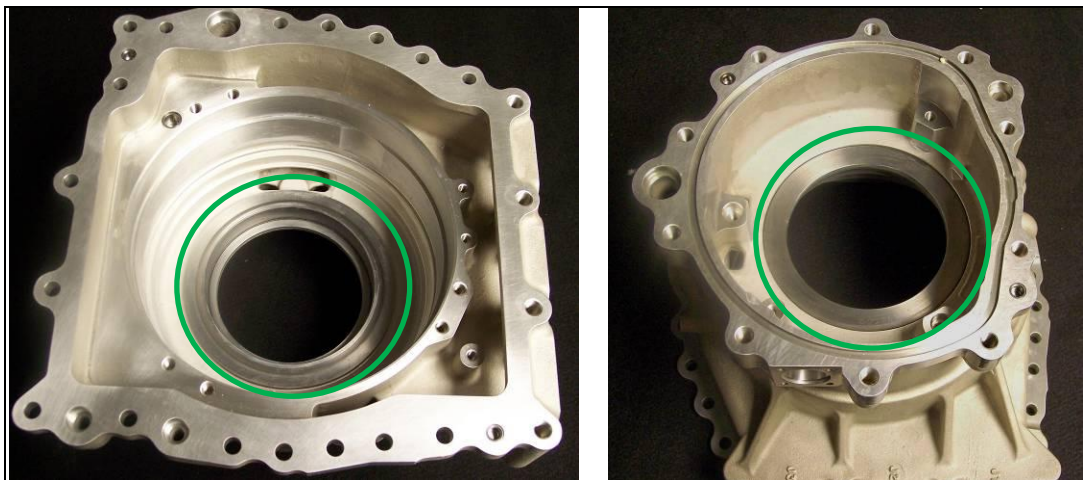


Figure 6. New magnesium component for the F-35 Joint Strike Fighter with pressed-in steel liner. Left: (top view) steel liner raised about the magnesium casting. Right: (bottom view) steel liner flush with the magnesium casting.

The basis for the masking technology developed for the used magnesium components designated in Task I is the aluminum covers, along with threaded aluminum stud covers, used to mask the steel liners. An example of the use of aluminum covers to mask steel liners is shown in figure 7.

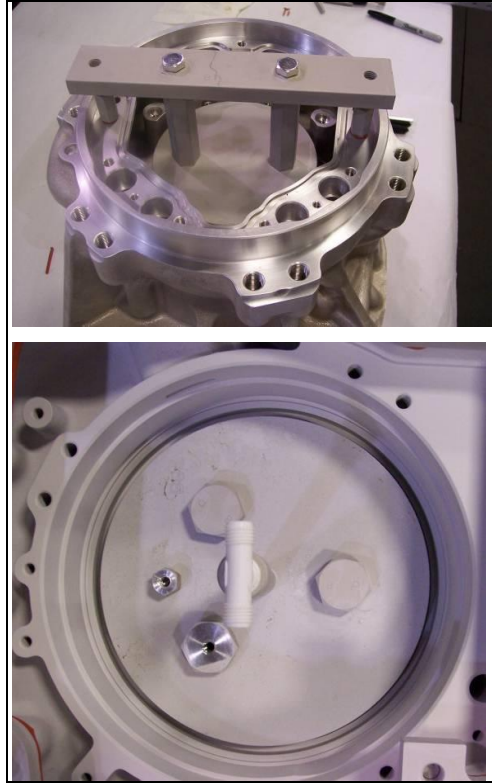


Figure 7. After installation of aluminum covers on F-35 part. Top: installed top cover. Bottom: installed bottom cover with bolts.

3.1 Task IIa: Evaluation of Dymax UV Curable Maskant

TAG is always considering new types of masking techniques. One potential type of masking used in the anodize industry is UV light–curable maskants. Our previous experience with these types of maskants was not favorable. However, Dymax (Torrington, CT) introduced a line of UV-curable maskants formulated specifically for the anodization market in 2010. These maskants have a gel-like consistency and can be brushed on, hand applied, spray painted, or dispensed by syringe. The maskant material is then “cured” when it is exposed to a specific wavelength of UV light for a given amount of time. The maskants evaluated in this project are SpeedMask 728-G and SpeedMask 730-BT (figure 8).



Figure 8. Dymax 728-G Maskant (left) and 730-BT Maskant (right).

The purpose of this evaluation was to evaluate the effectiveness of these Dymax maskants to:

1. Survive the Tagnite pretreatment process (table 3).
2. Survive the Tagnite anodization process (table 4).
3. Protect the bare magnesium under the maskants during the entire Tagnite process.
4. Protect any mixed metal inserts (steel, titanium, Cad plated) during the entire Tagnite process.

Table 3. Summary of operating conditions for pretreatment baths used in the Tagnite process.

Pretreatment Tank	pH	Operating Temperature (°C)	Typical Dwell Time in Tank (min)
Alkaline degreaser	10–11	50–60	3–30
Mild alkaline etch	9.3–10.1	70–80	1–15
Fluoride activator	6.4–7.1	70–80	30–180

Table 4. Summary of operating parameters used during the Tagnite anodization step.

Operating Voltage	pH	Operating Temperature (°C)	Typical Dwell Time in Tank (min)
15–400	12.7–13.4	2–18	6–45

Maskant evaluations took place on 4- × 5-in test coupons made from the magnesium alloy ZE41A. The test protocol is summarized in figure 9.

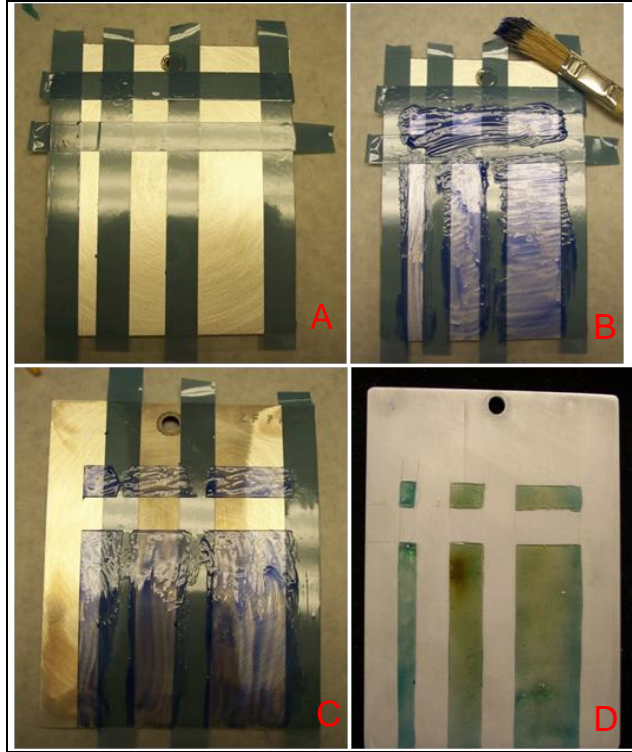


Figure 9. (a) Use plater's tape to partition panel, (b) brush on maskant, (c) remove plater's tape and cure maskant, and (d) evaluate pretreatment and Tagnite coat panel.

Initial investigations with the Dymax maskants focused on which maskant gave the best performance after being run through the Tagnite process. The following variables were investigated:

1. Maskant Types: 728-GT and 730-B
2. Number of coats of maskant
 - One thick coat (minimum thickness of 0.001 in)
 - Two thin coats (minimum total thickness of 0.001 in)
3. UV cure time
 - 5 s
 - 10 s
 - 15 s
 - 20 s

The panels all received the same Tagnite treatment, which consisted of:

1. 3 min in alkaline degrease
2. 1 min in alkaline etch
3. 60 min in fluoride activator
4. Tagnite coating applied for 12 min at 9 A/ft²

Panels were evaluated for cure completion, maskant adherence during the entire process, and crispness of masked area after maskant removal. Examples of panel evaluations are shown in figures 10–12.

In figure 10, the cure was tested by pressing a finger into the cured maskant. If the finger sticks to the maskant, the cure is incomplete. The cure was then checked for maskant adhesion around the edges. If lifting is present, the cure is incomplete.

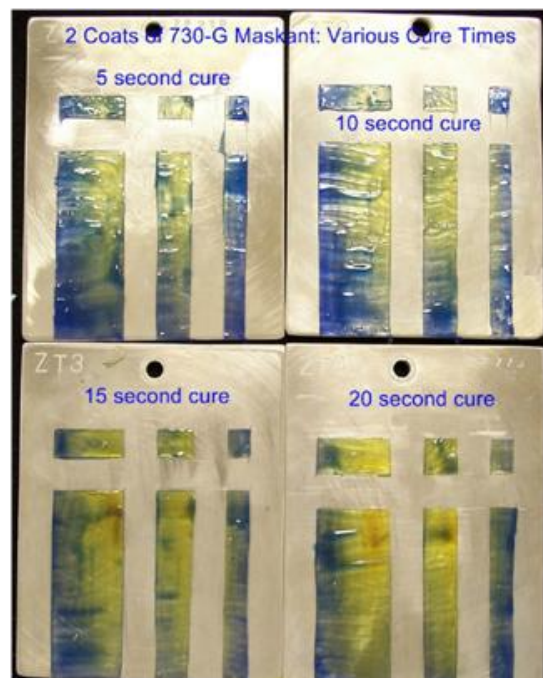


Figure 10. Two coats of 730-BT maskant after various cure times.

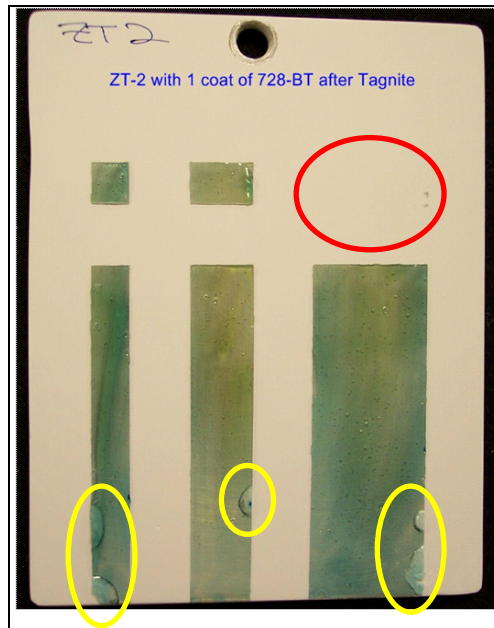


Figure 11. Panel with one coat of 728-G. Red shows area where maskant lost adhesion during Tagnite process. Yellow shows lifting of maskant after Tagnite.

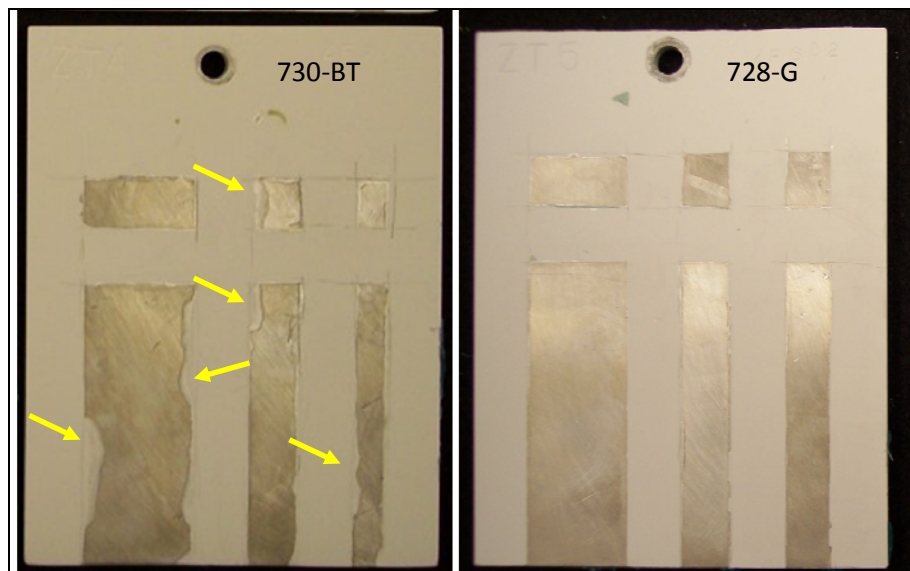


Figure 12. Both panels were placed in fluoride activator for 1 h and were Tagnite coated for 12 min at $9A/ft^2$. Left: 730-BT maskant had significant lifting (yellow arrows) during the Tagnite process. Right: 728-G maskant remained intact throughout the entire process, leading to well-defined masked areas.

UV Maskant Conclusions:

1. Maskant selection: Dymax 728-G and 730-BT were applied to panels and underwent same cure times, pretreatment, and Tagnite processing.

- 728-G
 - Maskant was firm but not brittle for most cure times.
 - Allowed for smooth removal, occasionally torn during removal after Tagnite.
 - Little to no failure during fluoride pretreatment or Tagnite anodize steps.
- 730-BT
 - Maskant was soft regardless of cure time.
 - Maskant was extremely easy to remove.
 - Failed universally due to lack of adhesion.

Conclusion: Dymax 728-G was the best maskant for the Tagnite process.

2. Optimum cure time for Dymax 728-G for two thin coats of maskant, 1-h soak in fluoride activator followed by 12 min of Tagnite anodization at 9 A/ft².

- 5-s cure time
 - Incomplete cure—maskant was sticky and had no adhesion.
- 10-s cure time
 - Was soft after curing.
 - Fails periodically during Tagnite anodize.
 - Difficult to remove from test coupons.
- 15-s cure time
 - Firm but not brittle after curing.
 - Consistently holds adhesion during Tagnite process.
 - Can tear during maskant removal but not often.
- 20-s cure time
 - Extremely brittle.

- Lack of adhesion around the edges.
- Very difficult to remove from test coupons.

Conclusion: The 15-s cure time was optimum for the 728-G maskant at a thickness of 0.001 to 0.0015 in.

3. Effective of dwell time in fluoride activator. Dymax 728-G maskant was applied to test coupons and cured for 10 or 15 s. The panels were placed in the fluoride pretreatment at 80 °C for 1, 2, or 3 h, then underwent Tagnite anodization for 12 min at 9 A/ft².

- 1-h soak in fluoride
 - 10-s cure: maskant was somewhat soft—large amounts of lifting.
 - 15-s cure: maskant was fairly firm—minimal lifting.
- 2-h soak in fluoride
 - 10-s cure: maskant was fairly soft—no lifting.
 - 15-s cure: maskant was somewhat firm—no lifting.
- 3-h soak in fluoride
 - 10-s cure: maskant was very soft—no lifting.
 - 15-s cure: slightly firm—small amount of lifting.

Conclusion: The 728-G maskant should not soak in the fluoride activator solution for more than 2 h. Longer than 2 h of dwell time in the fluoride activator could result in significant degradation of the maskant with a strong potential of lifting of the maskant from the base material.

3.2 Task IIb: Masking of UH-60 Magnesium Components

Initial masking efforts for this IBIF project focused on the following two UH-60 components (these parts did not contain any steel liners):

- Center gearbox housing assembly (P/N 70357-06305-042)
- Gearbox housing (P/N 70358-26607-042)

See figures 13 and 14.

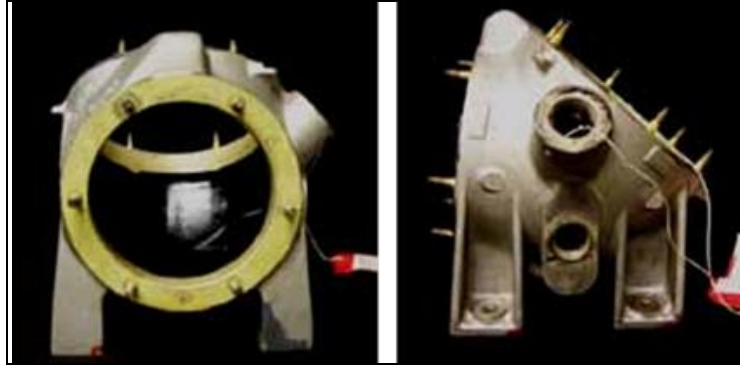


Figure 13. The as-received condition of the H-60 center housing.



Figure 14. H-60 gearbox housing shown in as-received condition.

The parts were sent to Able Engineering (Phoenix, AZ) for media blast cleaning. Figures 15 and 16 show the parts after the old coatings had been removed.

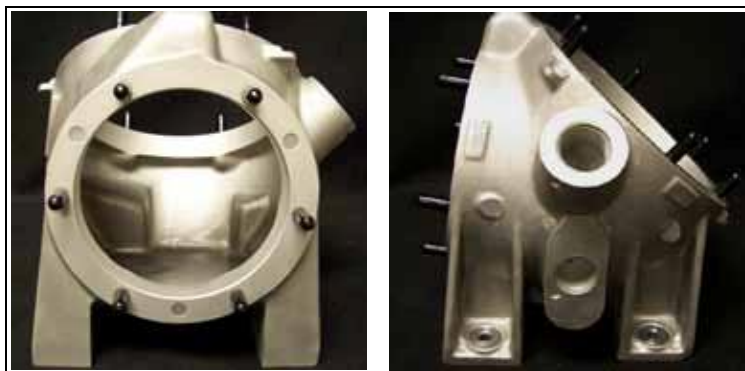


Figure 15. H-60 center housing after media blast cleaning.



Figure 16. H-60 gearbox housing after media blast cleaning.

After media blast cleaning, the parts were thoroughly examined, and the mixed metal inserts could be classified into five different categories (figure 17):

1. Threaded studs
2. Helicoils
3. Bottom end of threaded studs
4. Mounting pad bushings
5. Machine face buttons

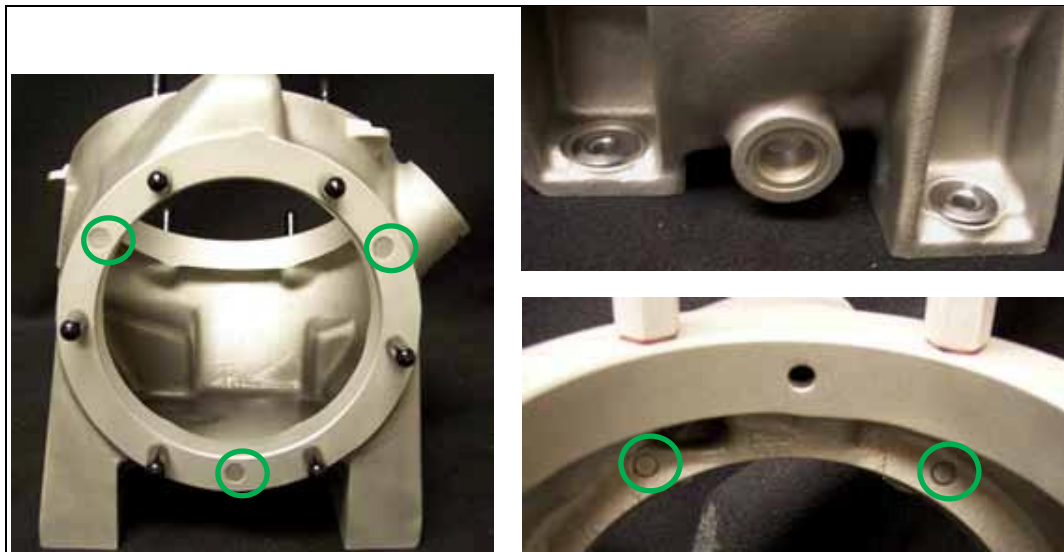


Figure 17. Mixed metal types on H-60 magnesium components. Left: threaded studs with black caps and machine face buttons (green). Upper right: mounting pad bushings. Lower right: bottom of studs penetrated through the as-cast surface (green).

The threaded studs were masked using threaded stud covers made from 6061 aluminum along with O-rings. An example of this type of threaded cover is seen in figure 18. The helicoils were masked using threaded 6061 aluminum inserts/O-rings that matched the thread count of the helicoils. These masking tools, developed during prior research, worked very well with these parts.



Figure 18. Masked H-60 components. Left: aluminum stud covers on center housing, right: stud covers and helicoil covers (red) on gearbox housing.

The mounting pad bushings were initially masked using top and bottom covers with O-rings, where the bottom cover threaded into the top cover to provide the necessary seal. Initial attempts at masking these bushings were met with high failure rates due to leakage around the top part of the bushing, as seen in figure 19. The machine face buttons were masked using 6061 aluminum covers with O-rings that were held in place with a bridge attached to the aluminum stud covers (figure 20). The initial masking attempt suffered from minor leakage due to alignment problems with the covers, as seen in figure 20, lower right. The bottom of the studs that penetrated the as-cast surface (figure 17, lower right) were first masked using a matching cover with an O-ring connected by a linkage to the other masking tools, as seen in figure 21. This methodology worked well, but installation was very complicated.

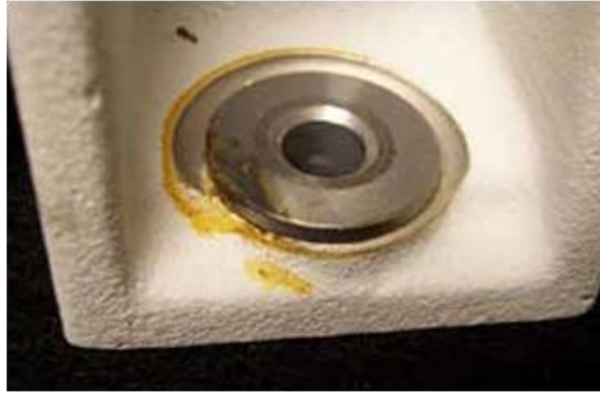


Figure 19. Example of masking tool failure around mounting pad.

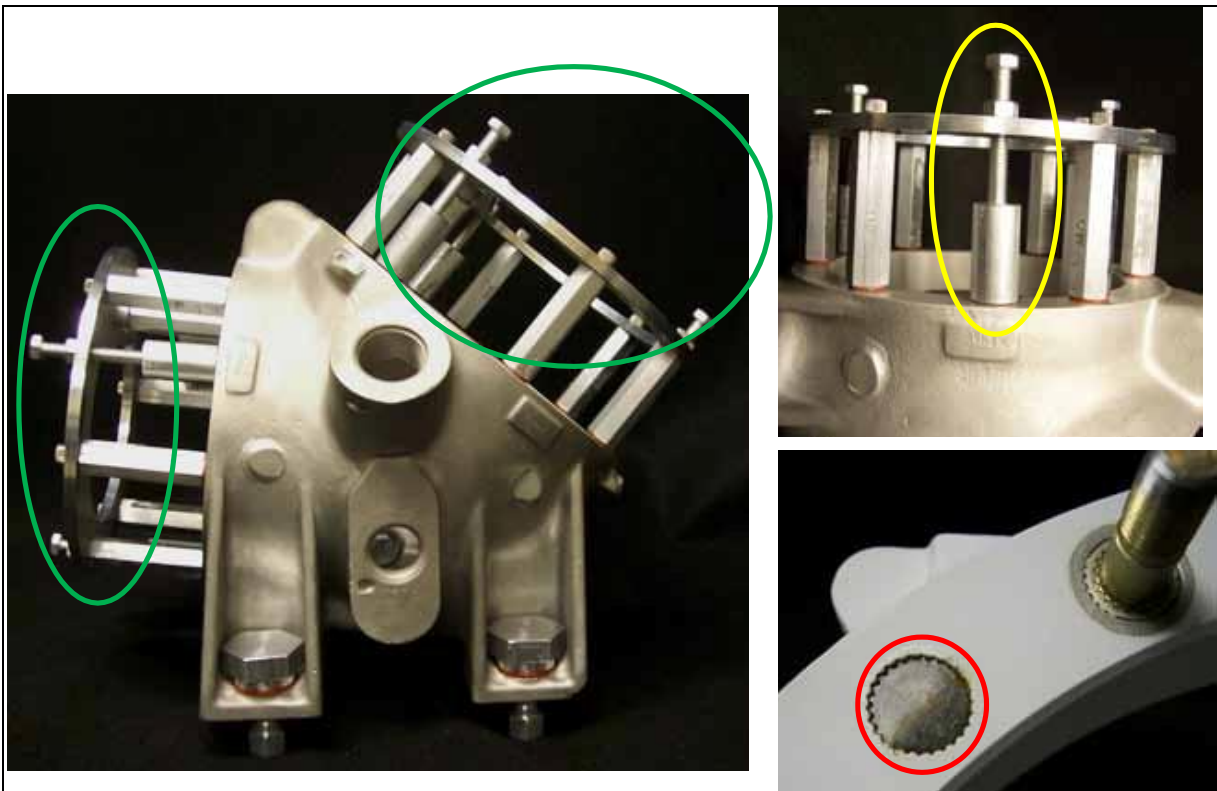


Figure 20. Masking of machine face buttons on H-60. Left: bridges (green) that support machine face button covers. Upper right: machine face button cover (yellow). Lower right: damage to button after Tagnite (red).

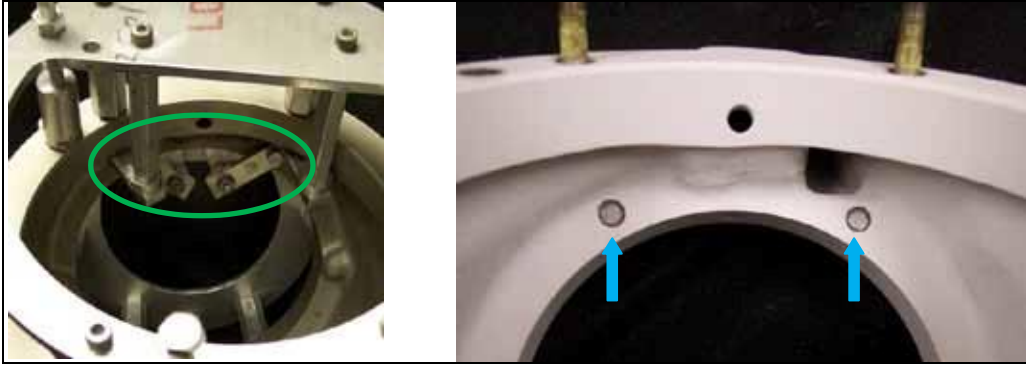


Figure 21. Masking for stud bottoms on H-60 components. Left: masking for stud bottoms using linkage to bridge. Right: close-up of stud bottoms after Tagnite (no damage).

The first attempt at masking the H-60 components was plagued by two problems:

1. Buttons on the machine face were not consistently masked off because of alignment problems with the insert covers mated to the bridge.
2. Covers on the mounting feet were very difficult to seal because of the varying depth of base metal around the mounting pad bushings.

During the second attempt at masking these parts, the following approaches were used to remedy the leakage problem:

1. UV curable maskant was applied to the buttons on the machine faces instead of using the bridge with the insert covers. Also, the bottom studs were masked using the UV maskant because the initial linkage masking arrangement was cumbersome and the installation time consuming (figure 22).

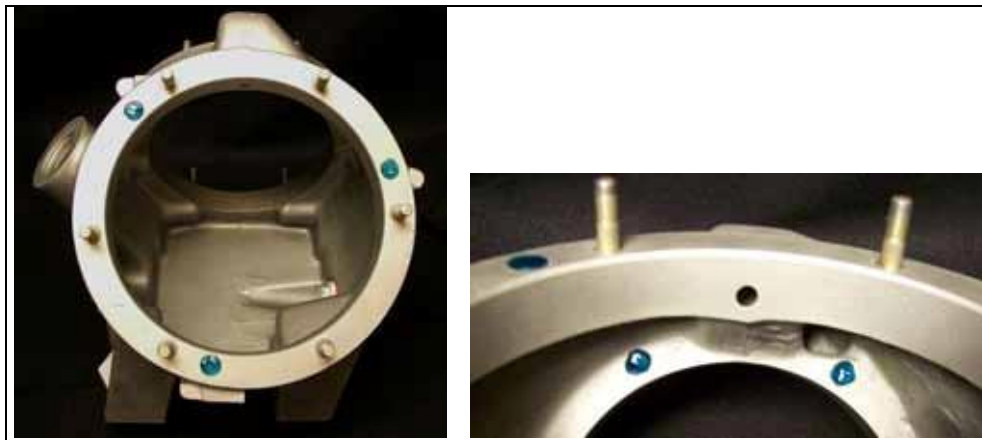


Figure 22. UV curable maskant on H-60 component. Left: UV maskant covering buttons on machine face. Right: UV maskant covering stud buttons on inside lip of component.

2. The covers for the mounting pad bushings were redesigned to incorporate a shoulder on the cover to better hold the O-ring in position. The hex head of the top cover was downsized to allow for easier access for tightening during installation.

After the modifications were made to the mounting pad covers and the UV maskant was applied, the parts were coated in the Tagnite bath. When the masking was removed, the following observations were noted:

- The UV maskant held up well, but to get the best results, the UV maskant must completely cover the buttons or stud bottoms along with some overlap (1/32 to 1/16 in) onto the magnesium portion of the casting.
- The shoulder on the mounting pad bushing cover could force the O-ring below the lip of the bushing, which would cause a gap between the O-ring and the cover. This movement would result in Tagnite electrolyte reaching the surface of the bushing and oxidizing the surface. We must exercise care when installing the cover to avoid pushing the front part of O-ring out of position.

Conclusion:

Using these modifications and taking our time in masking the parts, we were able to successfully coat the H-60 magnesium components without damaging the mixed metals.

3.3 Task IIc: Masking of AH-64 Magnesium Components

AMRDEC engineers identified the following three magnesium components on the AH-64 as having significant corrosion issues, hence making them good candidates for this IBIF effort.

- Tail rotor gearbox housing (P/N 7-311340011-9)
- Tail rotor gearbox cover (P/N 7-311340012-5)
- Mechanical drive housing, a.k.a. intermediate gearbox (P/N 7-311330011)

The tail rotor gearbox housing and tail rotor gearbox cover (figures 23–25*) are mating pieces that share common components, such as studs, helicoils, and inserts.

* Items in figures 23–25 are pictured as-received from the Aviation and Missile Research, Development, and Engineering Center (AMRDEC) Aviation Engineering Directorate (AED).

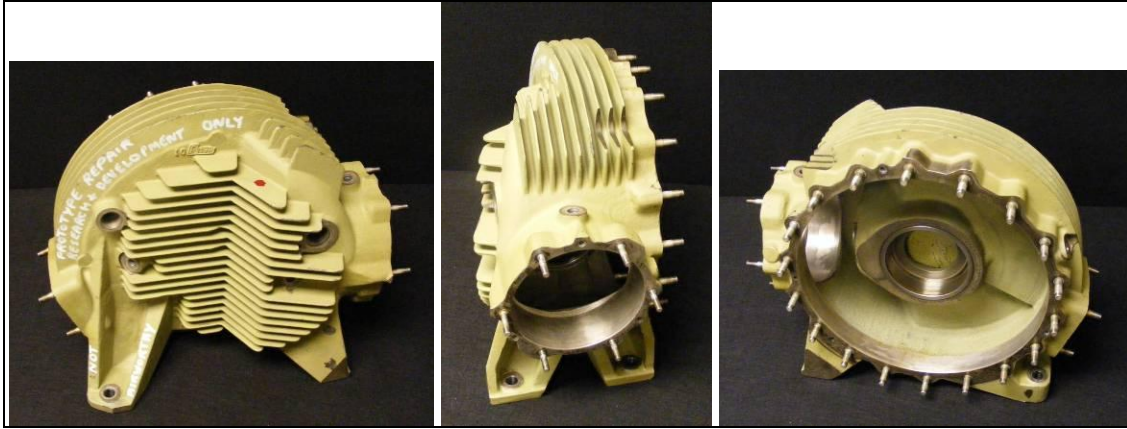


Figure 23. Tail rotor gearbox housing.



Figure 24. Tail rotor gearbox cover.



Figure 25. Mechanical drive housing.

The parts were sent to Able Engineering (Phoenix, AZ) for the same type of media blast cleaning done to the H-60 components. Figures 26–28 show the parts after the old coatings were removed.

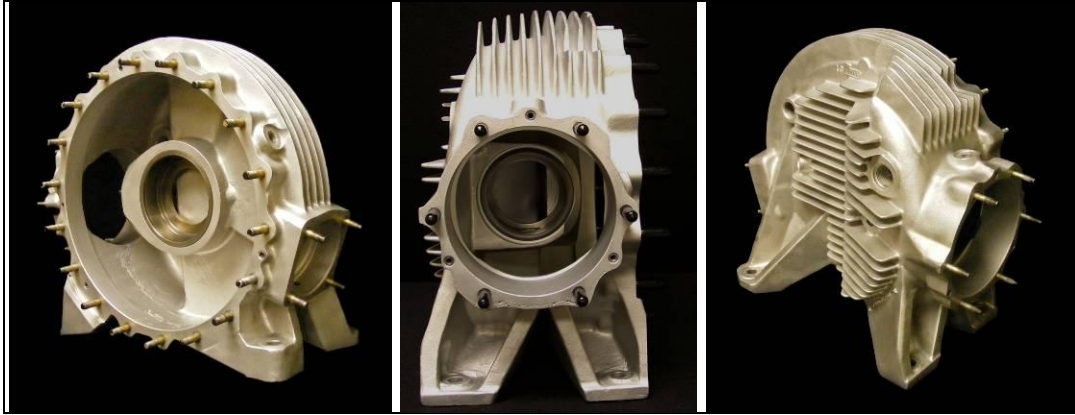


Figure 26. H-64 tail rotor gearbox housing after media blast.



Figure 27. H-64 tail rotor gearbox cover after media blast.

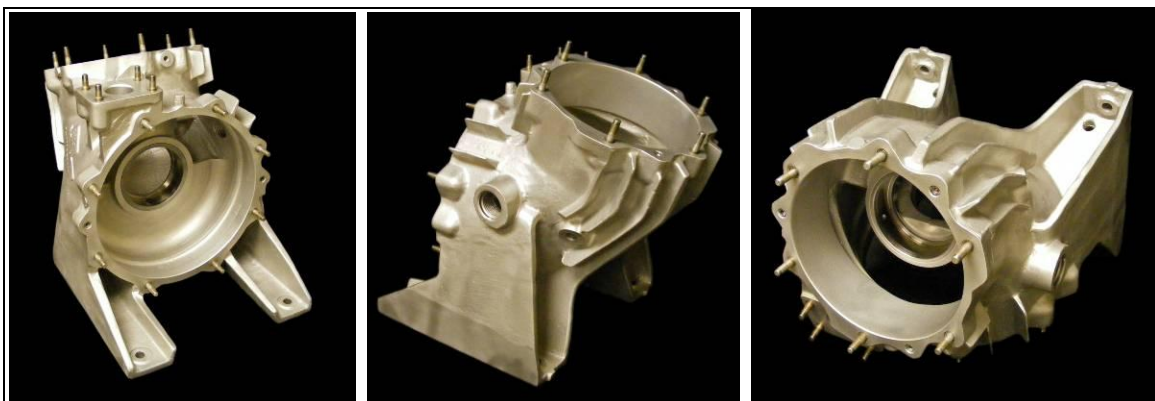


Figure 28. H-64 mechanical drive housing after media blast.

3.3.1 H-64 Tail Rotor Gearbox Housing: Masking Tool Development

The first step in the masking tool development was to identify the types and number of mixed metal inserts. Figures 29–32 illustrate the mixed metal content of this housing.



Figure 29. Tail rotor gearbox housing. Large machine face contains 18 studs (black caps), 3 helicoil inserts (yellow), and steel liner in housing body (green).

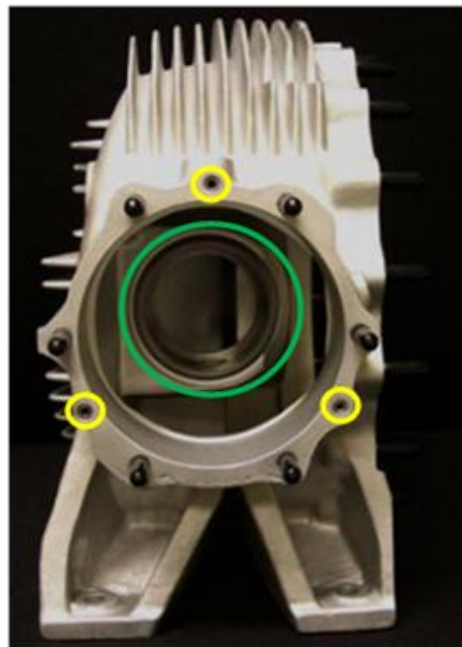


Figure 30. Tail rotor gearbox housing. Small machine face contains six studs (black caps), three helicoil inserts (yellow), and steel liner in housing body (green).

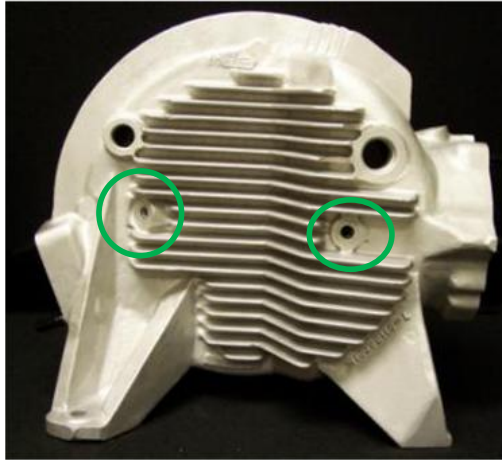


Figure 31. Tail rotor gearbox housing; profile contains two inserts (green).

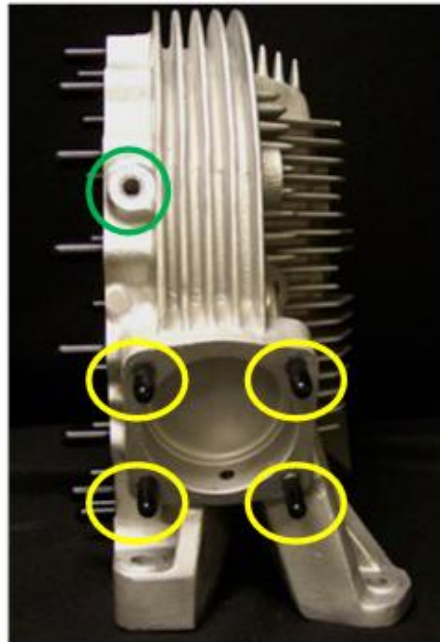


Figure 32. Tail rotor gearbox housing; profile contains four studs (yellow) and one insert (green).

The base of the studs was covered with threaded aluminum covers with O-rings, while the helicoils and inserts were covered using threaded inserts with O-rings as seen in figure 33.

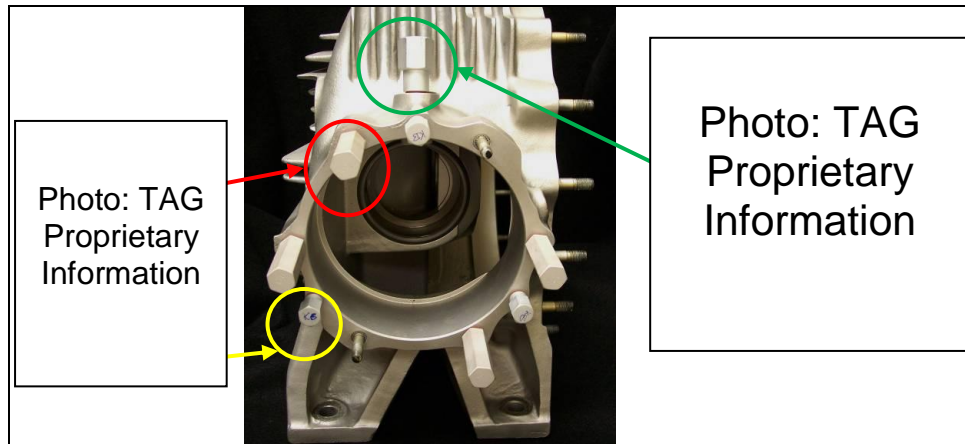


Figure 33. Masking of studs, helicoils, and inserts on tail rotor gearbox housing: stud covers (red), helicoil covers (yellow), and insert cover (green).

The primary masking challenge on the tail rotor gearbox housing was the masking of the two steel liners inside the housing. The difficulties with these liners were as follows:

1. There was solid magnesium underneath the liners, which eliminates the use of top and bottom covers (figure 34, blue shading).
2. One of the liners had a notch in the magnesium around the perimeter of the steel liner (figure 34, red oval).
3. The steel liners are mounted at a 90° angle to each other (figure 34, yellow).

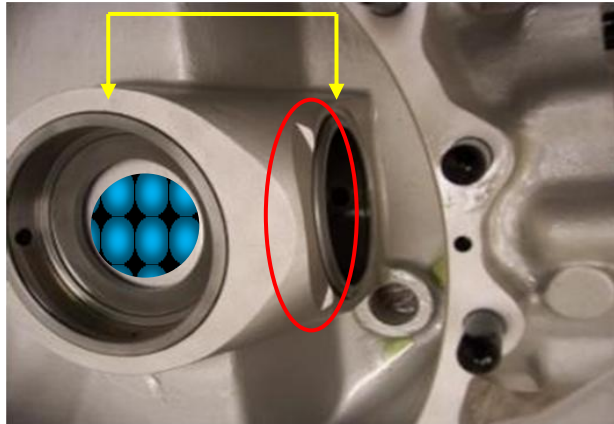


Figure 34. Tail rotor gearbox housing steel liners.

The masking approach shown in figure 35 used to protect these steel liners was to manufacture aluminum covers and place them over the top of the liners. The covers would be held in place by attaching an aluminum bridge to the threaded stud covers for the studs on the machine faces, then use long aluminum studs anchored in the bridge to hold and seal the aluminum cover into place over the steel liners.

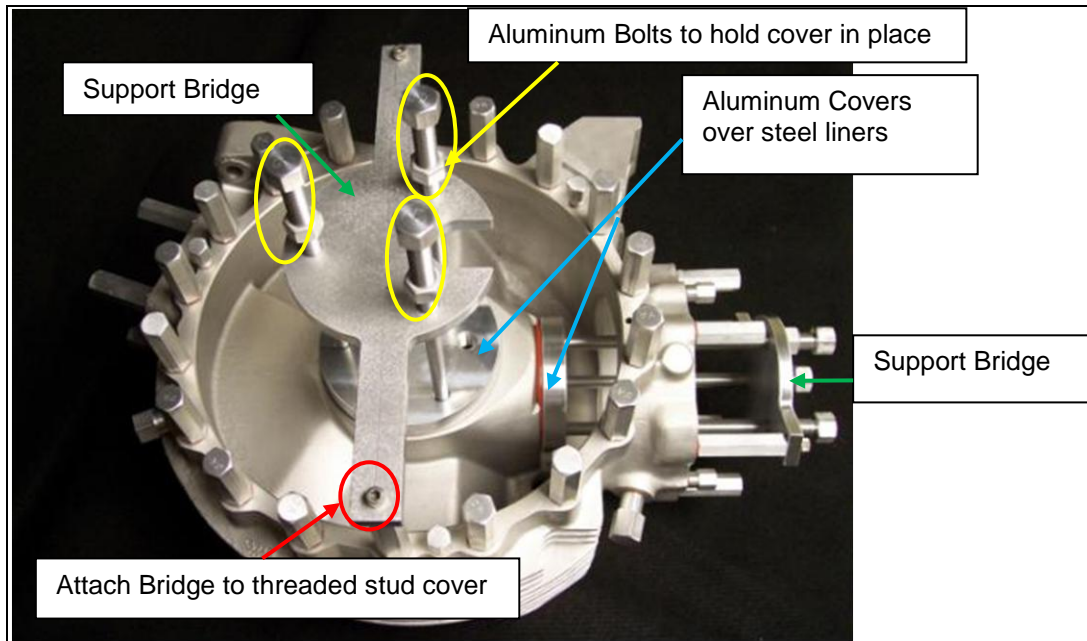


Figure 35. Masking of steel liners on H-64 tail rotor gearbox housing.

3.3.2 H-64 Tail Rotor Gearbox Housing: Tagnite Application on Masked Parts

The masked H-64 tail rotor gearbox housings were run through the Immersion Tagnite bath using the same conditions that a new tail rotor gearbox housing without any mixed metal would be processed in the TAG production line. After the immersion Tagnite process, the masking was removed and the parts were inspected. Multiple trials were done using the masking protocol, and there was never a single instance of damage to any mixed metal inserts on this part. Pictures of tail rotor gearbox housings after Tagnite are shown in figure 36.*

* The tail rotor gearbox housing and the tail rotor cover are made from QE22 magnesium. This particular alloy is coated in the Tagnite 8500 formulation, and as a result, the Tagnite coating has a dark yellow to chocolate brown color that is dependent on the final Tagnite thickness. This is the only magnesium alloy that is coated with the Tagnite 8500 formulation and has a yellow color.

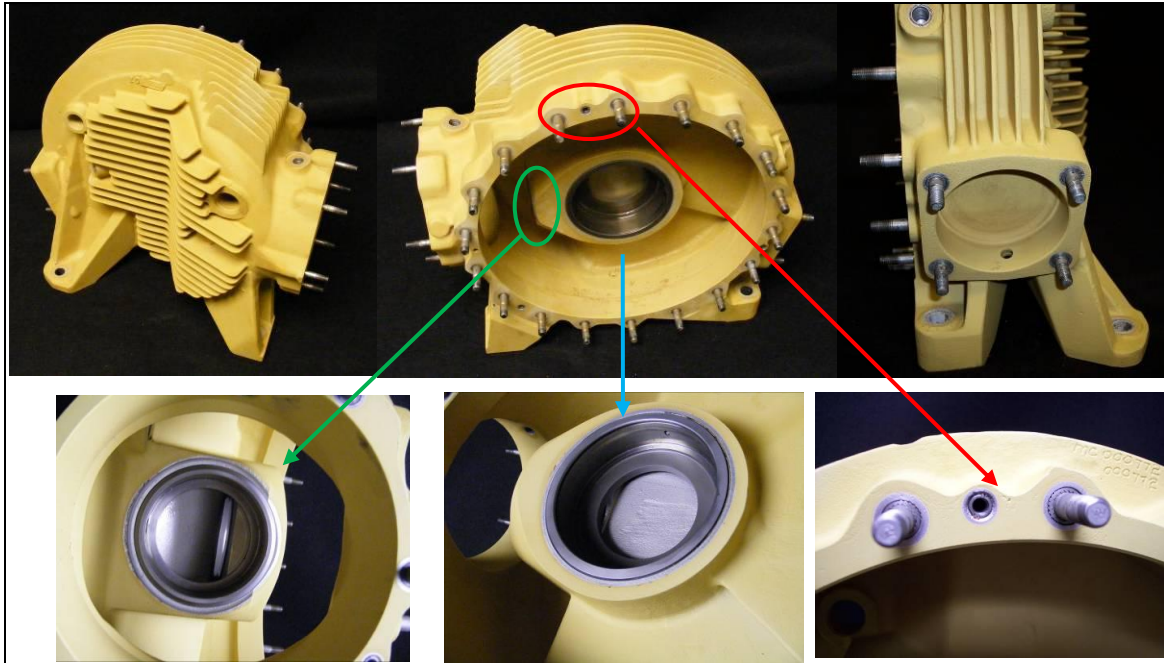


Figure 36. H-64 tail rotor gearbox housing after Tagnite 8500.

After Immersion Tagnite and inspection of the mixed metal inserts, the bare areas around the mixed metals were touched up using low-voltage Brush Tagnite (figure 37).



Figure 37. H-64 tail rotor gearbox housing after Brush Tagnite touchup around mixed metal inserts.

Note: Brush Tagnite coating is light gray in appearance.

3.3.3 H-64 Tail Rotor Cover: Masking Tool Development

As with the tail rotor gearbox housing, the first step in the masking tool development with the tail rotor cover was to identify the types and number of mixed metal inserts. Figures 38 and 39 show the mixed metal content of this housing.

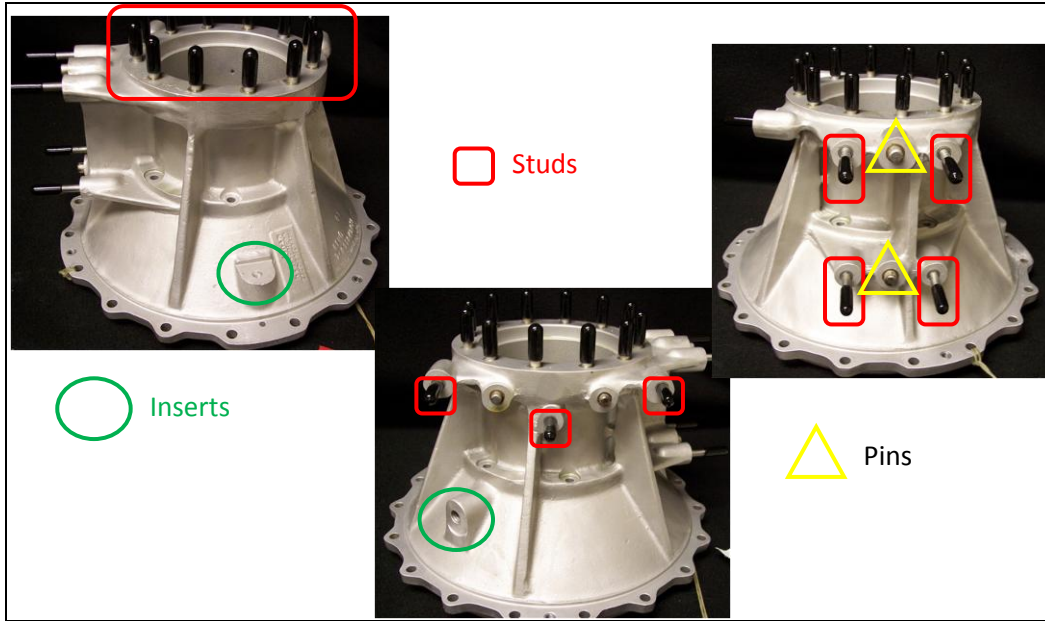


Figure 38. Tail rotor cover contains 12 studs on machine face (left), 7 extended studs (center and right), 2 alignment pins (right), and 2 inserts (left and center).

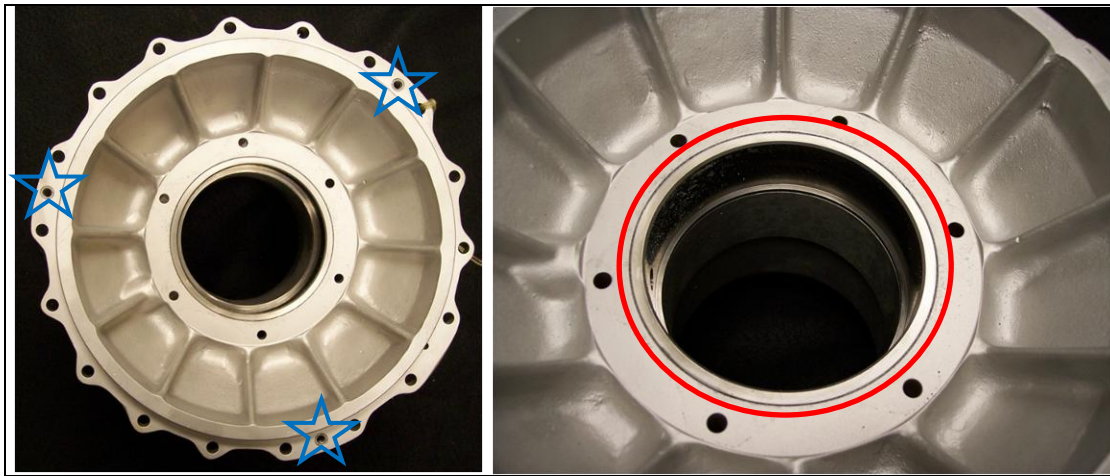


Figure 39. H-64 tail rotor cover contains three helicoil inserts (blue) and one pressed-in bearing liner (red).

The tail rotor gearbox housing and cover are mating parts. All of the studs on the mating faces and inserts were shared parts, and the same type of covers were used on both housings. Some extended studs, alignment pins, helicoils, and the steel inner liner of the tail rotor cover needed masking development. The same masking principles used to develop masking for the tail rotor gearbox housing were integrated into the development of the new masking tools for the tail rotor cover. The masking solutions for the different mixed metal inserts on the tail rotor cover are shown in figures 40 and 41.

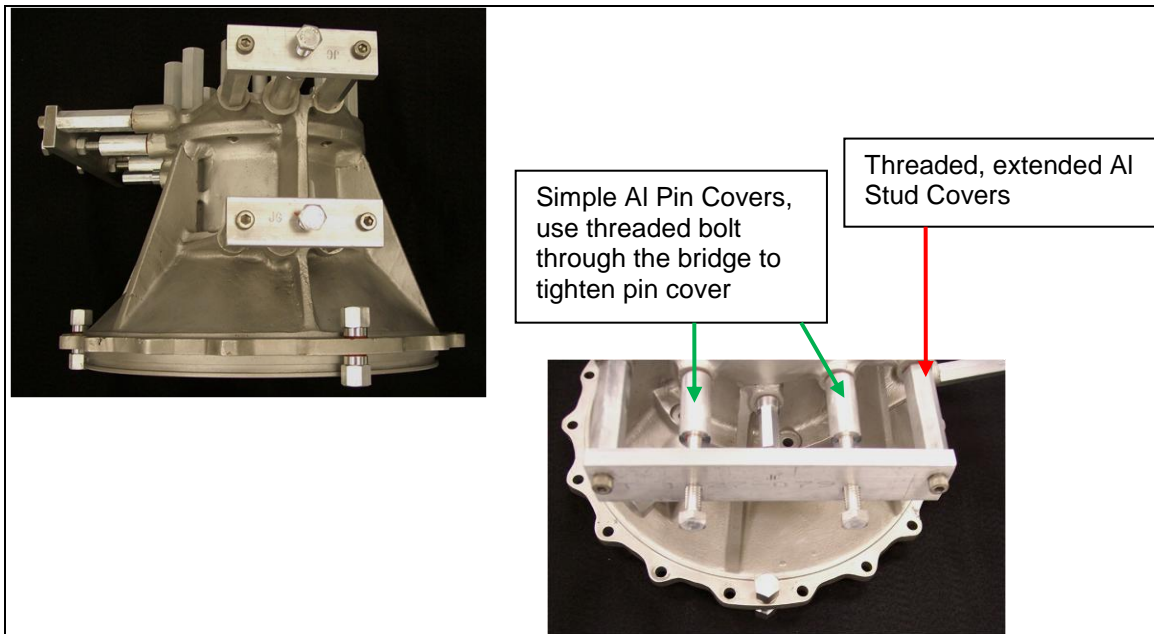


Figure 40. Two types of aluminum bridge designs used to cover alignment pins on H-64 tail rotor cover.

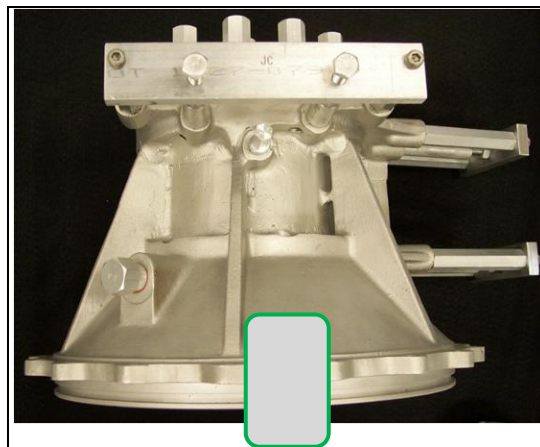


Figure 41. Examples of aluminum insert and helicoil covers.

There were studs on the small-diameter opening of the housing that went all the way through flange and broke out of the bottom of the flange, exposing the bottom of the studs (figure 42). The irregular surface in this area eliminated the use of aluminum covers and instead was masked off using the Dymax UV curable maskant applied using a syringe and medium-gauge needle.

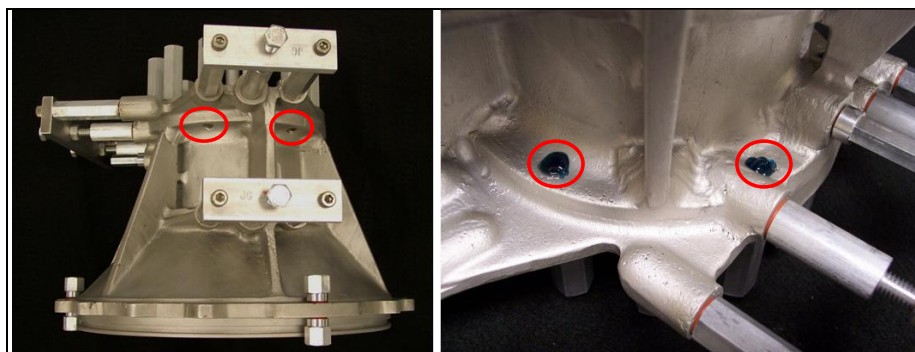


Figure 42. Left: location of stud bottoms that are exposed on bottom of the flange.
Right: stud bottoms after filling with Dymax UV maskant.

The steel liner on the inside of the housing had a raised lip on the inside diameter that was able to support an aluminum cover. This aluminum cover had a large O-ring around the outside diameter and was pressed into position on top of the steel liner. Another aluminum cover with an O-ring was placed over the bottom portion of the steel liner, and bolts were used to tighten the two covers together.

3.3.4 H-64 Tail Rotor Cover: Tagnite Application on Masked Parts

The masked H-64 tail rotor cover was run through the Immersion Tagnite bath using the same conditions that a new tail rotor cover without any mixed metal would be processed in the TAG production line. After the Immersion Tagnite process, the masking was removed, and the parts were inspected. The initial trial was done using the masking protocol developed in section 3.3.3, and there was never a single instance of damage to any mixed metal inserts on this part. However, there was damage to the Tagnite coating during the removal of the steel liner covers. The damage was easily repaired using Brush Tagnite, but the top cover to the steel liner was modified to eliminate the potential for damage during masking removal. Pictures of the tail rotor cover after Tagnite are shown in figures 43 and 44.*

* The tail rotor gearbox housing and the tail rotor cover are made from QE22 magnesium. This particular alloy is coated in the Tagnite 8500 formulation, and as a result, the Tagnite coating has a dark yellow to chocolate brown color that is dependent on the final Tagnite thickness. This is the only magnesium alloy that is coated with the Tagnite 8500 formulation and has a yellow color.

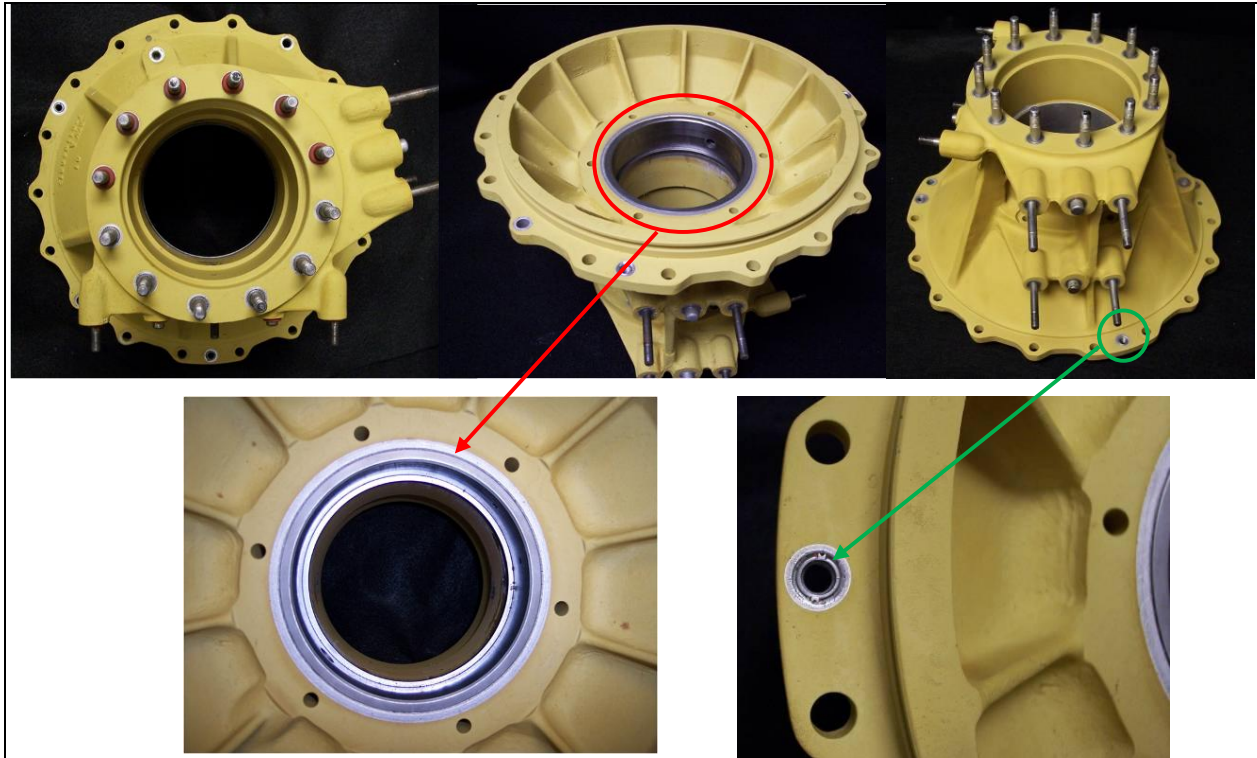


Figure 43. H-64 tail rotor cover after Immersion Tagnite 8500. Lower left: close-up of steel liner bottom after masking removal. Lower right: close-up of helicoid after masking removal.



Figure 44. Damage to interior of H-64 tail rotor cover during masking removal.

The masking was then installed on a second H-64 tail rotor cover. During the installation of the covers for the steel liner, it was discovered that the steel liner on the second tail rotor cover was installed flush with the interior wall of the cover. Therefore, the lip that the top cover could rest on was no longer present. So the top cover was modified to fit on a second lip that was higher up the interior diameter. The drawback to this approach was that a large area of uncoated magnesium would be present after the masking was removed above the steel liner (figure 45). This would have to be touched up with Brush Tagnite.

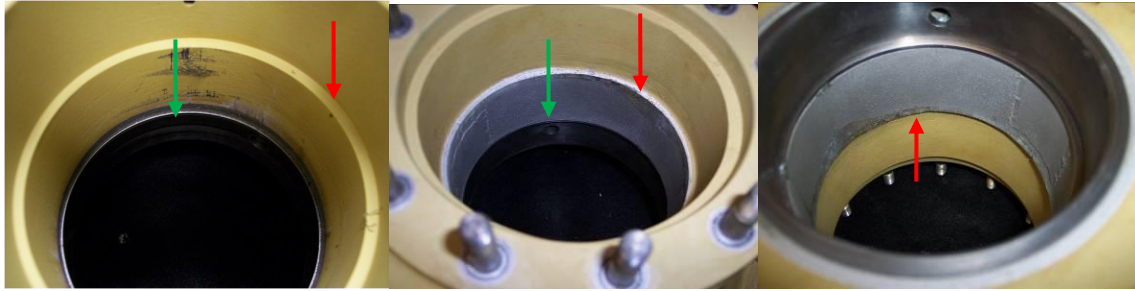


Figure 45. H-64 tail rotor cover – steel liner masking. Left: original cover had a raised steel lip that the cover could rest on (green arrow). Second cover did not have the raised lip and cover was installed on lip in the as-cast section of the interior diameter (red arrow). Center and right: second cover after Tagnite showing the large uncovered area after the masking removal.

On the second cover, there was no failure of the masking, but there was a larger area of uncoated magnesium that needed brush Tagnite touch-up.

3.3.5 H-64 Mechanical Drive Housing (a.k.a. Intermediate Gearbox): Masking Tool Development

The different types and number of mixed metal inserts are shown in figures 46–50.

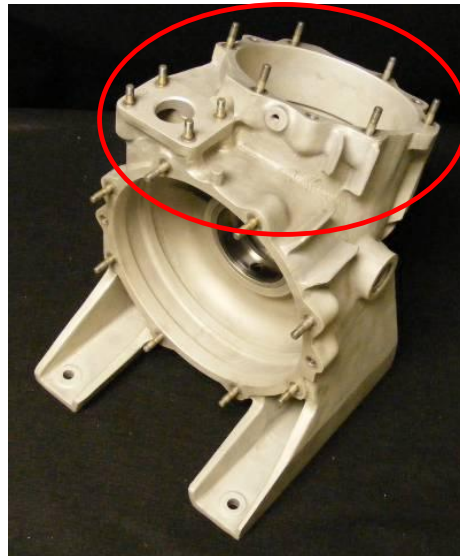


Figure 46. H-64 intermediate gearbox – top of housing contains 10 studs, 3 helicoil inserts, and steel liner in housing body.

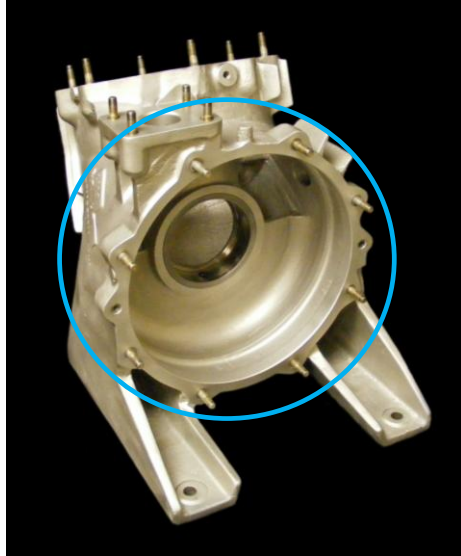


Figure 47. H-64 intermediate gearbox – front of housing contains 8 studs, 3 helicoil inserts, and steel liner in housing body.

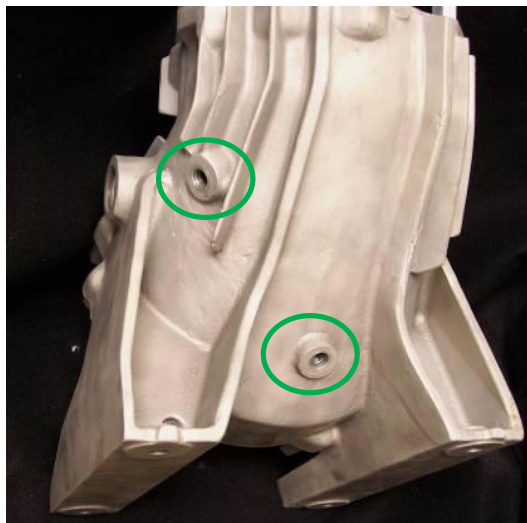


Figure 48. Location of two inserts on backside of H-64 intermediate gearbox.

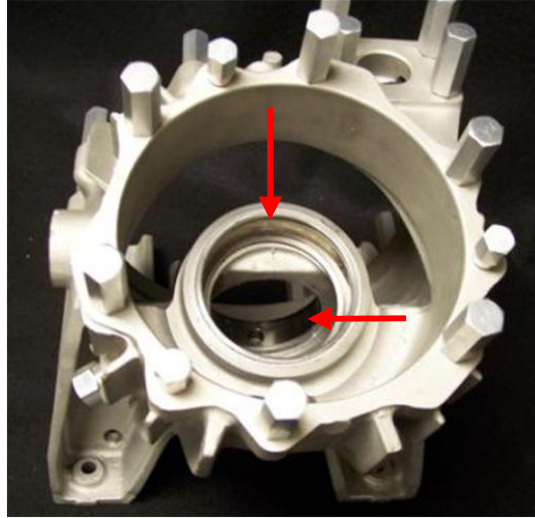


Figure 49. Location of two steel liners in the interior of H-64 intermediate gearbox looking from the top.

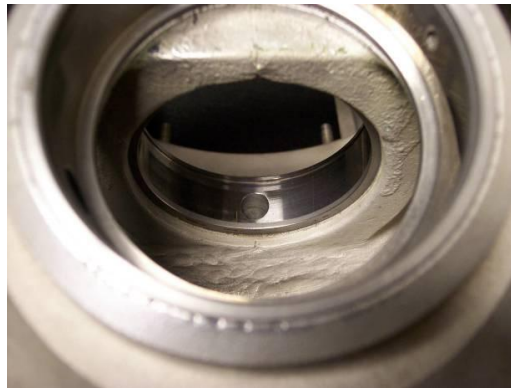


Figure 50. Close up view of two steel liners looking from the top. Steel liners are mounted at a 90° angle.

The studs, helicoils, and inserts were masked using the covers developed for the tail rotor components (figures 51 and 52).

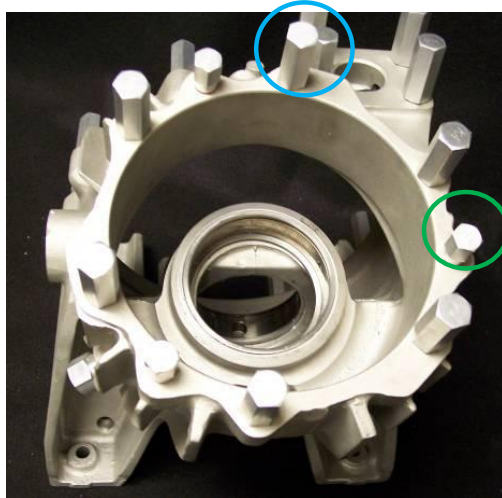


Figure 51. Threaded aluminum stud covers (blue) and helicoil covers (green) installed on the H-64 intermediate gearbox.

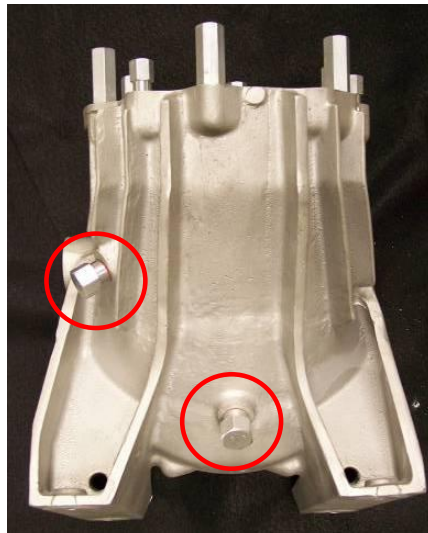


Figure 52. Threaded aluminum insert covers installed on the H-64 intermediate gearbox.

The primary challenge on this component was the two steel liners seen in figures 49 and 50, which are in the interior of the component. Additional challenges with these liners are as follows:

- The top steel liner rests on a three-quarters moon-shaped hole in the casting (figure 50). The ledge underneath the top liner makes it difficult to seal the bottom portion of this liner.

- The bottom lip of both liners has varying depths in the casting. Sometimes the lower lip of the liner is recessed into the casting, while at other locations the liner is flush with the casting or sticks out.
- The type of aluminum covers developed to fit the tail rotor liners cannot be used on the bottom portion of the liners in the intermediate gearbox because the openings are too small to fit through the openings in the steel liners.

The original masking concept for the steel liners in the H-60 intermediate gearbox was to cast molds of the interior of the steel liners. The molds would protect the inside of the steel liners, and these molds would be held in place by aluminum support plates on the bottom side of the mold. Bolts would run through the support plate and mold would then be attached to an aluminum cover with nuts.

When this masking concept was assembled, TAG determined that the mold material would be pulled through the steel liner while tightening the nuts used to hold the aluminum covers in place. This problem was due to the small size of the back-supporting plate on the mold. The support plate was made small to pass it through the opening of the steel liner. However, when tightening the bolts, the support plate was not large enough to grab the bottom lip of the casting that holds the steel liner.

After many attempts to solve the problem with the mold inserts, this concept was abandoned because the mold material was too flexible and would not seal properly. The primary issue was the inability to get a proper seal on the backside of the steel liners.

The focus shifted to developing masking tools with rigid back-supporting plates with gaskets instead of mold material in order to get an effective seal on the backsides of both steel liners. The problem with the bottom liner with the full opening was the ability to get a support plate that was large enough to cover the entire opening while still being able to get it through the opening of the steel liner. The issue was solved by making the back support plate in two pieces and connecting them after installation. Gasket material is used between the support plate and the as-cast surface of the housing to get a watertight seal. Threaded spacer bolts are used to provide connection points with the top cover.

The top cover for this liner has another gasket on the bottom side of the cover, and bolts are inserted through the cover into the spacer bolts attached to the bottom support plate.

The upper or top steel liner (figure 53) is difficult to seal because of the three-quarters moon-shaped bottom of the liner. All of the leakage occurred next to this small shelf on the bottom of the liner. After multiple attempts at sealing this liner, the best approach was to provide multiple layers of protection.

The first step is to install a back support plate that takes into account the three-quarters moon shape of the liner as well as the back support plate for the bottom liner. The next step is to

develop masking material that can be compressed against the back plate to seal off the bottom of the liner. This was accomplished by using mold material sized to the shape of the liner walls. The mold material is compressed with a plate to force the mold material into the voids of the support plate and the steel liner/magnesium as-cast interface. Lastly, a cover is needed for the top part of the liner.



Figure 53. Top steel liner of H-64 intermediate gearbox. Blue shaded area represents primary leakage areas.

After masking was installed, the part was checked for leaks then run through the Immersion Tagnite 8200 process. The masking was removed and the part was checked for leaks or attack on the mixed metals (figure 54). There was no evidence of leaks or damage. This process was repeated on two other H-64 Intermediate Gearboxes. All three gearboxes were coated without any damage.

TAG personnel were concerned about the complexity of the masking for the steel liners on this part and wanted to see what a commercial masking vendor had to offer. TAG contacted Acme Masking Company, Avon, Indiana, who specializes in developing masking for aluminum anodizing and other magnesium anodizing processes such as DOW 17 and HAE. Their proposed solution was to develop tightly fitting rubber covers for the steel liners that are held in place by press-in aluminum sleeves as seen in figure 55.

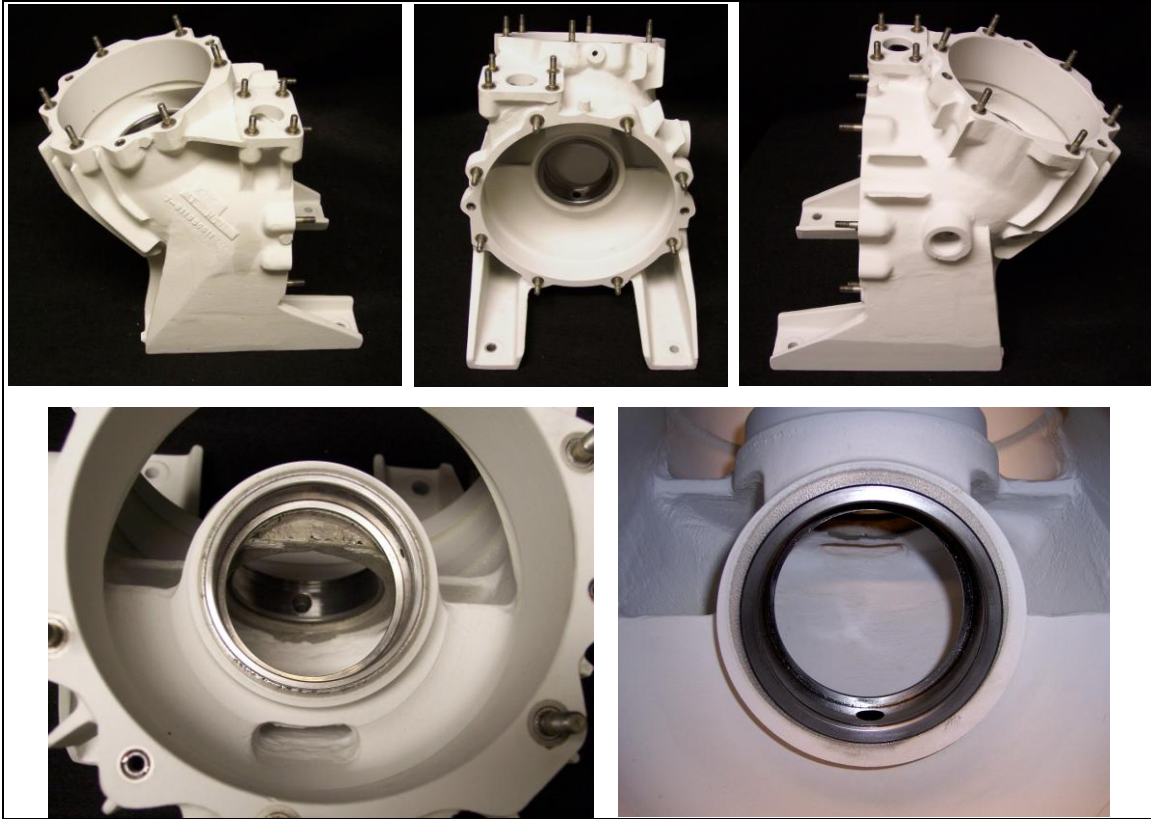


Figure 54. H-64 intermediate gearbox after Immersion Tagnite 8200 and removal of masking tools.
 Bottom left: top steel liner after Tagnite. Bottom right: bottom steel liner after Tagnite.

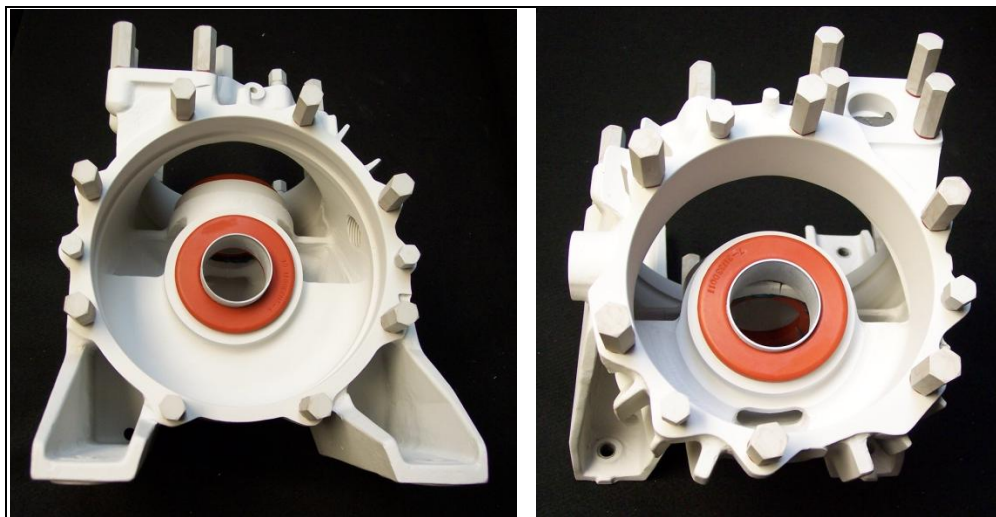


Figure 55. Installation of Acme masking tools on steel liners of H-64 intermediate gearbox.
 Left: masking on bottom steel liner. Right: masking on top steel liner.

During the installation process, TAG personnel discovered that the masking inserts did not protect the bottom of the liners (figure 56). The solution was to attempt to seal the bottom areas of the steel liners with the Dymax UV curable maskant. Inspection of the UV maskant after the Immersion Tagnite process showed that the UV maskant held up well.

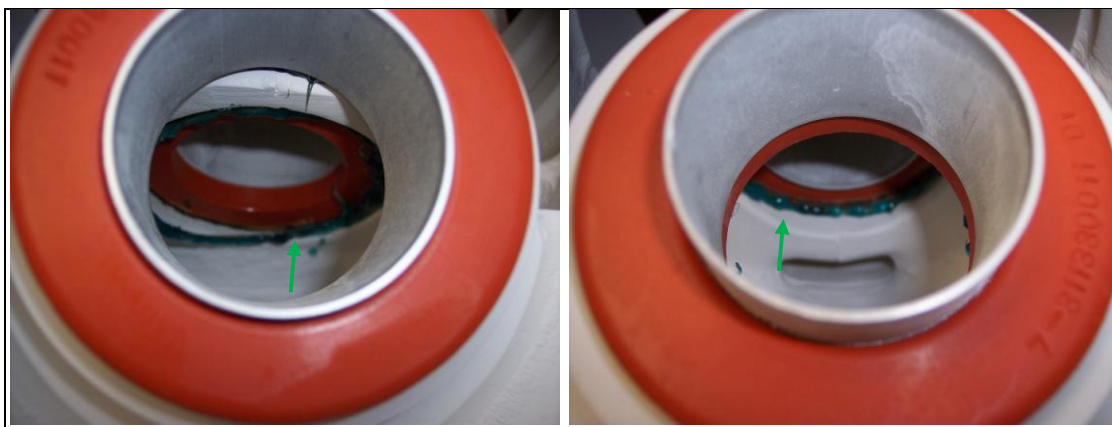


Figure 56. View of UV maskant around the bottom of the steel liners after Tagnite.

Once the steel liner covers were removed after Tagnite, it was immediately evident that the Acme masking tools were not robust enough to survive the Tagnite process. The steel liners had lots of damage caused by a total lack of sealing around the steel (figure 57). After the rust was removed, there was evidence of pitting on the steel, which indicated that the leakage was present during the Tagnite anodize portion of the process; this leakage left the steel liner unusable. The Acme masking was quickly abandoned because of the extensive leaking during the Tagnite process.

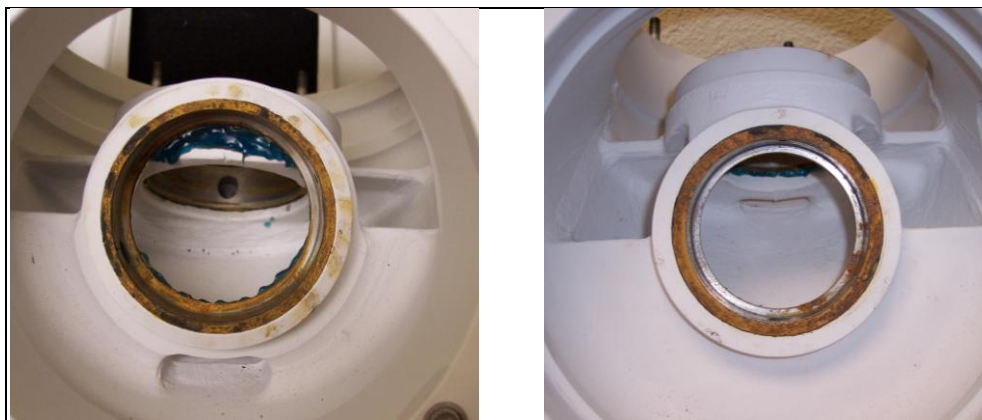


Figure 57. Extensive damage to the steel liners after removal of Acme masking tools. Left: top steel liner. Right: bottom steel liner.

Conclusions:

- The masking tools for all three (H-64) parts were successfully developed and tested.
- The H-64 intermediate gearbox was the most difficult to mask because of the two steel liners mounted on the inside of the casting at a 90° angle to each other.
- Commercially available masking is not robust enough to provide protection during the Tagnite anodizing process. Extensive modifications would be required to this type of masking; these modifications would minimize any manpower savings due to the perceived simplified installation process.

3.4 Task IId: Masking of CH-47 Magnesium Components

The original work plan was to focus on the H-60 and H-64 platforms. As the project proceeded, the masking tools for the H-60 and H-64 parts were coming in under budget. TAG was looking for a complex aviation magnesium component that would challenge the current masking technology at TAG. After some discussion, AMRDEC engineers concluded that the H-47 accessory gearbox (P/N 145D2309-3) was a suitable “reach” component to test the limits of the masking technology. Two accessory gearboxes (figure 58) were obtained from the AMRDEC AED at Corpus Christi Army Depot (CCAD).



Figure 58. As-received pictures of two H-47 accessory covers from CCAD/SAFR.

The parts were sent to Able Engineering (Phoenix, AZ) for the same type of media blast cleaning done on the H-60/H-64 components. Figure 59 shows the parts after the old coatings had been removed.



Figure 59. H-47 accessory cover after media blast cleaning.

3.4.1 H-47 Accessory Cover: Masking Tool Development

We took a visual survey of the accessory cover to identify the types and number of mixed metal inserts. Figures 60 and 61 summarize the mixed metal content of this housing.

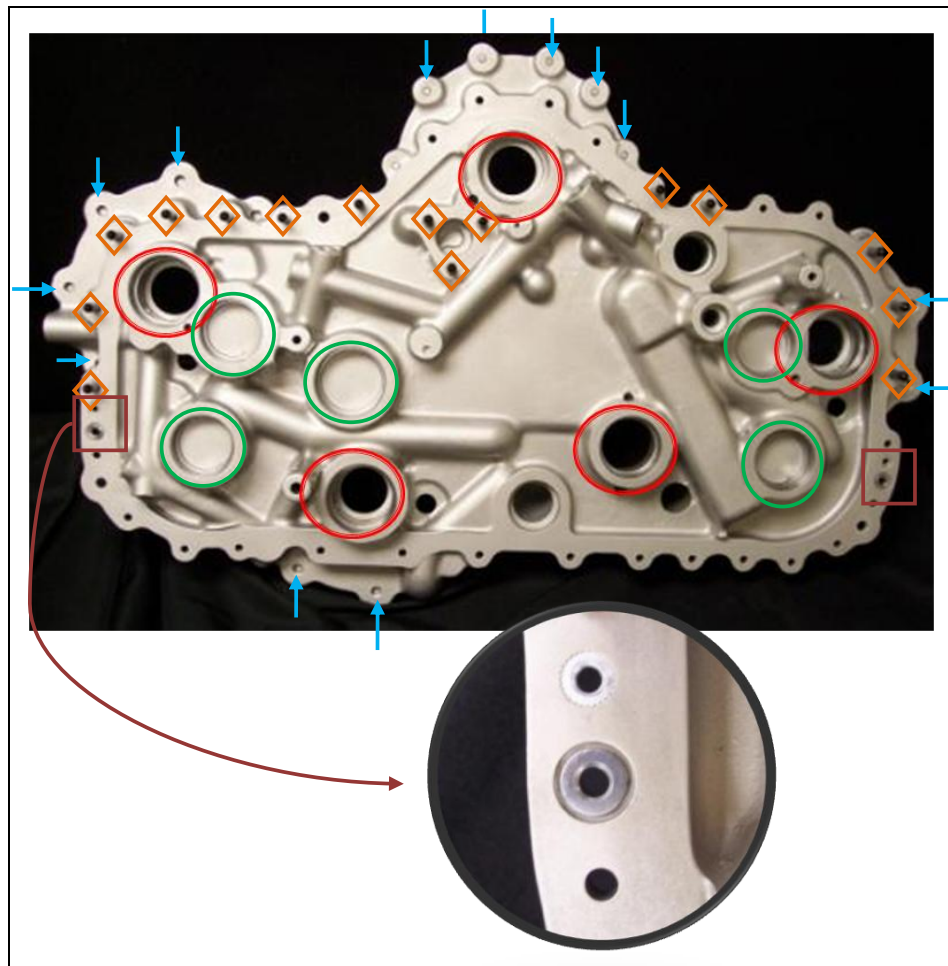


Figure 60. H-47 accessory cover – bottom contains 15 threaded studs, 5 bearing races with through holes, 5 bearing races (enclosed), 13 stud bottoms for UV maskant, and 4 inserts.

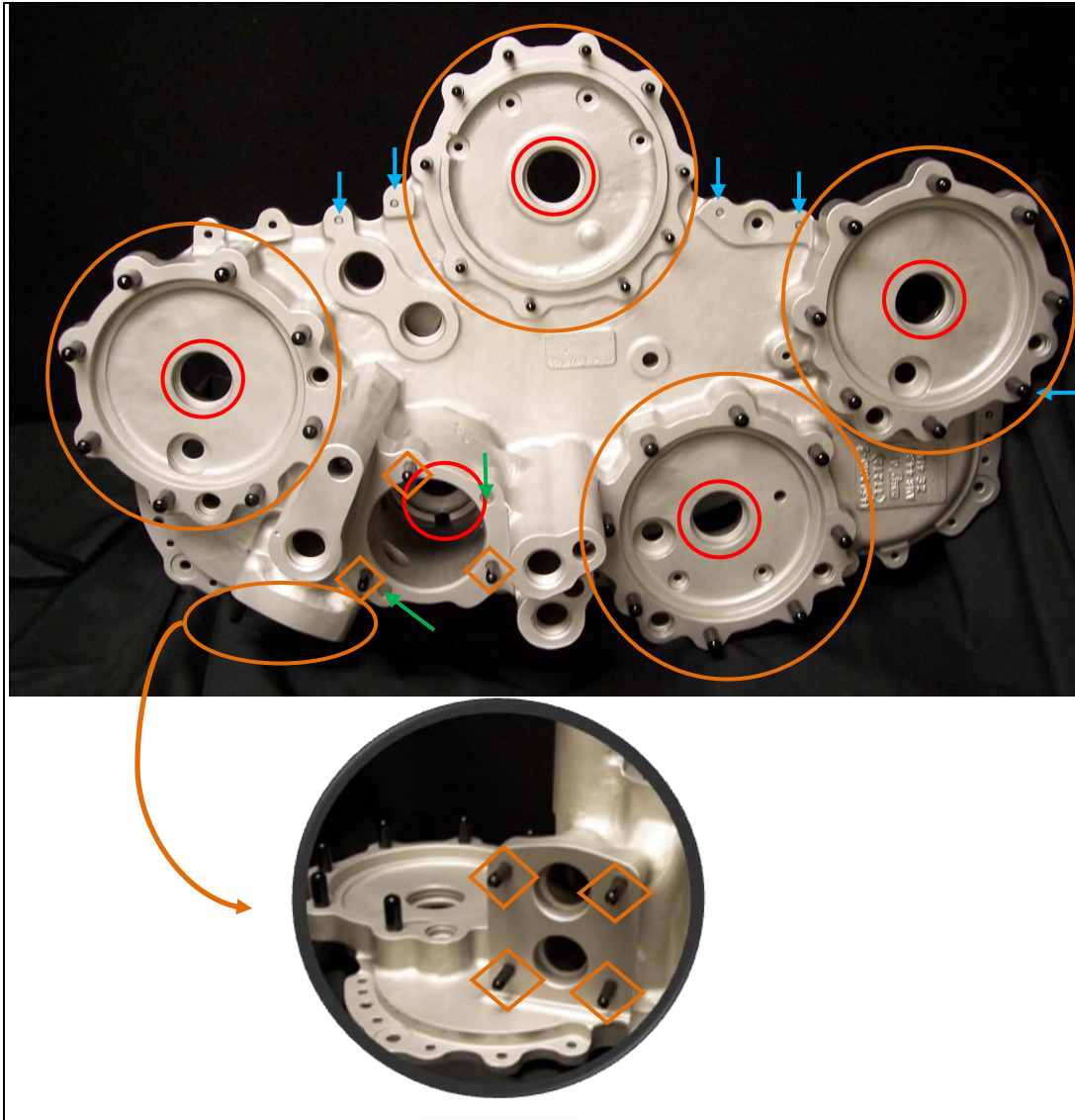


Figure 61. H-47 accessory cover – top contains 41 threaded studs, 5 bearing races with through holes, 2 inserts, and 5 stud bottoms for UV maskant.

The steel bearing races on the accessory cover are more complicated than the liners on the H-60 and H-64 platforms. Each bearing race has oil drainage holes in the steel or right underneath the steel. There are also two drain holes out of each bearing race that leads to the outside of the housing. Examples of these drain holes are shown in figure 62. These drain holes must all be plugged to prevent Tagnite electrolyte from making contact with the steel races.

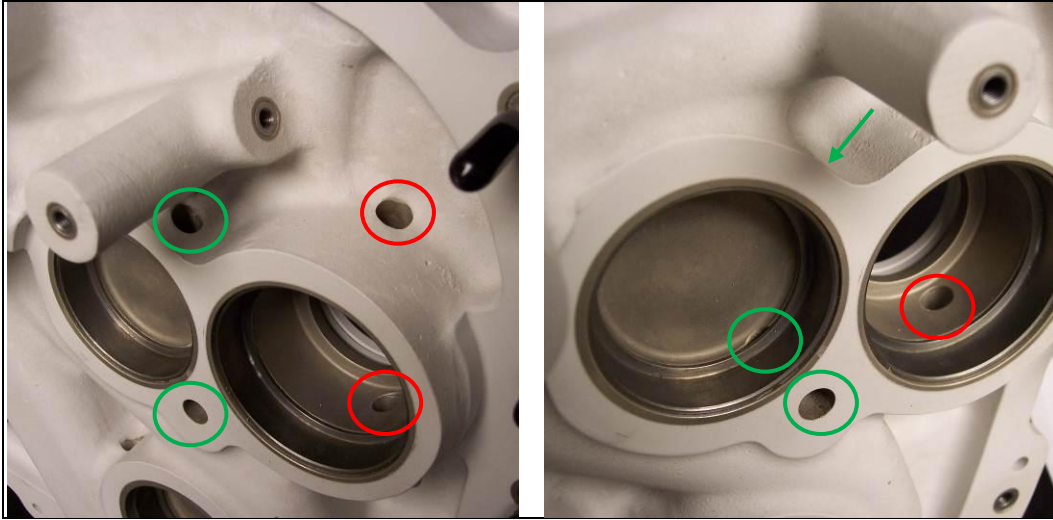


Figure 62. Drainage holes for bearing races on H-47 accessory cover. Drainage holes for recessed bearing races (left) and drainage holes for bearing races with through passageways (right).

The studs were covered with threaded aluminum covers with O-rings on the base of the studs (figure 63).

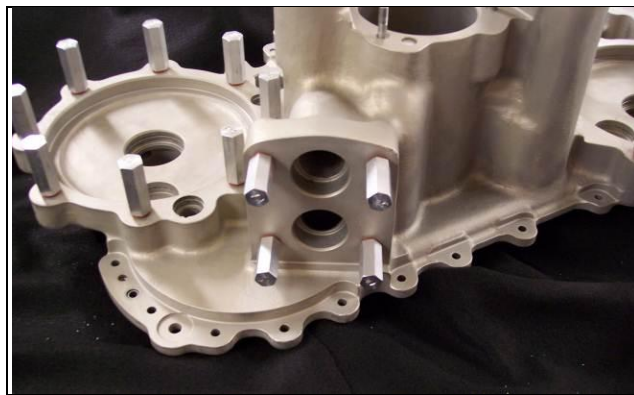


Figure 63. Typical masking on threaded studs.

The inserts were handled by two different methods:

1. Threaded inserts with O-rings.
2. Aluminum covers with O-rings held by a support bridge.

The masking for the bearing races with the through passageways consisted of top and bottom covers held together with threaded bolts.

The masking for the recessed bearing races (blind hole) consisted of a top cover held in place with a large support bridge/threaded bolt arrangement.

The outside drainage holes were plugged using silicon plugs that were cut down to size and the exposed stud bottoms were masked off using the UV curable maskant (figure 64).



Figure 64. Example of UV curable maskant on stud bottoms of H-47 accessory cover.

3.4.2 H-47 Accessory Cover: Tagnite Application on Masked Parts

The masked H-47 accessory cover was run through the Immersion Tagnite bath using the same conditions that a new aerospace magnesium casting without any mixed metal would be processed in the TAG production line. After the Immersion Tagnite process, the masking was removed, and the part was inspected (figure 65). There was only one problem seen after the removal of the masking: one of the recessed bearing races had some rust. The rust was easily removed, and the source of the leak was traced to a silicone plug that had fallen out. There was no pitting on the bearing race, which implies that the rust formation occurred after the Tagnite process (figure 66).

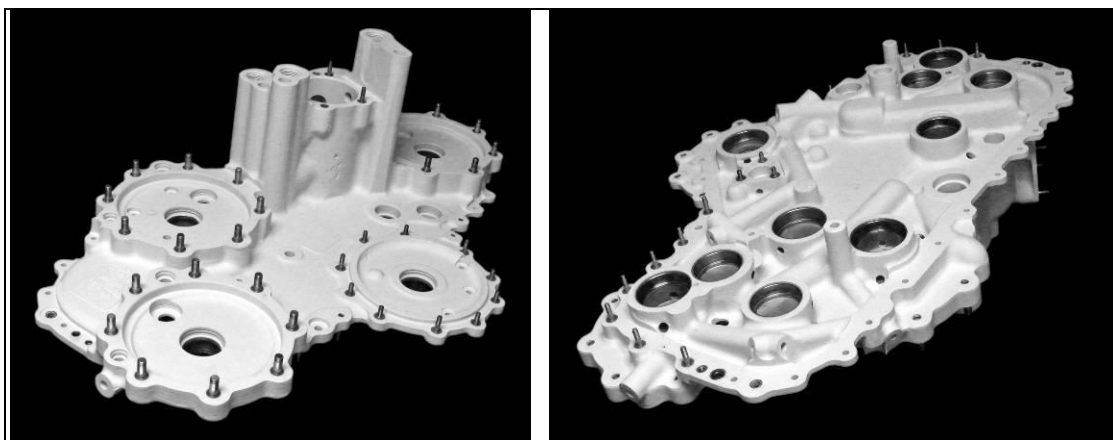


Figure 65. H-47 accessory cover after Tagnite and removal of masking tools.



Figure 66. Various mixed metal inserts on H-47 accessory cover after Immersion Tagnite process. Left: perimeter inserts. Center: recessed and through bearing races (no damage). Right: through bearing races with light rust damage.

3.4.3 H-47 Accessory Cover: Masking Tool Development – Cover No. 2

During the masking development stage, TAG personnel noticed that the second H-47 accessory cover had additional inserts that were not present on the first cover. The new inserts were evaluated for ferrous content by holding a magnet over the inserts. These new inserts are shown in figures 67–69. Some of the inserts had a strong attraction to the magnet, while others had no attraction. The inserts with no magnetic attraction were assumed to be aluminum inserts. Aluminum will take a coating during the Tagnite anodization process, and therefore no masking was needed for these inserts. The other inserts were all threaded inserts that were installed flush to the magnesium casting and were easily masked with threaded aluminum insert covers and O-rings.

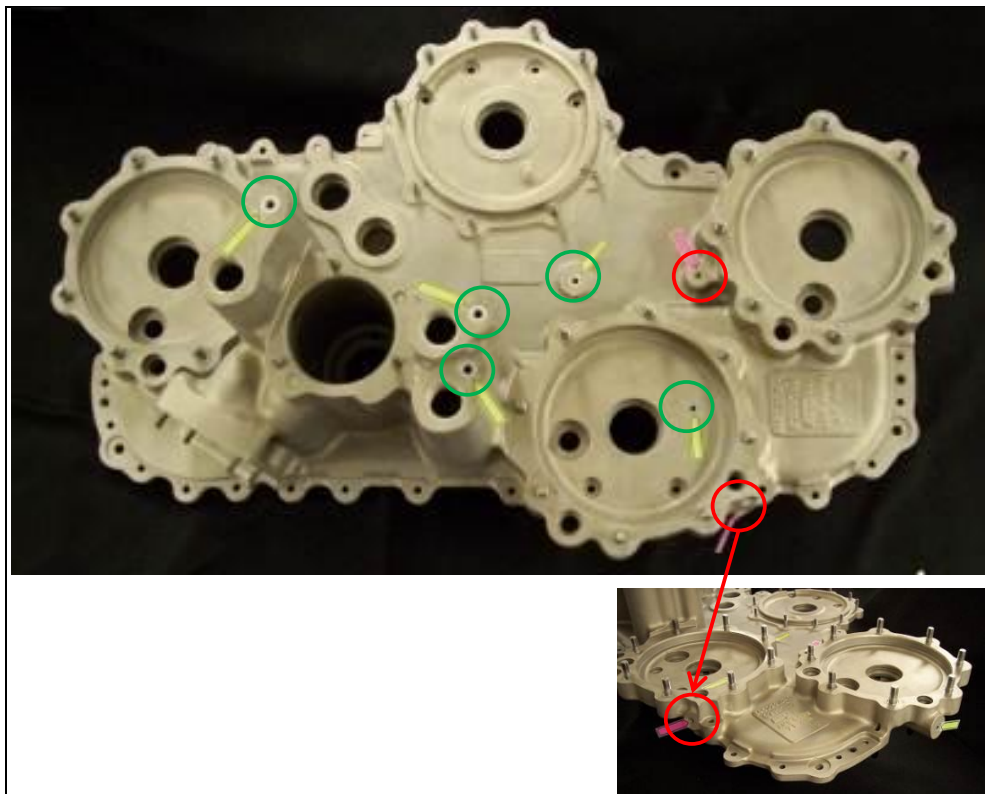


Figure 67. Additional inserts on top of second H-47 accessory cover (view 1): nonmagnetic (green) and magnetic (red).

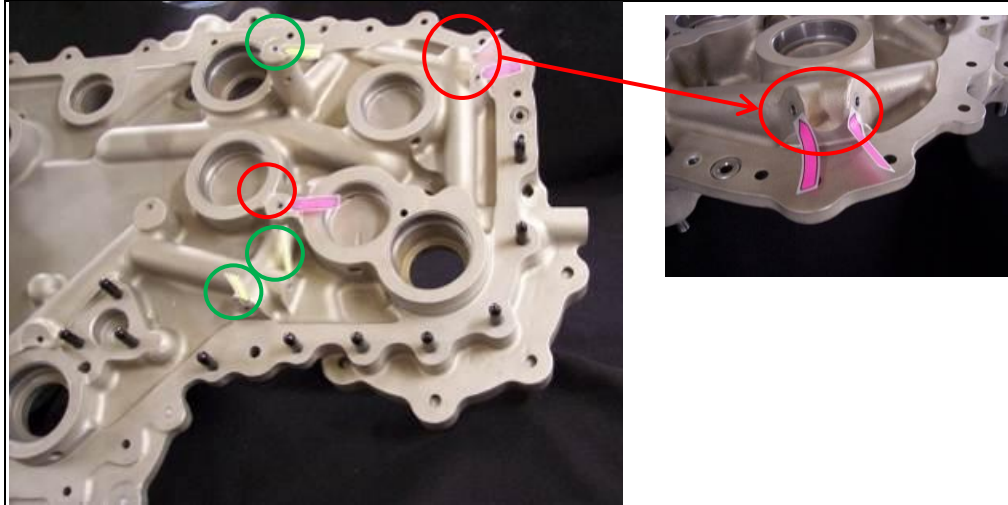


Figure 68. Additional inserts on bottom of second H-47 accessory cover (view 2): nonmagnetic (green) and magnetic (red).

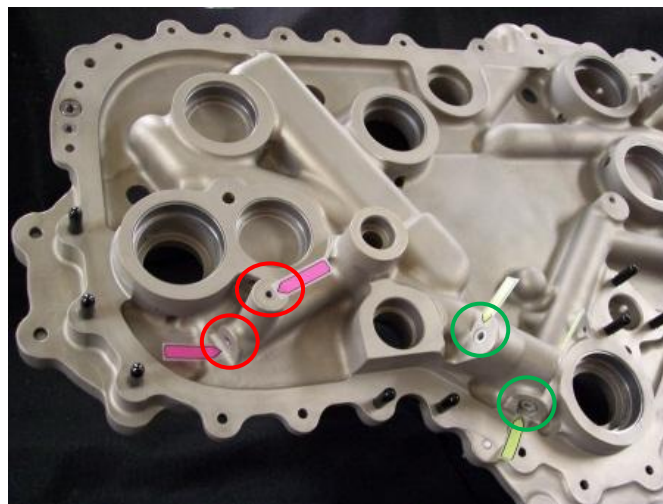


Figure 69. Additional inserts on bottom of second H-47 accessory cover (view 3): nonmagnetic (green) and magnetic (red).

After masking the additional inserts, the second H-47 accessory cover was coated in the Immersion Tagnite process. An examination of this part after the masking tools were removed showed no evidence of damage to the mixed metals. The extra inserts that were nonmagnetic accepted a Tagnite coating and therefore must be aluminum inserts.

Conclusions:

- The H-47 accessory cover contained a wide variety of mixed metal inserts that were all successfully masked off.
- The number of mixed metal inserts and complexity of the installed masking tools require a significant amount of man-hours to install (2–3 man-hours) and test, but given the replacement cost, this process is still very cost effective.
- Modifications can be made to the masking tools to simplify installation, particularly to the large support bridge, which need additional reinforcement to prevent warping or shifting during the installation process.

3.4.4 H-47 Accessory Cover: Cold Spray Repair of Corrosion Damage

In February 2011, the IBIF advisory team was present at TAG's Grand Forks, ND, production facility. During a break in the meeting, Jim Holiday of AMRDEC, CCAD, inspected the Tagnite-coated H-47 accessory cover. He pointed out the area on the housing that had enough corrosion damage to have the component removed from service. The corroded area was a through hole with no mixed metals present. An oil tube is inserted in the hole and held in place with a snap ring. Over time, galvanic corrosion occurred in the snap ring groove, and eventually the corrosion caused the snap ring groove to exceed its allowable dimensions. Mr. Holiday, along with several other attendees, remarked that the type of corrosion damage seen in figure 70 is an ideal candidate for aluminum cold spray repair.

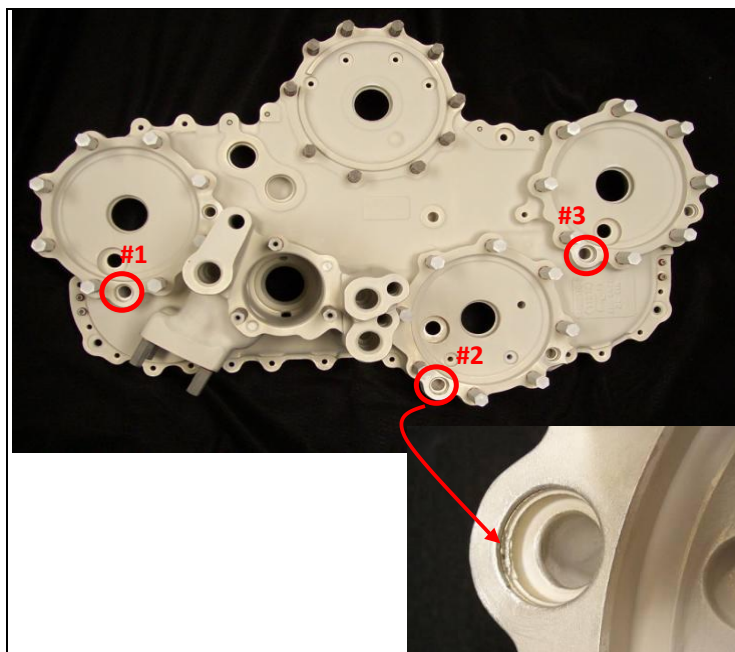


Figure 70. Location of snap ring grooves with corrosion damage. Insert shows location with greatest corrosion damage in snap ring groove.

After a detailed examination of the corroded areas, location no. 2 was deemed the best candidate for cold spray repair. The accessory cover was sent to the U.S. Army Research Laboratory (ARL), Adelphi, MD, for high-pressure cold spray repair using 6061 aluminum. Location no. 2 was over-drilled to enlarge the hole, then cold spray was applied around the interior perimeter and remachined to original tolerances (figure 71). In addition, some porosity holes on the as-cast surface (figure 72) were also over-sprayed (figure 73).



Figure 71. H-47 accessory cover – snap ring groove cold spray repair. Left: after cold spray and remachining. Right: after Immersion Tagnite.

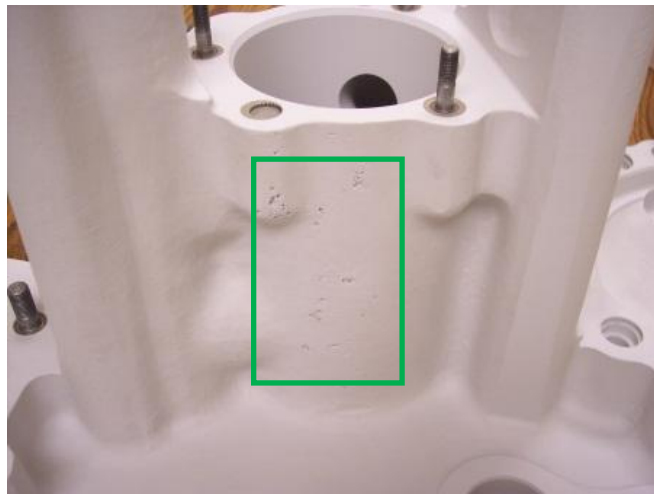


Figure 72. Location of porosity on as-cast surface to be cold spray repaired.

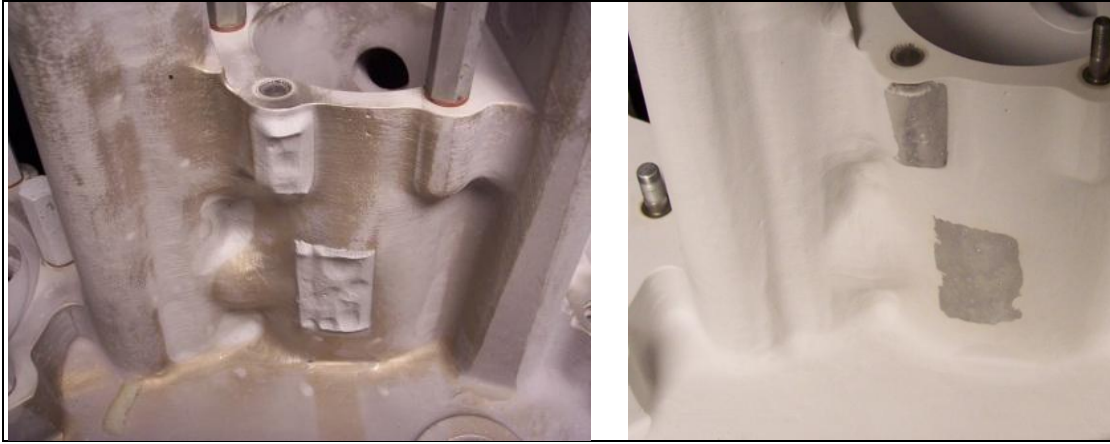


Figure 73. Cold spray repair of as-cast surface on H-47 accessory cover. Left: after cold spray repair. Right: after blending of repair and Immersion Tagnite.

The part will be returned to Mr. Jim Holiday at CCAD for evaluation. If the part has been restored to dimensional tolerances, the plan is to place the part on a helicopter.

Conclusions:

- The aluminum cold spray was sprayed into the snap ring groove and remachined to original tolerances after some adjustments to the cold spray deposition process and careful remachining.
- The Tagnite coating was readily accepted by the aluminum cold spray layer. There was no apparent damage or loss of adhesion of the cold spray because of the Tagnite anodization step.

3.5 Task IIe: IBIF Demonstration at TAG (February 2012)

In order to prove the validity of masking mixed metal aerospace magnesium components and applying an anodized coating, a demonstration of this technology was made at the Technology Application Group production facility in Grand Forks, ND, on 8 February 2012 (figure 74). In addition, TAG wanted to demonstrate that more than one mixed metal part could be masked and coated at one time.

During a teleconference of the IBIF advisory board, board members agreed to have TAG mask and apply Immersion Tagnite to four H-64 tail rotor gearbox housings simultaneously as well as four H-60 center housing assemblies. Additional H-64 tail rotor gearbox housings and H-60 center housing assemblies were obtained from the SAFR facility at CCAD. The parts were sent to Able Engineering for media blast cleaning.



Figure 74. H-60 center housings and H-64 tail rotor gearbox housings for IBIF demonstration (as-received condition).

The parts were masked and then racked onto TAG's production flight bars prior to the arrival of the IBIF demonstration attendees. There were two flight bars prepared—one flight bar held four masked H-60 center housing assemblies and the other flight bar held the four H-64 tail rotor gearbox housings. Each flight bar of parts would allow the four components to be coated at the same time. The parts were immersion Tagnite coated, and the masking was removed in the presence of the IBIF attendees. The four H-64 tail rotor gearbox housings were inspected, and no evidence of damage was seen on any of the parts. After masking removal on the H-60 center housing assemblies, some minor rust was found on several of the mounting pad bushings; however, the attendees inspected the parts and deemed them acceptable.

Conclusion:

The engineers in attendance at the demonstration agreed that the project goals were achieved.

4. Task III: Develop Precleaning Protocol

In order to apply a high-quality Immersion Tagnite coating on used magnesium components, all of the old coatings must be removed prior to the Tagnite process. Any remaining coatings that are present during the Immersion Tagnite process will probably be undermined by the Tagnite deposition process. The danger arises when the old coatings are so thick that the Tagnite pretreatment process cannot remove the coating, leaving the metal underneath the coating lacking the necessary surface activation. The result is that the Tagnite deposition process undermines the old coatings and attacks the base metal. The attack can cause rapid oxidation at the surface; this oxidation leads to “burning” of the metal and significant metal loss.

As mentioned earlier in this report, the old coatings were removed by a media blast process at Able Engineering in Phoenix, AZ. This company has a vast background in removing old coatings from overhauled parts. The parts that were media blasted at Able Engineering were closely inspected by TAG personnel and were found to be completely void of old coatings. Because of trade secrets, Able Engineering would not reveal the exact media blast procedure, but

they did tell TAG that the process consisted of various plastic media and glass media steps. This cleaning procedure was approved by the Federal Aviation Administration for use on civilian aircraft parts.

TAG was so impressed by the quality of the parts received from Able Engineering that the decision was made to forego any investigations into anodic precleaning in order to use the funds to expand the number of parts that could be masked and Tagnite coated for this IBIF effort.

5. Task IV: Early Warning Electrolyte Leakage Mitigation

In most magnesium aerospace components, the mixed metal components that are difficult or impossible to replace are the steel liners and bearing races. Because of the complexity of the masking used to protect these parts, extra measures must be taken to prevent the contact of Tagnite electrolyte with the steel during all phases of the Tagnite process. Knowledge developed during the masking efforts for the magnesium components led TAG to the use of additional safeguards to prevent damage to the steel liners during the Tagnite process.

The original proposal called for the development of early warning indicators of electrolyte leakage. At the time of proposal, TAG personnel had the idea that sensors could be installed in the aluminum covers that could sense the presence of liquid in the masked-off areas. TAG was unable to find any sensors that could survive the high voltage (>300-V DC) and high current (>9 A) that are present during the Tagnite anodization process. The use of sensors was then abandoned.

5.1 Masking Tool Costing and Manpower Requirements

During this IBIF effort, TAG personnel kept detailed records of the amount of time needed to apply and remove the masking tools for the components summarized in this report. The process steps that were documented were:

- Time to apply UV maskant
- Time to apply masking tooling
- Time to remove UV maskant and tooling
- Time to Brush Tagnite touchup the bare areas left after masking was removed

The times needed to perform the process steps for the H-60, H-64, and H-47 components are listed in tables 5–7. Based on this information and the standard cost to apply the Immersion Tagnite coating, TAG was able to arrive at the estimated cost to apply Tagnite to these used components on a routine basis. Knowing the replacement cost of each component and the cost for applying Tagnite with the masking technology, a cost-benefit analysis can be undertaken.

Table 5. Masking time and tooling costs for H-60 components.

H-60 Components	Center Gearbox Housing (70357-06305-042)	Gearbox Housing (70358-26607-042)
Masking Time	UV Maskant – 25 min Al Covers – 30 min	UV Maskant – 25 min Al Covers – 30 min
Unmasking Time	20 min	20 min
Brush Tagnite Time	40 min	40 min
# of Parts per Run in Tagnite	4 - 16	4 - 8
Approximate Masking Tools Cost per Part.	\$1,200	\$1,400

Table 6. Masking time and tooling costs for H-64 components.

H-64 Components	Intermediate Gearbox Housing (7-30033011)	Tail Rotor Gearbox (7-311340011-9)	Tail Rotor Cover (7-311340012-5)
Masking Time	UV Maskant – NA Al Covers – 40 min	UV Maskant – NA Al Covers – 60 min	UV Maskant – 10 min Al Covers – 40 min
Unmasking Time	20 min	25 min	20 min
Brush Tagnite Time	60 min	120 min	60 min
# of Parts per Run in Tagnite	4 – 8	4 – 8	4 - 8
Approximate Masking Tools Cost per Part	\$1,000	\$1,700	\$1,500

Table 7. Masking time and tooling costs for H-47 components.

H-47 Components	Accessory Cover (145D2309-3)
Masking Time	UV Maskant – 30 min Al Covers – 150 min
Unmasking Time	60 min
Brush Tagnite Time	180 min
# of Parts per Run in Tagnite	1 - 2
Approximate Masking Tools Cost per Part	\$2,800

The results in table 8 show that the proposed system for masking used magnesium castings and applying the Immersion Tagnite/Brush Tagnite coatings can be done for a fraction of the replacement cost. The typical cost for this finishing system is about 8%–10% of the replacement cost. Highlights of this analysis include the following:

- Of the components containing mixed metal, the H-47 accessory cover had the best value, which was driven primarily by the high replacement cost. This component had the highest masking/coating costs of the components evaluated in this effort but still had the lowest percentage vs. the replacement cost.
- The H-60 components had the highest percentage cost vs. replacement cost due to the relatively low replacement cost and time spent to mask the part. This analysis does not include any cost savings due to coating multiple parts per run in Immersion Tagnite. It also does not account for the anticipated increase in corrosion protection and subsequent decrease in life cycle costs. There will also be cost benefits due to the elimination of hexavalent chromium in the depots and maintenance facilities.

This analysis does not include any cost savings due to coating multiple parts per run in Immersion Tagnite. It also does not account for the anticipated increase in corrosion protection and subsequent decrease in life-cycle costs. There will also be cost benefits due to the elimination of hexavalent chromium in the depots and maintenance facilities.

Table 8. Estimated cost of masking components and applying Tagnite and Brush Tagnite as a percentage of the replacement cost.

Component	Part Number	Estimated Replacement Cost	Estimated Tagnite/Brush Tagnite Cost	Tagnite/BT Coatings as Percentage of Replacement Cost
H-60 Center Gearbox Housing	70357-06305-042	\$3,900	\$600 - \$800	15 – 20 %
H-60 Gearbox Housing	70358-26607-042	\$1,700	\$600 - \$800	35 – 45 %
H-64 Tail Rotor Gearbox Housing	7-311340011-9	\$18,500	\$1500 - \$1850	8 – 10 %
H-64 Tail Rotor Cover	7-311340012-5	\$13,500	\$1000 - \$1350	7.5 – 10 %
H-47 Accessory Cover	145D2309-3	\$59,200	\$3000 - \$4000	5 – 7 %

5.2 Conclusion

Even with the increased man-hours needed to mask, unmask, and apply Brush Tagnite along with the slightly increased cost of the Tagnite anodize, the overhauled magnesium component will have better protection than a “new” magnesium component for 10%–15% of the cost of a replacement component.

6. Task V: Evaluation of Flight Critical Components

The IBIF Advisory Panel for this project deemed this task outside the realm of TAG’s responsibility and was not undertaken by TAG personnel.

7. Task VI: Parts Washer After Brush Tagnite

During the course of this effort, TAG personnel realized that a lot of time and effort was needed to clean parts after Brush Tagnite touchup. The Brush Tagnite electrolyte is very caustic and viscous, which results in dried electrolyte on the part. This dried electrolyte is difficult to remove. The best method of removal was found to be immersion or washing with very hot water

followed by vigorous scrubbing and additional rinsing. There is the potential that cleanup after Brush Tagnite can take as long or longer than the actual Brush Tagnite application.

Based on this information, a parts washer was designed and manufactured per TAG's specification. The design is based on a commercially sized dishwasher typically used in a school or hospital setting. The parts washer consists of:

- Loading tray large enough to hold a H-60 main transmission housing.
- Washing bay with randomly rotating nozzles on the top, bottom, and both sides.
- Tankless water heater capable of producing 180 °F water for 4–6 min.
- Fresh water rinse.
- Heated air knife dryer.
- Unattended operation.
- Programmable controller that allows operator to set water temperature, length of wash cycle, length of rinse cycle, and pressure out of the nozzles.

This parts washer should drastically reduce the operator time needed to clean up and rinse a magnesium housing after Brush Tagnite.

8. Conclusions

1. TAG was able to successfully demonstrate that used magnesium aviation component containing mixed metals can be coated with Immersion Tagnite without damage to the mixed metal components.
2. TAG was able to apply the masking/Tagnite/Brush Tagnite coating scheme to:
 - Three magnesium components on the AH-64
 - Two magnesium components on the UH-60
 - One magnesium component on the UH-47
3. This coating scheme was demonstrated to Army Aviation engineers and scientists at the TAG facility.
4. A preliminary cost analysis shows that the proposed masking/Tagnite/Brush Tagnite scheme can be applied to most used magnesium housings for about 8% to 10% of the replacement cost for a new housing.

5. This coating scheme can also be applied to new magnesium castings as seen on the F-35 magnesium components. Using this scheme on new housings will result in cost savings due to elimination of several machining steps and increased lifetime of the part by having Immersion Tagnite on the machined mating faces where galvanic corrosion typically occurs.
-

9. Galvanic Corrosion Study

Scientists at the Center for Surface Protection at North Dakota State University undertook a detailed galvanic corrosion study. This study looked at the galvanic corrosion interaction between common cad-plated fasteners and ZE41 magnesium metal finished with a variety of commonly used magnesium coatings. Three anodized coatings were studied: Immersion Tagnite, DOW 17, and HAE. Three touch-up coatings were studied as well: Brush Tagnite, DOW 7, and DOW 19. The published report from the Center for Surface Protection is found in the appendix.

The conclusion of the report was that the Immersion Tagnite and Brush Tagnite coatings provided superior galvanic corrosion protection vs. the other commonly used coatings.

INTENTIONALLY LEFT BLANK.

Appendix. Performance of Corrosion Protective Coatings on Magnesium Alloy ZE41

This appendix appears in its original form, without editorial change.

PERFORMANCE OF CORROSION PROTECTIVE***COATINGS ON MAGNESIUM ALLOY ZE41*****Dante Battocchi, PhD,**

NDSU CSP

1735 NDSU Research Park Drive, Fargo ND 58102

Dante.Battocchi@ndsu.edu

Ph: 701-231-6219

Nicholas Wilson, PhD,

NDSU, CSP

1735 NDSU Research Park Drive

Nick.Wilson.1@ndsu.edu

Ph: 701-231-5656

Research Project sponsored by Technology Applications Group in support of IBIF III Contract SP4701-10-C-0021 and the ND-COE program.

Table of Contents

Executive Summary.....	B-3
1. Electrochemical impedance spectroscopy and potentiodynamic scan on blocks of Mg alloy ZE41.....	B-4
1.1 EIS of samples with Rockhard topcoat.....	B-4
1.2 EIS of samples without Rockhard topcoat.....	B-8
1.3 Potentiodynamic scan.....	B-12
2. Scanning electron microscopy of TAG8200 on ZE41.....	B-15
3. Neutral salt fog corrosion test (B117 protocol).....	B-26
4. Galvanic corrosion and potentiodynamic scan of six types of Mg alloy ZE41 surface treatment.....	B-33
4.1 Galvanic corrosion.....	B-33
4.2 Potentiodynamic scan.....	B-36
5. Initial inhibitor studies.....	B-40
Notations and abbreviations.....	B-43

Executive Summary

Magnesium and its alloys are gaining wide acceptability due to its light weight and good mechanical properties. Magnesium alloy ZE41 is used extensively for a range of helicopter transmission casings, and is the material of choice for many new helicopter programs including the MD500, Eurocopter EC120, NH90, and Sikorsky S92. However, its use has introduced new issues in the design and lifetime of these structures. In particular, steel fasteners and jointed parts in close proximity to ZE41 are often the source of electrochemical galvanic cells that lead to galvanic corrosion.

The NDSU Center for Surface Protection (CSP) investigated several approaches to corrosion protection of Mg alloys based on anodized and chromated coatings, via a range of electrochemical techniques, scanning electron microscopy, energy dispersive x-ray spectroscopy, and neutral salt fog corrosion test (B117 protocol).

It was found that all specimens afforded excellent corrosion protection to Mg alloy ZE41 with a Rockhard specialty coating. The electrochemical performance of all Mg coating was dominated by the Rockhard topcoat. In order to differentiate between different coatings for Mg, further electrochemical experiments and corrosion testing were performed on non-topcoated specimens.

Electrochemical impedance spectroscopy (EIS) revealed that TAG8200 (from Technology Applications Group) was superior to other anodized coatings, namely HAE and DOW17. TAG8200 is a dense, but porous coating, with an average pore size of 0.5-2 μm . However, at the end of the prolonged exposure in corrosive electrolyte, TAG8200 exhibited barrier properties ten times higher than HAE and DOW17. The presence of a well-defined pitting potential in potentiodynamic scans (PDS) of TAG8200 and Brush Tagnite from Technology Applications Group indicated higher resistance to electrochemical stress compared to the other four tested systems, a crucial aspect to consider when designing protective coatings for multi-metal structures.

Galvanic corrosion and PDS results indicate that TAG8200 affords the best long-term corrosion protective performance. At the same time, application of Brush Tagnite could be considered adequate for short-term protection of Mg alloys. Superior barrier properties of TAG8200 and Brush Tagnite lead to corrosion being confined to the defect site in galvanic corrosion experiments. Conversely, corrosion inhibition of DOW7 and DOW19 chromates passivates the defect, but does not stop corrosion from expanding outside the defect area across the metal surface.

CSP has identified several environmentally friendly corrosion inhibitors for protection of Mg alloys and have performed preliminary electrochemical tests of two of the inhibitors in various corrosive environments. The addition of Inhibitor A, whose chemical composition is not disclosed in this report, reduces the current above E_{pit} by almost 5 orders of magnitude. Similarly, Inhibitor A raises the pitting potential for Brush Tagnite and results in the lowest I_{corr} about E_{pit} . More research is required in order to optimize the amount of inhibitor, its composition, as well as consider synergistic phenomena that may arise from utilizing a mixture of corrosion inhibitors for protection of Mg alloy ZE41 in multi-metal structures.

1. Electrochemical impedance spectroscopy and potentiodynamic scan on blocks of Mg alloy ZE41

Several samples of coated Mg alloy ZE41 (4% Zinc, <1% rare earth alloying elements) were received from Technology Application Group (TAG) in the form of blocks. Five ZE41 blocks had been first subjected to three types of proprietary anodization procedures, namely:

- DOW17 that created a green coating, 2 panels;
- HAE that resulted in a tan color coating, 2 panels; and
- TAG8200, off-white in appearance.

One DOW17, one HAE, and the one TAG8200 anodized blocks were additionally coated with Rockhard topcoat. One ZE41 block had no anodization applied to it and was coated with the Rockhard topcoat. The TAG8200-coated Mg alloy ZE41 was received in the form of a 4" x 3" panel. Table 1 shows the sample matrix for the PDS and EIS experiments.

Table 1. Sample identification.

Sample ID	Substrate	Anodization	Topcoat
1	ZE41 panel	Tag8200	-
2	ZE41 block	Tag8200	Rockhard
3	ZE41 block	HAE	-
4	ZE41 block	HAE	Rockhard
5	ZE41 block	DOW17	-
6	ZE41 block	DOW17	Rockhard
7	ZE41 block	-	Rockhard

All electrochemical experiments were performed in 1% NaCl. The low concentration of the electrolyte was chosen in order to slow down the corrosion of the very active Mg alloy. Electrochemical impedance spectroscopy (EIS) and potentiodynamic scan (PDS) experiments were conducted in a three-electrode cell on a Gamry-family potentiostat, with a saturated calomel electrode (SCE) as the reference electrode, and a platinum mesh as the counter electrode. EIS was performed in the frequency range between 0.1 Hz and 100 kHz (instrumentation limit), with each EIS scan taking between 45 mins to 1 hour to complete.

1.1 EIS of samples with Rockhard topcoat

An electrochemical response of a coating to a small ac perturbation can be modeled by a combination of simple electric circuit elements, most frequently resistors and capacitors, connected either in series or in parallel. In ac circuits, the applied potential and resulting current are related through impedance, Z . Impedance is a vector, and, as such, can be represented graphically using two types of plots: complex plane, also known as Argand or Nyquist plots (Cartesian coordinates) and Bode plots (polar coordinates). The complex plane plot is a plot of Z'' versus Z' , that is, the imaginary versus the real components, plotted for various frequencies. The log of Impedance modulus $|Z|$ and the phase angle are plotted versus log frequency in the

Bode plot. Each representation of impedance has its advantages and drawbacks. For example, the frequency information can only be easily obtained from the Bode plot; however, the existence of several time constants associated with different physical and electrochemical processes may be easier to discern from the Nyquist plot.

$$(Eq. 1.1) \quad Z = Z_{Re} + jZ_{Im} \quad \text{or} \quad Z = R + jX_C$$

Z_{Re} is the real component of impedance, or resistance R . Resistance is independent of frequency, and its corresponding phase angle is always zero. Z_{Im} is the imaginary component of impedance, called reactance X . In the case of a capacitive coating, the imaginary component is called capacitive reactance, X_C .

$$(Eq. 1.2) \quad X_C = -1/2\pi fC, \text{ where } f \text{ is the frequency, and } C \text{ is the coating's capacitance.}$$

Equations 1.3 and 1.4 show the relationships between real and imaginary components of impedance and its modulus and phase angle.

$$(Eq. 1.3) \quad |Z| = (Z_{Re}^2 + Z_{Im}^2)^{\frac{1}{2}} = R^2 + X_C^2$$

$$(Eq. 1.4) \quad Phase = \arg\left(Z_{Im}/Z_{Re}\right)$$

Figure 1 shows a typical EIS spectrum as a Bode plot. In the high-frequency end of the spectrum, the coating response comes from its capacitive component, whereas the low end of the frequency spectrum depicts the resistive component. The low-frequency impedance is composed of R_s , solution resistance, and R_p , polarization resistance. R_p is the response of the electrochemical cell to a small ac perturbation, and can be due to many physical phenomena taking place in the cell.

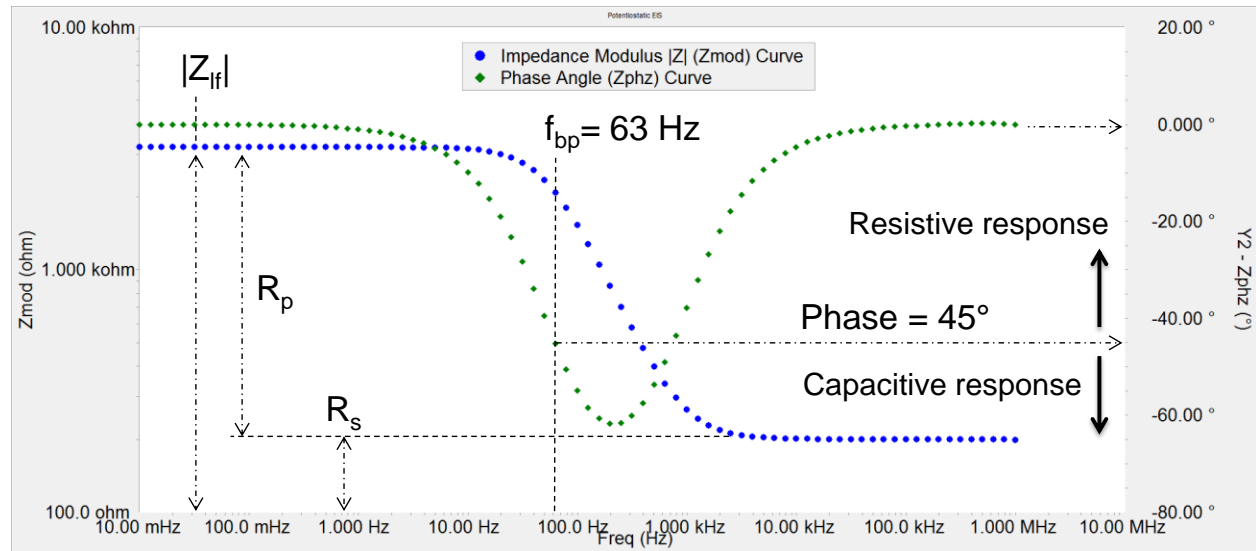


Figure 1. Bode plot of a typical EIS spectrum.

In the case of Figure 1, the Bode contains one breakpoint or corner frequency, f_{bp} . The breakpoint frequency f_{bp} indicates a boundary in a system's frequency response at which the electrochemical behavior of a system changes from resistive to capacitive. At f_{bp} , the real and imaginary components of impedance modulus are equal, and the phase angle is equal 45° .

When coating resistance is monitored as a function of time, f_{bp} can be useful for estimating the area fraction of physical defects as shown in Equation 1.5:

$$(Eq. 1.5) \quad f_{bp} = \left(\frac{1}{2\pi\epsilon\epsilon_0\rho} \right) \frac{A_d}{A}, \text{ where}$$

A_d – defect area where electrochemical reactions operate,
 A – total exposure area, and
 ρ – resistivity of coatings at defects.

The low-frequency impedance modulus, $|Z_{lf}|$, parameter is useful for coating systems with high impedance values. An excellent coating system, free of defects, will have a very low breakpoint frequency that will be undetected during an EIS experiment with a typical frequency range of 10 mHz – 100 kHz. While current electrochemical instrumentation allows impedance measurement at frequencies as low as several μ Hz, doing so is impractical as it significantly increases the measurement time and is prone to noise pickup due to the very small currents being measured. Additionally, when a breakpoint frequency cannot be detected above the min scan frequency, this only occurs with excellent coating with impedance values above the $10^9 \Omega\text{-cm}^2$ threshold that would qualify them as excellent coatings. However, in the case of an excellent coating, the phase angle never becomes zero within the experimental frequency range, and the modulus spectrum never plateaus into the resistive region. Therefore, true resistance cannot be obtained experimentally and can only be estimated as being above the highest $|Z|$ being measured at the lowest frequency, the $|Z_{lf}|$ value, sometimes depicted as $|Z_{f \rightarrow 0}|$.

The EIS spectra for TAG8200 coated with RockHard are shown in Figure 2. At the end of the test that ran for 30 hours, and there was almost no variation in impedance modulus (Z_{mod}) of phase angle (Z_{phz}). The Z_{mod} spectra in Figure 2 form a single line that is composed of several identical overlapping Z_{mod} spectra taken at different immersion times. The phase angle value close to -90° indicated that the coating remained highly capacitive throughout the entire exposure period, with low-frequency impedance modulus values on the order of $10^{11} \Omega\text{-cm}^2$. The actual $|Z|$ values at DC limit ($Z_{f \rightarrow 0}$) may be as high as $10^{14-16} \Omega\text{-cm}^2$, but such values are impossible to measure directly due to the length of the experiment and the noise associated with very low currents. However, for all practical applications, a coating with a low-frequency $|Z|$ of $10^9 \Omega\text{-cm}^2$ and above is considered excellent in terms of corrosion protection, and Rockhard topcoat meets and exceeds the criteria for such coating.

Figures 3 and 4 show EIS spectra for HAE with Rockhard and Rockhard alone, respectively. It is easy to observe that the $|Z|$ behavior of ZE41 treated with HAE first and then top-coated with Rockhard (Figure 2, HAE + Rockhard) is identical to the EIS spectra of ZE41 coated directly with Rockhard (Figure 3, Rockhard). Moreover, EIS spectra of all three samples (2, 4 and 7) are indistinguishable, which indicates that in an undamaged coating, the EIS response is dominated by the layer providing the best barrier protection, namely Rockhard. Rockhard is a thick,

capacitive coating that cannot be easily degraded by non-destructive electrochemical evaluation techniques, such as electrochemical impedance spectroscopy.

For non-destructive methods, the only input to the system is the corrosive electrolyte that penetrates the coating and eventually reaches the metal surface. For systems containing Rockhard, natural ingress of electrolyte into an undamaged topcoat is a very slow process that may require months of immersion, and is, therefore far removed from the true field conditions of the parts being tested. For this reason, Sample 6 was not tested with EIS.

We have shown that corrosion protection afforded by undamaged Rockhard alone is sufficient to classify these systems as excellent in terms of corrosion protection of Mg.

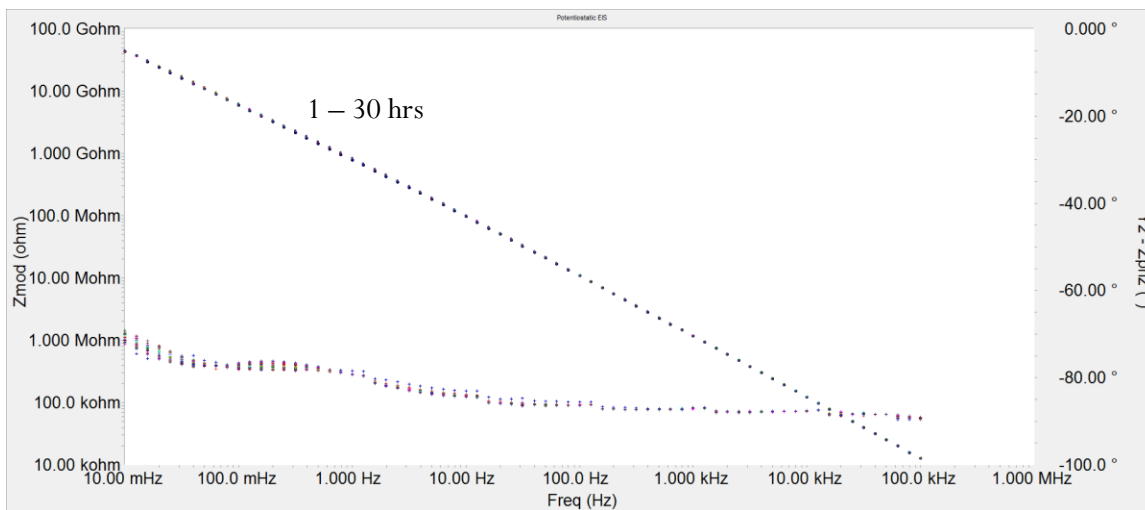


Figure 2. EIS for ZE41 with TAG8200 + Rockhard topcoat (Sample 2).

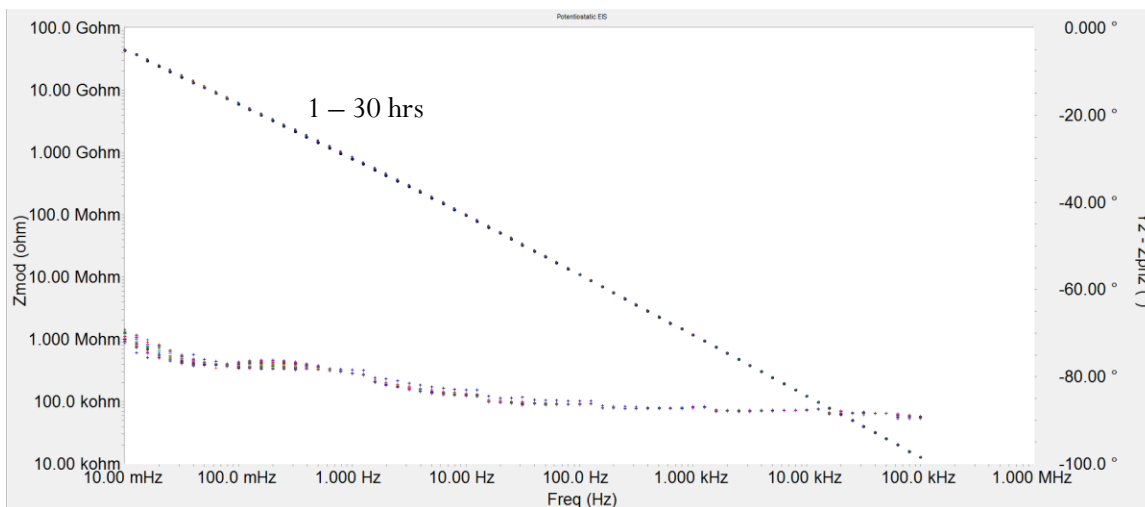


Figure 3. EIS for ZE41 with HAE + Rockhard (Sample 4).

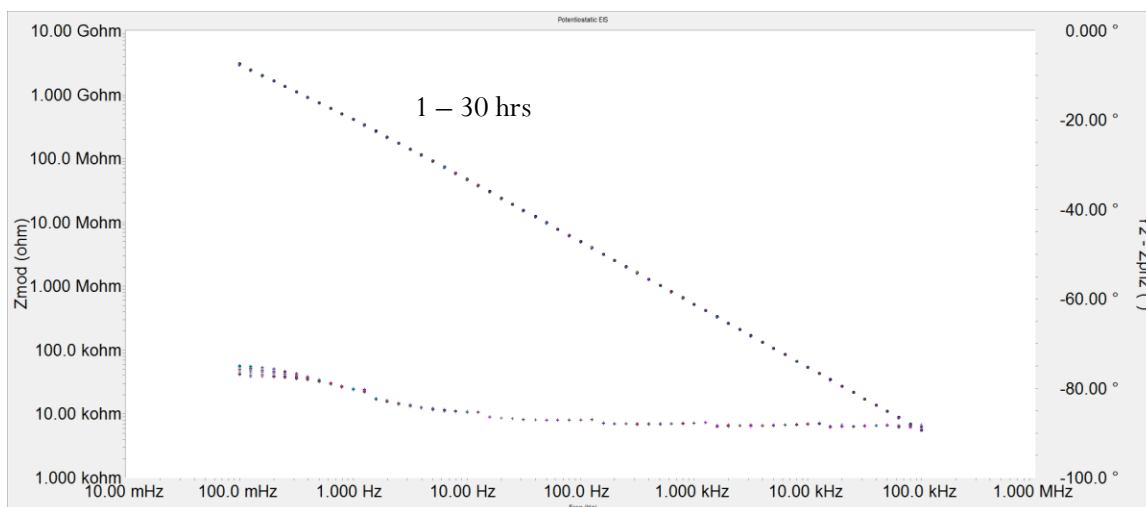


Figure 4. EIS for ZE41 with Rockhard only(Sample 7).

1.2 EIS of samples without Rockhard topcoat

Samples 1, 3 and 5 represent three types of anodization on ZE41. The EIS spectra of ZE41 modified with TAG8200 (Sample 1), HAE (Sample 3), and DOW17 (Sample 5) reveal that these surface treatments possess much lower impedance modulus values than their Rockhard-coated counterparts. For the purposes of this report, in order to establish a parallel to the conventional coating systems composed of a primer and topcoat, the anodization surface treatments may be referred to as primers.

Figures 5 and 6 show the EIS spectra and open circuit potential (OCP) records for the HAE primer on Mg alloy ZE41. Initially, the coating has a low-frequency $|Z|$ on the order of a few hundred kilo-Ohm, which is typical for primers. However, the coating deteriorates quickly during the first EIS run upon immersion in 1% NaCl. The OCP of -1.65V (vs. SCE) suggests the metal undergoes corrosion at the very start of the experiment, that is, after 20 minutes of soaking in electrolyte, the primer does not prevent the electrolyte from contacting the metal.

One hour into immersion, the OCP moves in the positive direction due to the formation of corrosion products. The EIS spectra show the gradual decrease of the low-frequency modulus, as simultaneously with the formation of corrosion products, the area affected by corrosion increases due to further degradation of the coating. Eventually, the entire coating layer is removed, and only corrosion products remain on the surface. At the 20-hr mark, the corrosion seems to accelerate again, which is indicative of further removal of corrosion products and exposing a new area for further contact with electrolyte. At the 20-hr mark, the trend for OCP going more positive changes direction, and the OCP values begin to trend more negative, back to the OCP values of the bare metal. This is due to more metal being exposed at prolonged exposure.

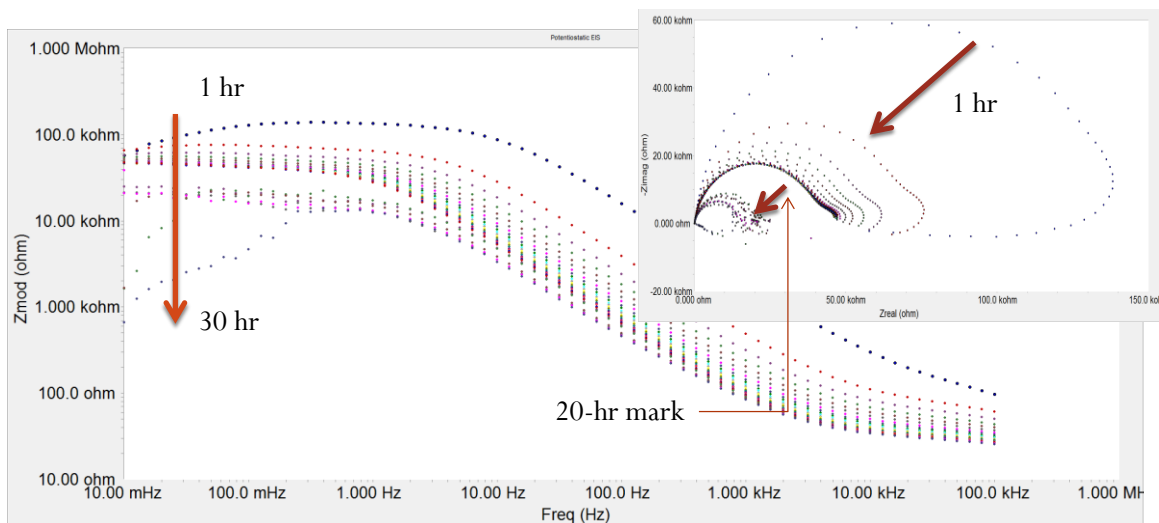


Figure 5. EIS for ZE41 with HAE: Bode (main) and Nyquist (inset) diagrams.

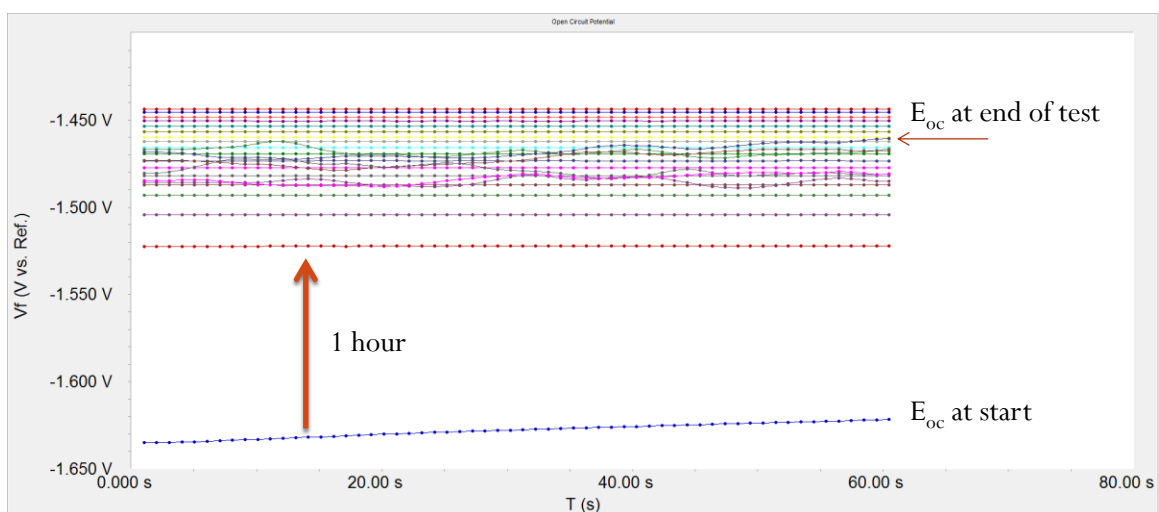


Figure 6. EIS for ZE41 with HAE: Open circuit potential (vs. SCE).

Figures 7 and 8 show the EIS spectra and open circuit potential (OCP) records for the DOW17 primer on Mg alloy ZE41. DOW17 behaves similarly to HAE in that it, too, provides poor barrier protection from corrosion. However, it appears the DOW17 coating presents more of a protection layer than the HAE, judging by the OCP values, albeit not significantly.

The OCP reaches the value for bare Mg at the beginning of the 2nd EIS test (vs. 1st for HAE), after which it climbs positively for the duration of the experiment. It can be concluded from the EIS spectra that corrosion products gradually form on the surface, and by 30 hours of exposure in 1% NaCl, the film is still being broken down and corrosion products still form on the surface and occupy most of the area. There is no OCP trend reversal back to bare metal, and EIS spectra do not change their shape at the end of the test, unlike HAE (Figure 5), where at the end of the last two EIS runs, the modulus dips down to 1 k Ω -cm², indicating further exposure of Mg alloy underneath corrosion products upon their removal from the surface.

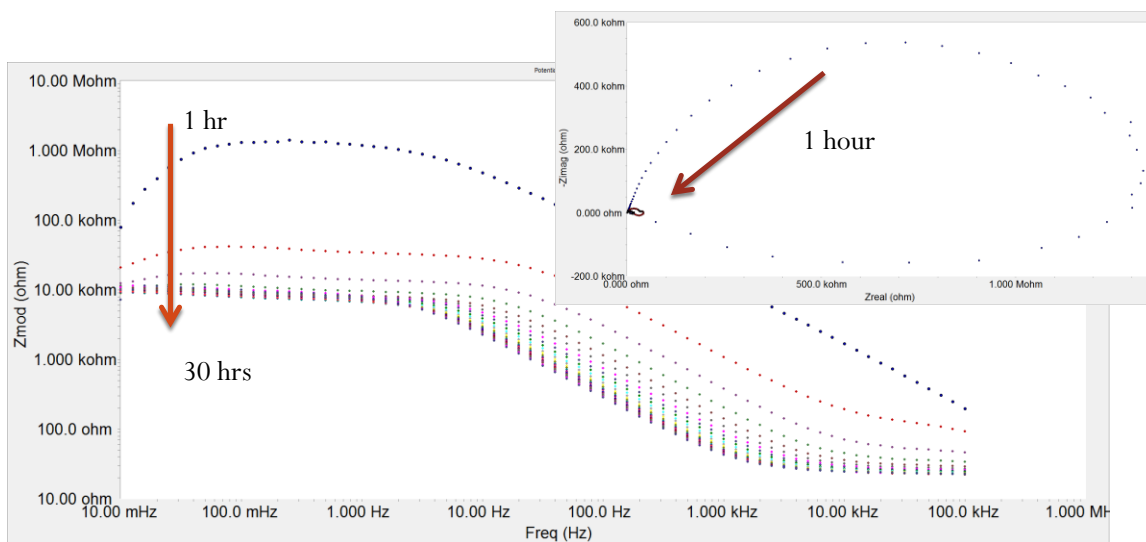


Figure 7. EIS for ZE41 with DOW17: Bode (main) and Nyquist (inset) diagrams.

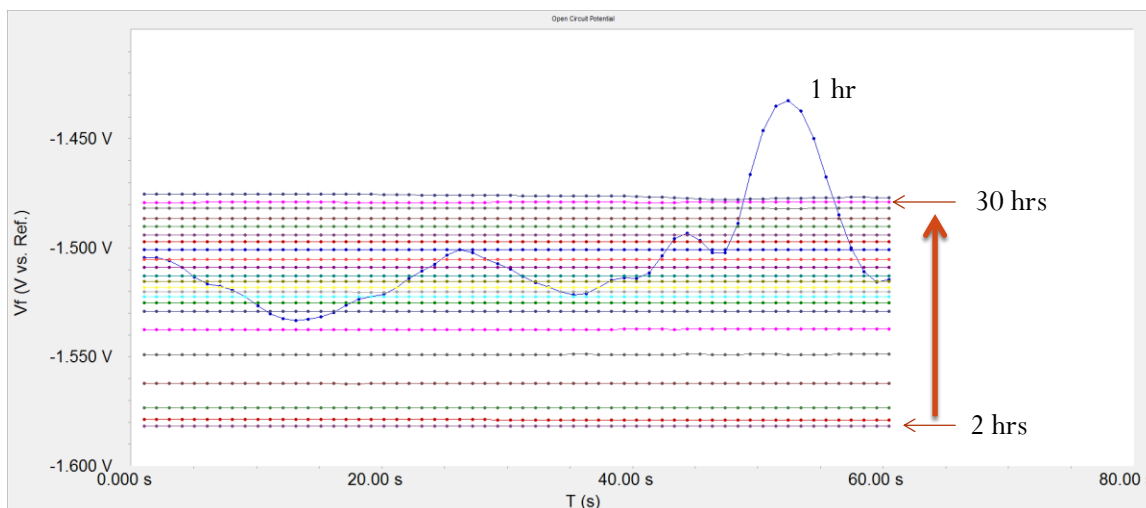


Figure 8. EIS for ZE41 with DOW17: Open circuit potential (vs. SCE).

At the end of EIS tests, once the corrosion products were washed from the surface, there were several areas of exposed metal clearly visible for both HAE and DOW17 primers, indicating complete degradation and removal of the primers during constant immersion in 1% NaCl.

EIS spectra for the uncoated TAG8200 (Sample 1) are shown in Figures 9 and 10. The TAG8200 EIS experiment contains the same number of EIS cycles as for HAE and DOW17. However, due to the active nature of Mg alloy ZE41, which manifests itself as the decrease of $|Z|$ in the low-frequency region of the EIS spectra for HAE and DOW17, the running time for one EIS cycle of TAG8200 was reduced by adjusting the lower frequency limit from 0.01 Hz to 0.1 Hz. Therefore, in the case of TAG8200, each cycle was completed in a slightly shorter amount of time due to the fewer frequency points in each EIS spectrum, thus reducing the total run time from 30 hrs to 25.5 hrs. However, it should be noted, that for the uncoated DOW17 and HAE, the discussion of EIS results would still be valid had the experiment been conducted for only 24

hrs, due to the fact that between 24 and 30 hrs of immersion only further accumulation of Mg corrosion products takes place—a process that is no longer affected by the failed coatings.

For the non-topcoated TAG8200, the low-frequency impedance modulus, $|Z_{lf}|$, indicative of the overall barrier properties of a coating system, decreased with time, as seen in Figure 9. The decrease was not gradual; in fact, $|Z_{lf}|$ increased initially, albeit slightly. Figure 10 shows the Nyquist diagram for TAG8200 – an alternative representation of EIS data in a complex impedance domain.

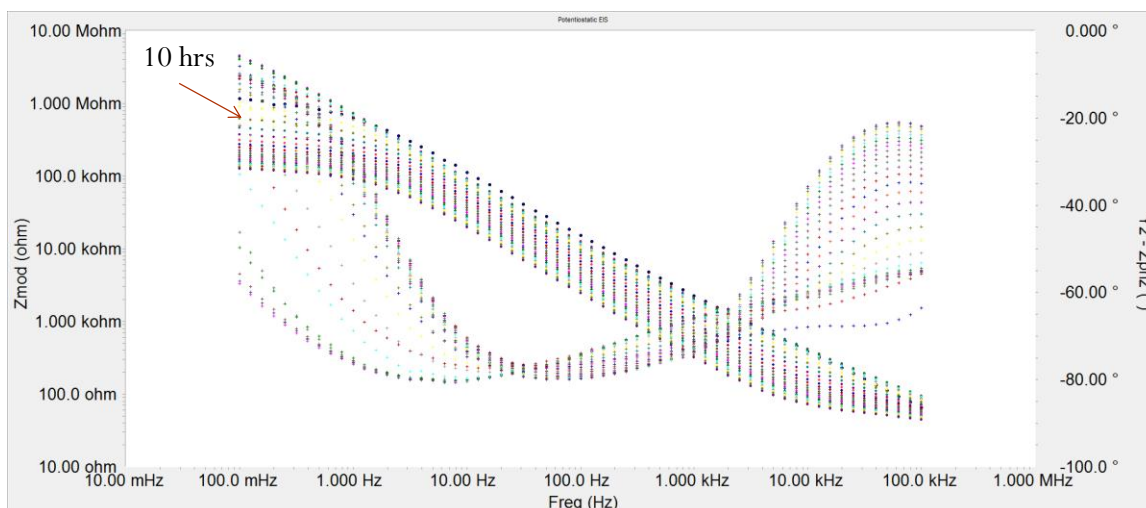


Figure 9. EIS for ZE41 with TAG8200 (Bode plot, $|Z|$ and Phase angle vs. log frequency).

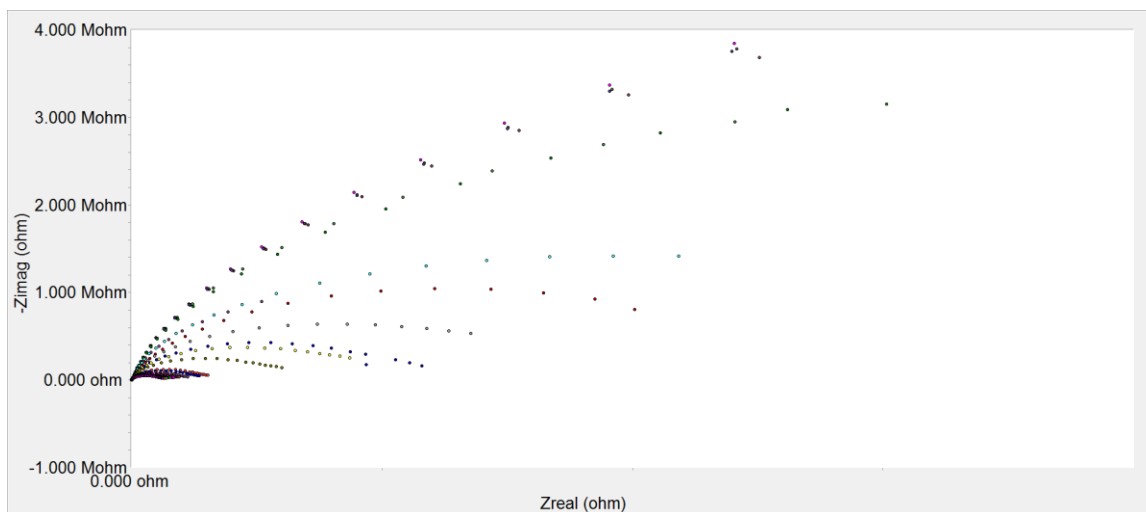


Figure 10. EIS for ZE41 with TAG8200 (Nyquist plot, $-Z_{Imag}$ vs. Z_{Real}).

The Nyquist plots suggest that the initial increase of $|Z_{lf}|$ is mainly brought about through the increase of the imaginary (capacitive) component of impedance modulus. Over the first 3-4 hours, the real (resistive) component increased from ~ 1 to $2.5 \text{ M}\Omega\text{-cm}^2$, whereas the imaginary component jumped from ~ 0.1 to almost $4 \text{ M}\Omega\text{-cm}^2$. The imaginary component is associated with the coating's capacitance. The increase in capacitance in this case is brought about by the water ingress into the film. As the electrolyte reaches the surface, corrosion products account for the

short-lived rise of the resistive (real) component. However, as the film starts to disintegrate and provides easier access of electrolyte to the surface, both resistive and capacitive components decrease, resulting in the lower $|Z_{lf}|$.

After 10 hrs in 1% NaCl, the value for $|Z_{lf}|$ decreased to the $10^6 \Omega\text{-cm}^2$ threshold, below which a coating is considered “poor” in terms of corrosion protection. However, the $10^6 \Omega\text{-cm}^2$ value applies to full coating systems. Therefore, if a topcoat is to be applied over the TAG8200, then the values below 10^6 are still meaningful for the purpose of ranking of various surface modification techniques.

At the end of the EIS test, once the corrosion products were removed from the surface, no areas of exposed metal were observed for TAG8200.

Overall, EIS results have demonstrated that TAG8200 is more resistant to corrosion on Mg alloys ZE41 than HAE and DOW17 anodization layers. For the non-topcoated systems, after a prolonged exposure to 1% NaCl, TAG8200 maintain impedance modulus values that were 10 times higher than those for HAE and DOW17. Additionally, no areas of exposed metal were visible on the surface of ZE41 coated with TAG8200 at the end of the constant immersion EIS experiment. Conversely, non-topcoated HAE and DOW17 were found to contain several large areas of severely corroded Mg substrate at the end of EIS test. While the degradation of non-topcoated TAG8200 scales linearly with immersion time, non-topcoated HAE and DOW17 lose most of its barrier potential within the first few hours of immersion in 1% NaCl. These findings indicate superior barrier properties of TAG8200 on ZE41 compared to HAE and DOW17.

1.3 Potentiodynamic scan

Potentiodynamic Scan (PDS) is a qualitative electrochemical technique used to assess the passivation tendencies of a metal. A typical potentiodynamic curve of the anodic (metal oxidation) reaction is shown in Figure 11. The potential is scanned in the direction of Point 1 \rightarrow Point 2. Point A on the curve represents the corrosion potential, E_{corr} , that is close to the open circuit potential of the system, E_{oc} . E_{oc} is the difference of electrochemical potentials between the working and reference electrode in the absence of current. E_{oc} is measured prior to electrochemical experiments to establish the electrochemical state of the system and the stability of its potential over time. In a stable system, E_{oc} will be close to E_{corr} , but there is typically a small difference on the order of a few millivolt present for almost any real system.

Region B represents the active region, or the anodic corrosion reaction—dissolution of the metal. For some systems there exists a passivation potential, depicted by point C, when the current decreases due to the formation of a passive layer. Point E is called the passivation region, a range of potential where the system is passivated, marked by a sharp decrease in corrosion current. Point F is the pitting potential, a value above which corrosion current increases (Region G) due to the pitting phenomena. Pitting is defined as localized corrosion that leads to the formation of small holes in the metal. Typically, a corrosion electrolyte containing chloride will attack the protective oxide or the passivation layer, thus accelerating corrosion of the metal.

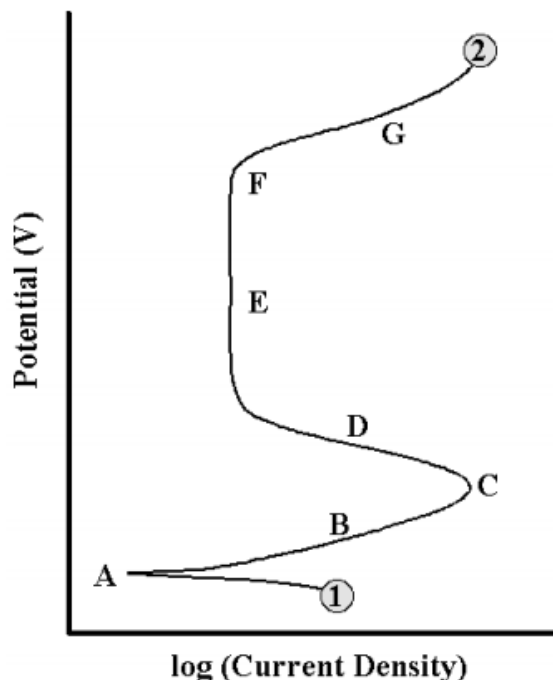


Figure 11. A typical potentiodynamic curve.

Notice that for many systems, Regions D and E may not be observed due to the lack of passivation. In that case, Region B continues into Region G without the passivation region.

Figure 12 depicts potentiodynamic (PDS) curves for all three types of surface modifications, namely TAG8200 (blue), DOW17 (green), and HAE (red). The DOW17 records a higher corrosion potential than HAE, which is consistent with the OCP values from EIS results. Higher OCP value is indicative of a somewhat higher initial protection afforded by this coating (relative to HAE). The small shoulder in the PDS records of DOW17 at 100 nA corresponds to a potential range of 70 mV. This is the area of passivation brought about by the brief formation and dissolution of corrosion products on the surface of the film. However, this passivation is very insignificant and should in no way be viewed as the evidence that DOW17 is the optimal coating for corrosion protection of Mg alloys. Both HAE and DOW17, as deposited, fail to protect Mg alloy from corrosion even in the presence of a mild electrolyte, such as 1% NaCl. Higher OCP for DOW17, -1.5 V vs. -1.7V for HAE, and the presence of passivation classifies DOW17 as providing marginally better protection for ZE41. However, the high corrosion current, on the order of microamps, makes both HAE and DOW17 poor choices for protection of Mg alloys.

For the TAG8200 sample, the corrosion potential is recorded at -1.42 V (vs. SCE), which is 260 mV above that for DOW17. Additionally, TAG8200 has a higher breakdown/pitting potential than the DOW17. The higher this potential, the more electrochemical stress can the film withstand. At -1.11 V (vs. SCE), E_{pit} for TAG8200 is 310 mV above its corrosion potential ($E_{corr} = -1.42$ V) and, thus, indicates a more protective system than HAE or DOW17.

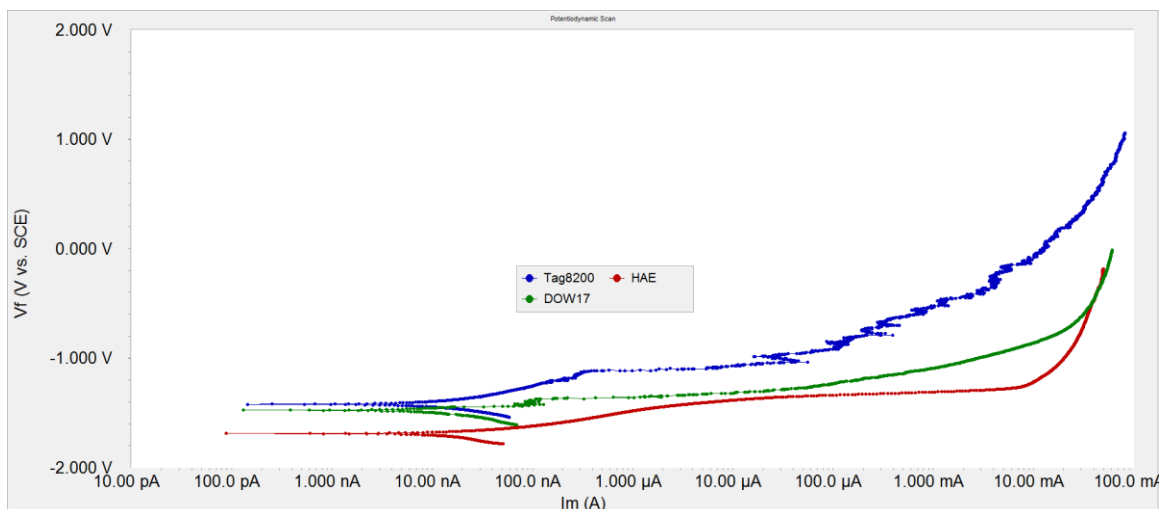


Figure 12. PDS for ZE41 with TAG8200, DOW17, and HAE.

In addition to the presence of a well-defined pitting potential, E_{pit} , TAG8200 records a smaller corrosion current on the order of tens of nanoamps, which is several orders of magnitude lower than that for HAE and DOW17. A significantly lower corrosion current of TAG8200 makes it a better candidate for corrosion protection of Mg alloys.

In conclusion, the presence of a well-defined pitting potential for the non-topcoated TAG8200 and its lower corrosion current, as determined from the potentiodynamic scan experiments, indicate that TAG8200 can withstand higher electrochemical stress than DOW17 and HAE. Corrosion protective properties of the three non-topcoated systems can be ranked in the following order of decreasing protection:

TAG8200 > **DOW17** > **HAE**.

2. Scanning electron microscopy of TAG8200 on ZE41

The TAG8200 sample was analyzed by scanning electron microscopy (SEM) and energy dispersive X-ray spectroscopy (EDS). The sample received from Tag was beveled on all side, which complicated Ar-ion milling. Additionally, the sample had to be coated with a layer of carbon and attached to Cu tape in order to dissipate heat and prevent charging of the surface.

Figures 13-15 show backscatter SEM micrographs at various magnification levels. The film thickness estimates from Figure 13 range between 8.5 – 9.2 μm . A backscatter detector registers stronger signals from heavier atom that scatter more radiation, resulting in brighter areas. Therefore, the white areas in Figures 13 and 14 are not voids, but rather heavier element present in the alloy. According to the EDS analysis, the white areas, identified as Area 5 in Figure 26, represent zinc. Tables 8 and 9 show weight % and atomic % of the EDS areas. Area 5 has the highest concentration of zinc.

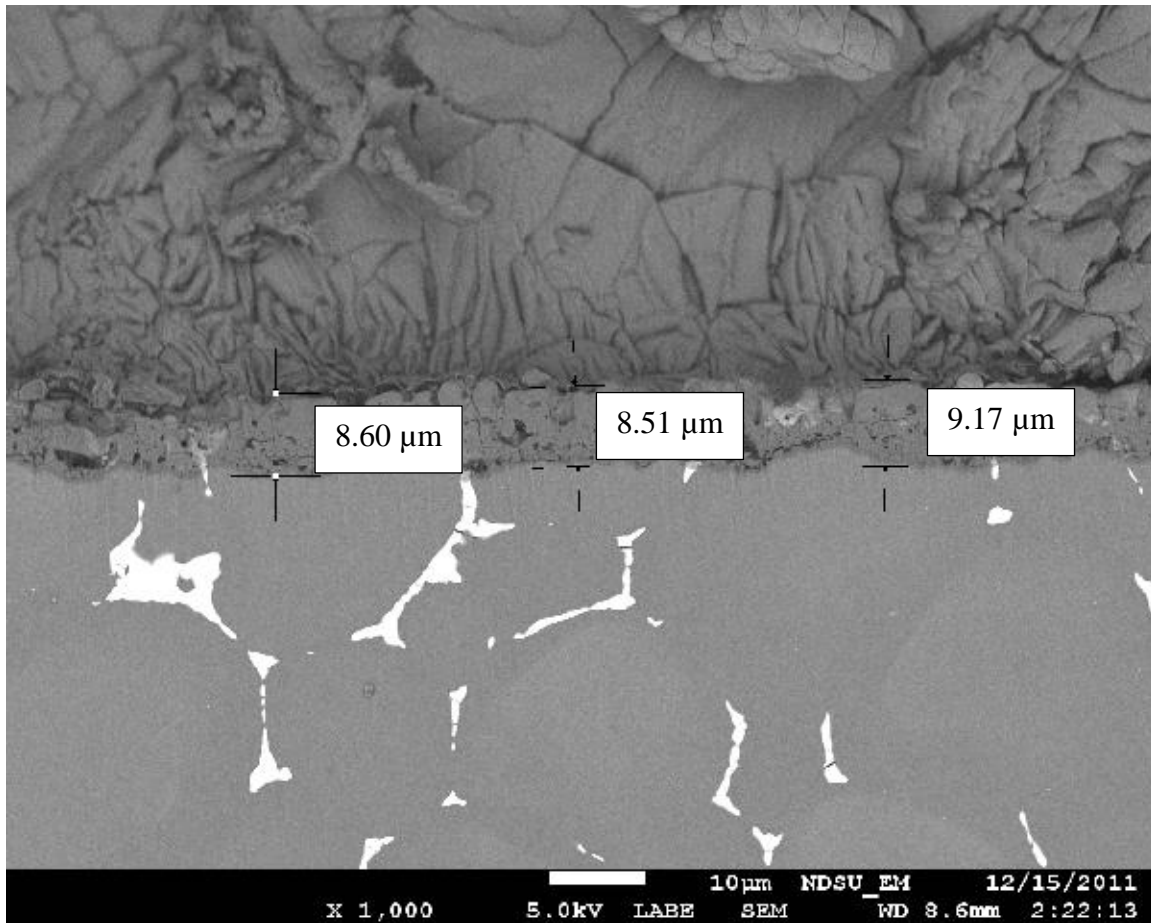


Figure 13. SEM micrograph of TAG8200 on ZE41.

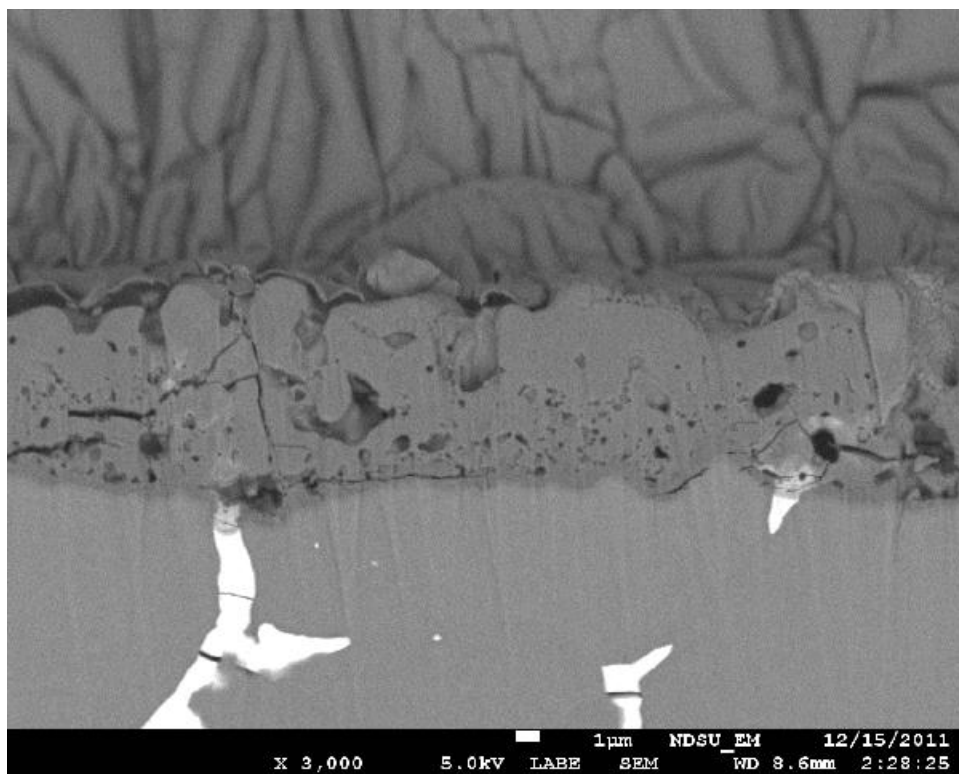


Figure 14. SEM of TAG8200 on ZE41 at x3000 magnification.

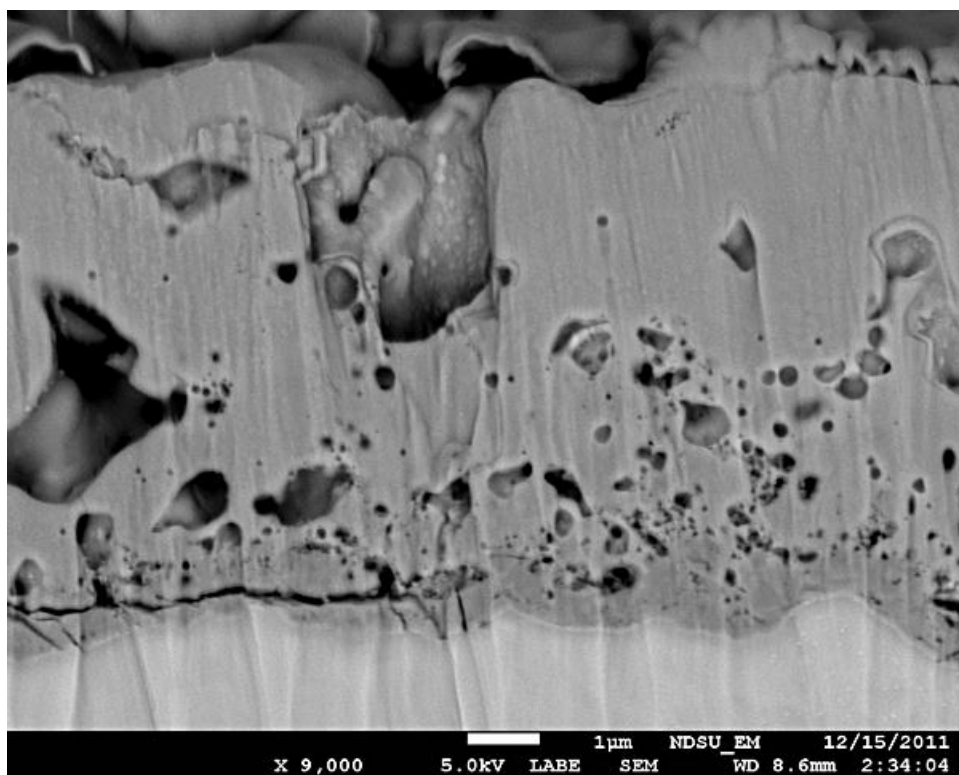


Figure 15. SEM of TAG8200 on ZE41 at x9000 magnification.

Upon closer examination of the TAG8200 film (Figures 14 and 15), two layers of variable lightness can be observed. The thickness of the bottom, darker layer is on the order of 1/10 of the thickness of the upper, lighter layer; and the bottom layer appears to be more porous than the top layer.

Figures 17-21 and Tables 8 and 9 present the results of the EDS analysis of the five areas identified in Figure 16. The amount of oxygen decreases as the location of the areas moves away from the surface of the film towards the interface and into the bulk metal. The amount of fluorine increases sharply between the topmost Area 1, within the light layer of the film, at 3.4 wt% / 3.55 at% to 24.3 wt% / 25.3 at% for Area 3 in the darker layer of the film.

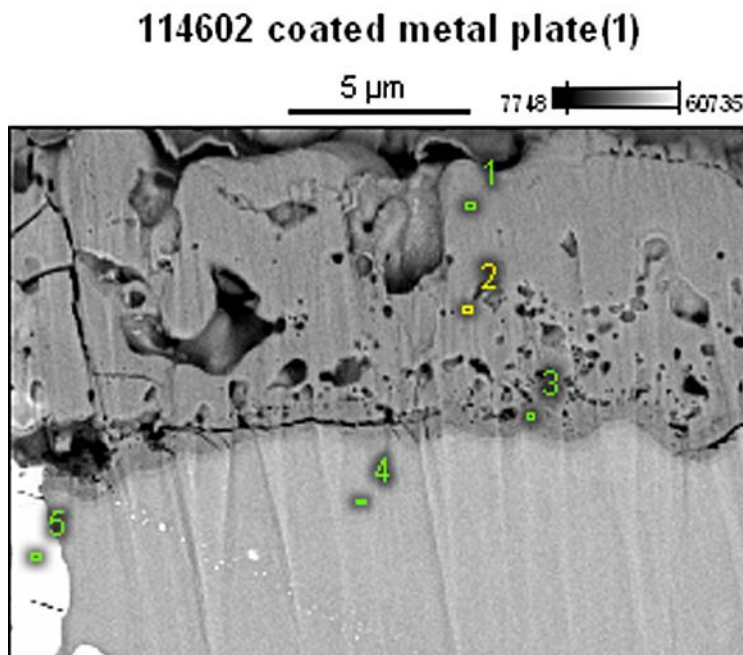


Figure 16. TAG8200 on ZE41, cross-sectional EDS areas.
Accelerating Voltage: 5.0 kV, Magnification: x6000.

Contrary to the trend for the amount of fluorine, the amount of silicon decreases as the EDS detector moves from the top area of the film towards the interface, from 17.2 wt% / 12.2 at% near the surface to 6.2 wt% / 4.3 at% near the interface. The diagram in Figure 22 shows the trends for atomic and weight percent compositions for oxygen, fluorine, and silicon. The oxygen is present in all 5 areas analyzed by the EDS due to the presence of natural oxides of Mg and alloying elements, denoted by the blue arrow pointing the direction of. However, silicon is introduced into the system during the film application process, and fluorine - pre-treatment process and it is present in the electrolyte. Therefore, silicon and fluorine can only be detected in the film itself, in areas 1-3.

Traces amounts of fluorine were detected in Area 5. However, the peak assignment for Area 5 was complicated due to the low amounts of the alloying elements. It is common for the analysis software to mislabel some elements in EDS micrographs due to the close proximity of their energy peaks and their low atomic amounts. Some prior knowledge of the system is required in order to make unambiguous peak assignment. For the bulk ZE41, what the software identified as

a fluorine peak may, in fact, be a peak corresponding to one of the alloying elements. At the same time, small amount of F could have been introduced into the film during the pre-treatment process. The exact assignment of the small peak in Area 5 in Figure 21 (30 wt% Mg and 58% wt% Zn) does not detract from the EDS analysis of the TAG8200 film.

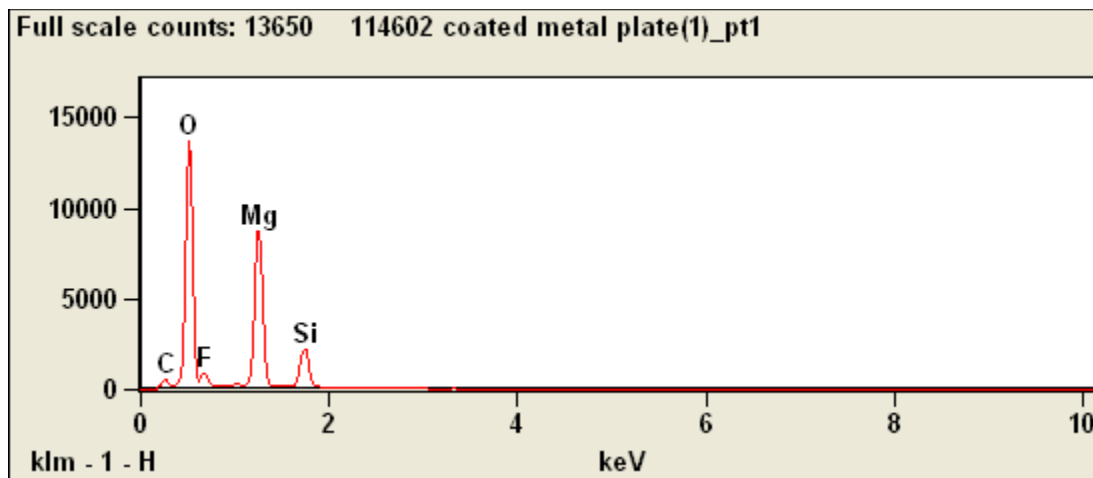


Figure 17. EDS peaks for cross-sectional view Area 1 of TAG8200 on ZE41.

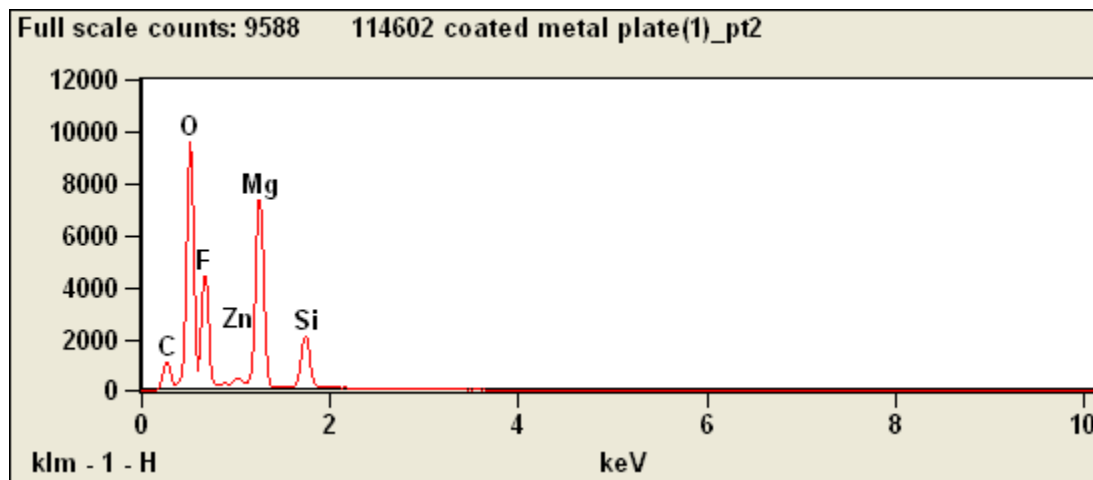


Figure 18. EDS peaks for cross-sectional view Area 2 of TAG8200 on ZE41.

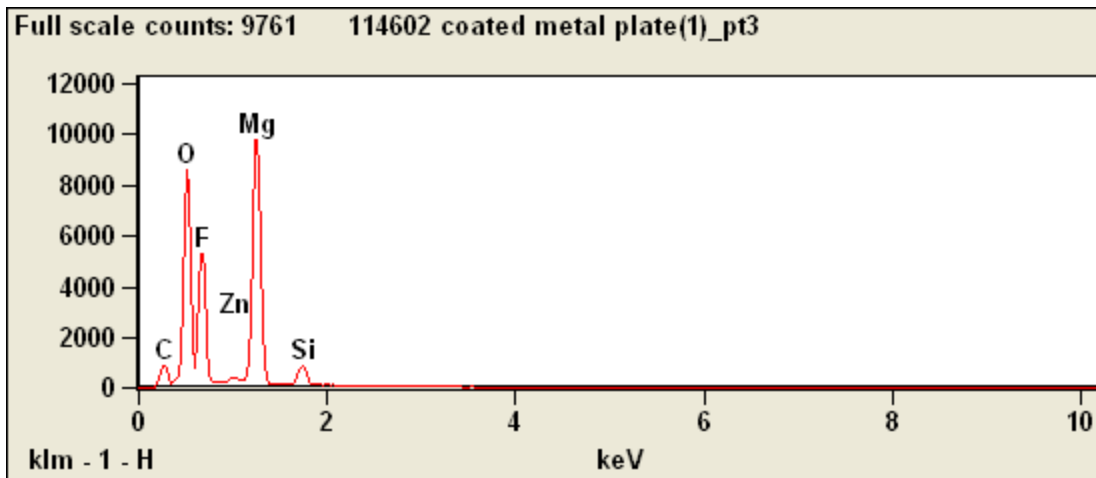


Figure 19. EDS peaks for cross-sectional view Area 3 of TAG8200 on ZE41.

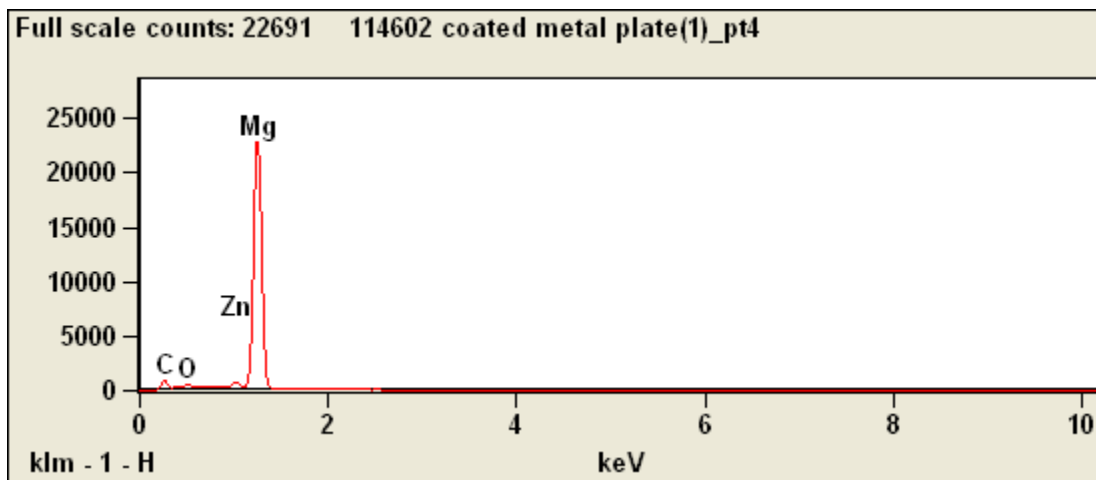


Figure 20. EDS peaks for cross-sectional view Area 4 of TAG8200 on ZE41.

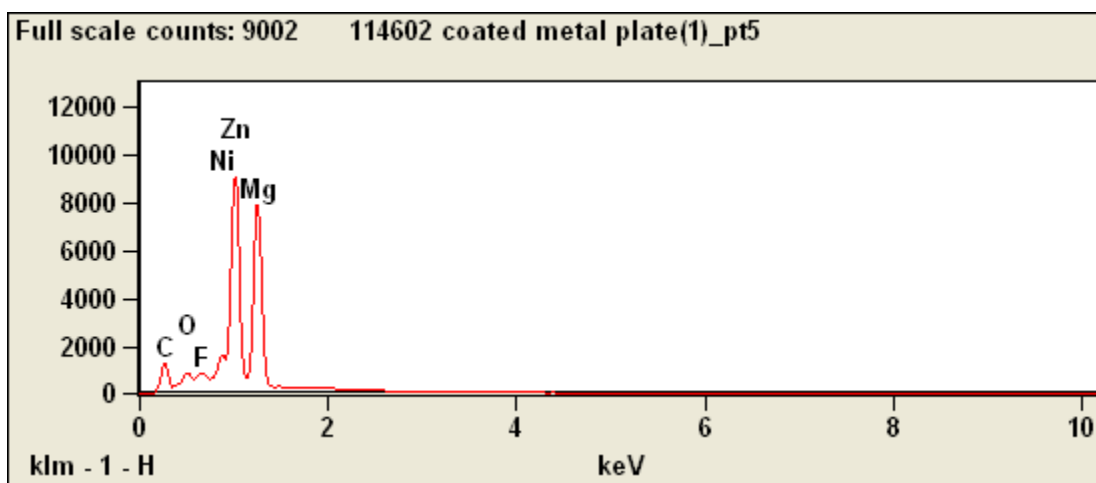


Figure 21. EDS peaks for cross-sectional view Area 5 of TAG8200 on ZE41.

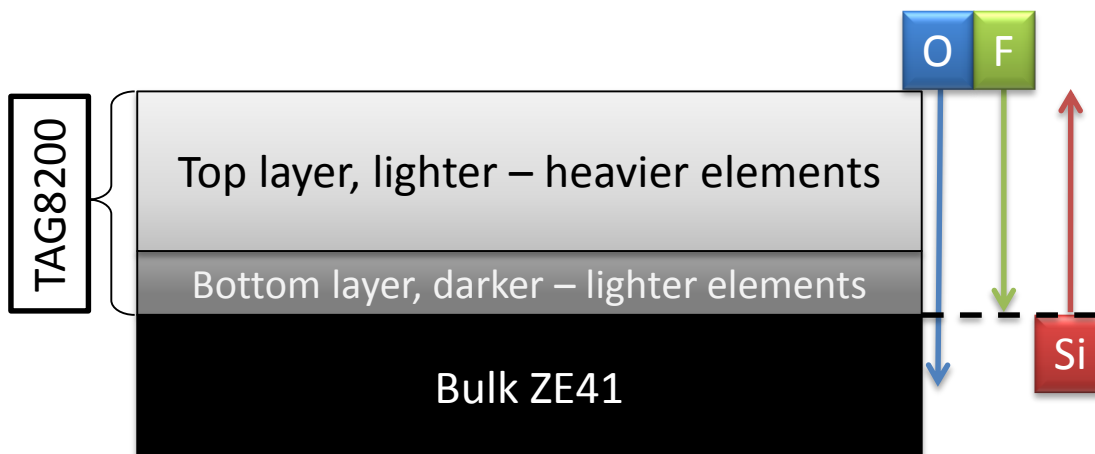


Figure 22. Schematic representation of cross-sectional EDS analysis areas.

Table 8. EDS of TAG8200 on ZE41, Weight %.

	<i>C-K</i>	<i>O-K</i>	<i>F-K</i>	<i>Mg-K</i>	<i>Si-K</i>	<i>Ni-L</i>	<i>Zn-L</i>
<i>114602 coated metal plate(1)_pt1</i>	1.65	43.04	3.40	34.68	17.24		
<i>114602 coated metal plate(1)_pt2</i>	5.89	28.97	20.06	28.75	15.30		1.03
<i>114602 coated metal plate(1)_pt3</i>	4.61	25.31	24.34	38.71	6.17		0.87
<i>114602 coated metal plate(1)_pt4</i>	7.16	1.35		89.45			2.05
<i>114602 coated metal plate(1)_pt5</i>	7.51	1.57	1.10	30.27		1.54	58.02

Table 9. EDS of TAG8200 on ZE41, Atomic %.

	<i>C-K</i>	<i>O-K</i>	<i>F-K</i>	<i>Mg-K</i>	<i>Si-K</i>	<i>Ni-L</i>	<i>Zn-L</i>
<i>114602 coated metal plate(1)_pt1</i>	2.72	53.30	3.55	28.27	12.16		
<i>114602 coated metal plate(1)_pt2</i>	9.61	35.50	20.70	23.20	10.68		0.31
<i>114602 coated metal plate(1)_pt3</i>	7.56	31.19	25.26	31.40	4.33		0.26
<i>114602 coated metal plate(1)_pt4</i>	13.57	1.91		83.80			0.71
<i>114602 coated metal plate(1)_pt5</i>	21.27	3.34	1.96	42.36		0.89	30.18

Figures 23 and 24 depict the top view of TAG8200 taken in the secondary electron imaging (SEI) mode of SEM at various magnifications. The SEI mode provides information on the topography of the surface. Unlike the backscatter electron emission, the light and dark areas in SEI micrograph and topographical in nature and do not represent heavier or lighter elements.

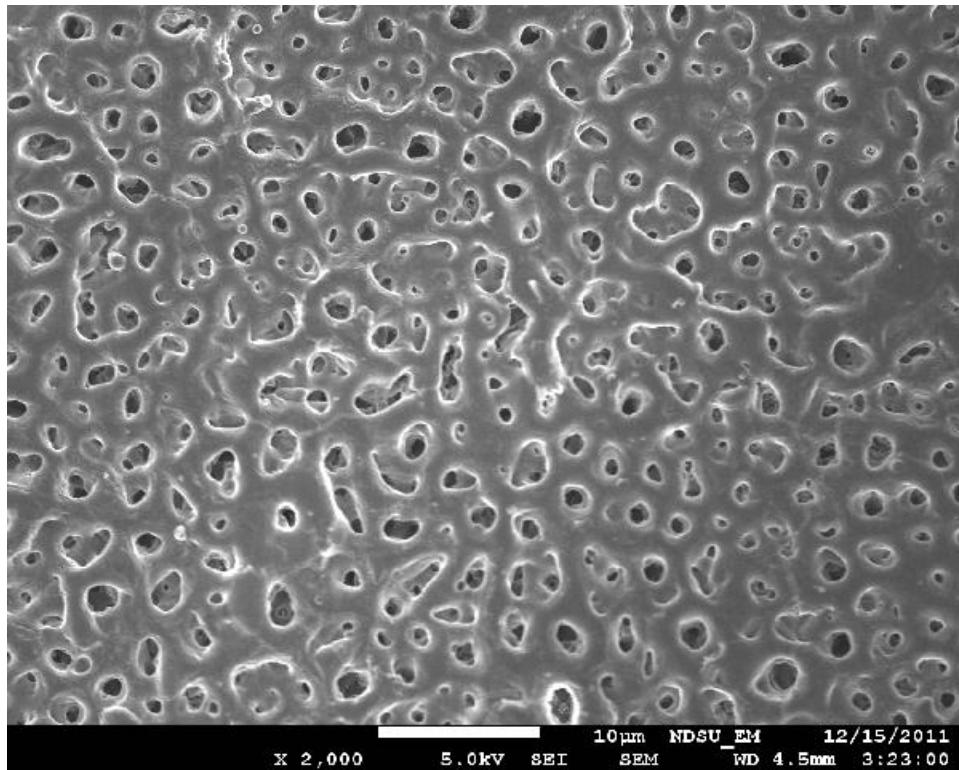


Figure 23. SEM of TAG8200 on ZE41, secondary electron emission.
Top View at x2000 magnification.

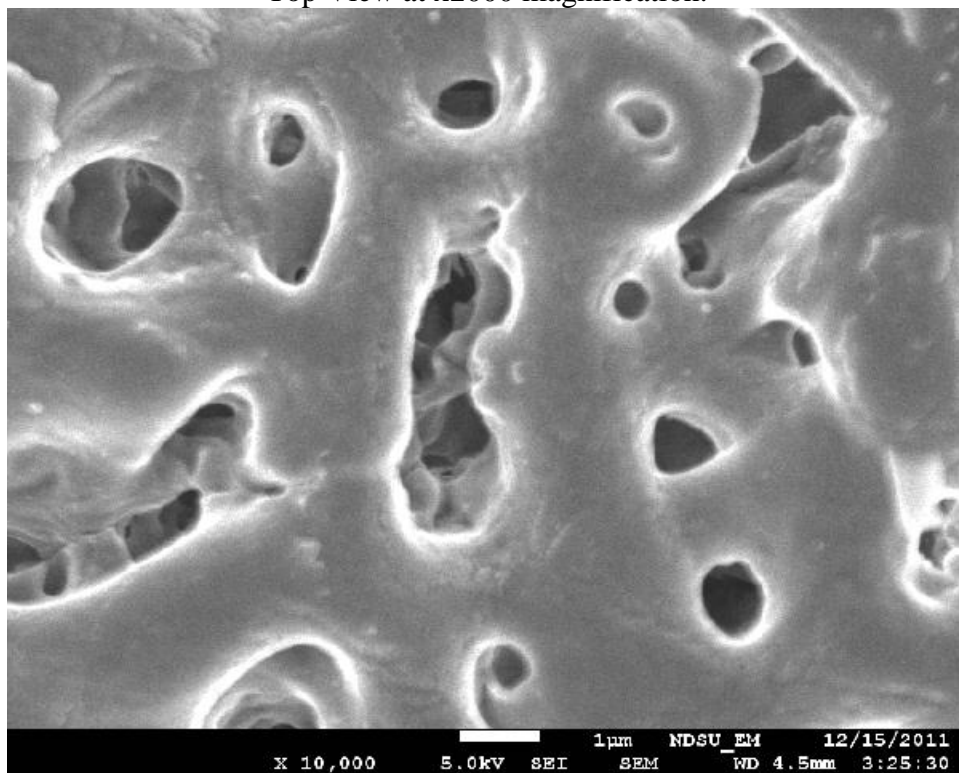


Figure 24. SEM of TAG8200 on ZE41, secondary electron emission.
Top View at x10,000 magnification.

It can be concluded from the SEI micrographs that the TAG8200 film is very uniform in nature. There is some cratering on the surface, most likely do to gas escaping the surface during deposition. Figures 23 and 24 allow visual estimation of the size of the craters, which range between submicron to 0.5 μm for round shapes, and between 3-4 μm for irregular-shaped pores at their longest dimension.

To complement the SEM view of the top surface of TAG8200, backscatter SEM imaging was also performed at magnification of x6000 and is shown in Figure 25. The voids appear darker in backscatter images, due to the material being composed of heavier, denser matter which scatters electrons more effectively. However, the shade of the material is uniform throughout the surface indicating uniform coverage of the substrate. This fact is confirmed by the EDS analysis of 3 areas located on the surface of the film.

Figure 26 shows the mapping of the EDS areas on the surface of TAG8200, while Figures 27-29 show peak assignments for the individual areas. From Tables 10 and 11, it can be observed that the amounts of oxygen and silicon are consistent across the entire surface of the film, with only a few percent variations.

Due to the areas analyzed in the top view EDS being above all 5 areas of the cross-sectional EDS, the atomic concentrations and weight-percent values given in Tables 10 and 11 must be compared to the Area 1 values in Tables 8 and 9. Comparison of atomic and weight percent values demonstrates that the amounts of silicone and fluorine on the surface of TAG8200 are consistent with the cross-sectional EDS.

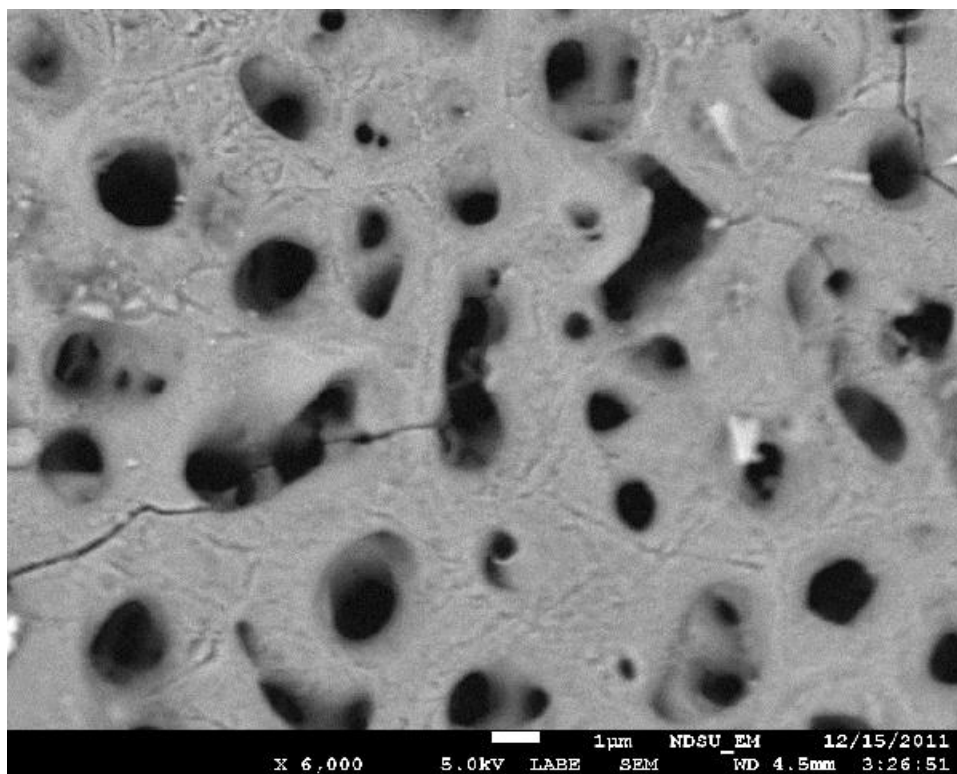


Figure 25. SEM of TAG8200 on ZE41, backscatter electron emission.
Top View at x6000 magnification.

114602 surface of coated metal plate(1)

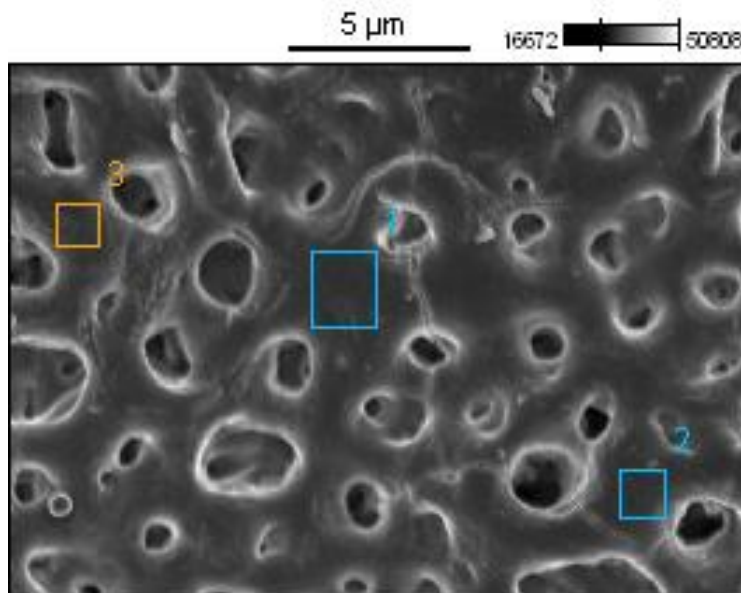


Figure 26. TAG8200 on ZE41, top view EDS areas.
Accelerating Voltage: 5.0 kV, Magnification: x6000.

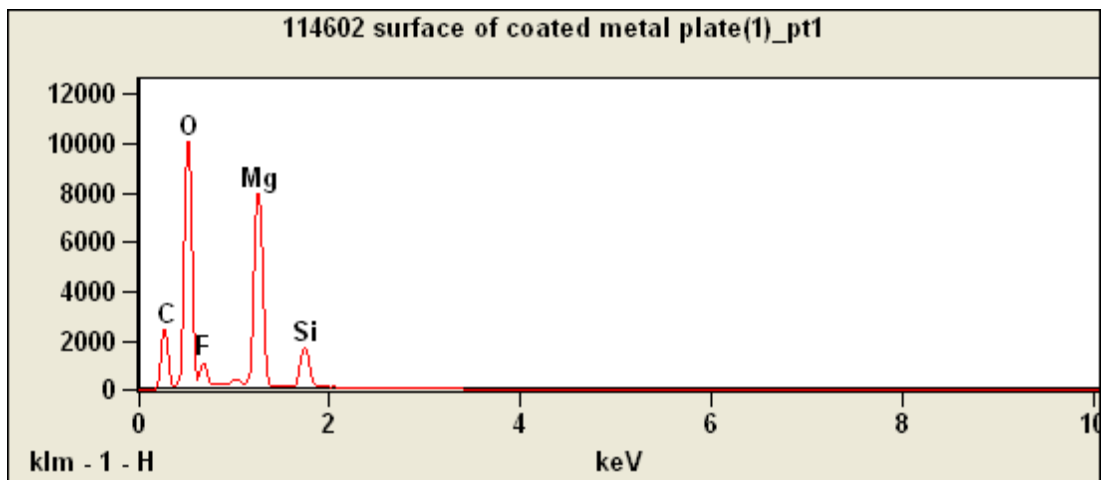


Figure 27. EDS peaks for top view Area 1 of TAG8200 on ZE41.

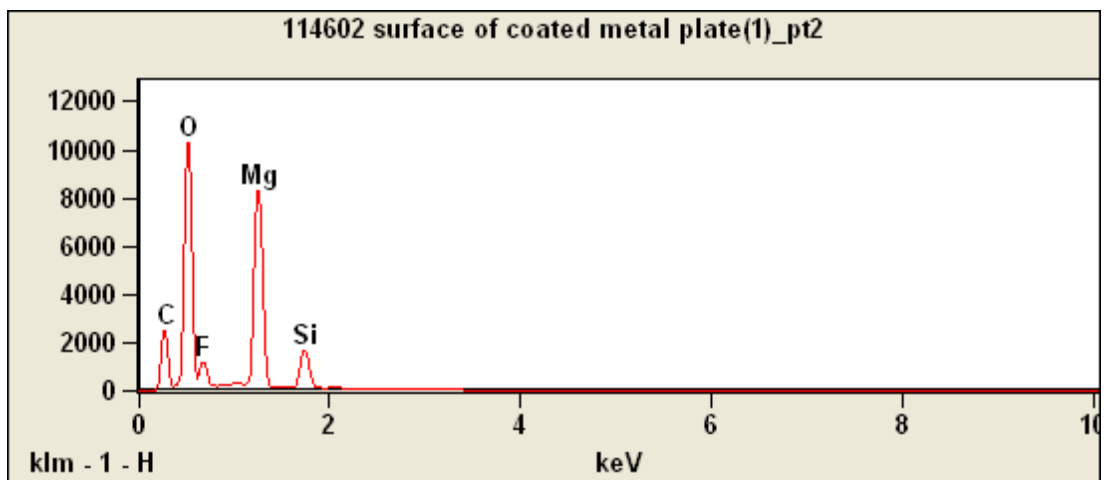


Figure 28. EDS peaks for top view Area 2 of TAG8200 on ZE41.

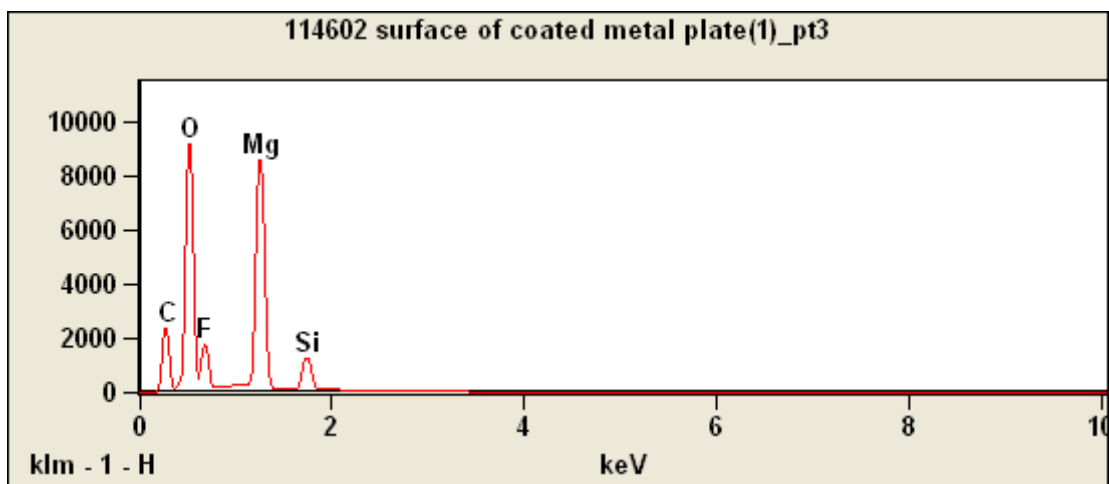


Figure 29. EDS peaks for top view Area 3 of TAG8200 on ZE41.

Table 10. EDS of TAG8200 on ZE41, Weight %.

	<i>C-K</i>	<i>O-K</i>	<i>F-K</i>	<i>Mg-K</i>	<i>Si-K</i>
<i>114602 surface of coated metal plate(1)_pt1</i>	15.57	34.81	4.98	32.00	12.64
<i>114602 surface of coated metal plate(1)_pt2</i>	15.33	34.19	5.89	32.19	12.39
<i>114602 surface of coated metal plate(1)_pt3</i>	15.11	31.52	8.80	35.22	9.35

Table 11. EDS of TAG8200 on ZE41, Atomic %.

	<i>C-K</i>	<i>O-K</i>	<i>F-K</i>	<i>Mg-K</i>	<i>Si-K</i>
<i>114602 surface of coated metal plate(1)_pt1</i>	23.57	39.55	4.77	23.93	8.18
<i>114602 surface of coated metal plate(1)_pt2</i>	23.26	38.93	5.65	24.13	8.04
<i>114602 surface of coated metal plate(1)_pt3</i>	22.98	36.00	8.46	26.48	6.08

3. Neutral salt fog corrosion test (B117 protocol)

Coated ZE41 helicopter gear parts were received from TAG and dissected at Mid-America Aviation.¹ The areas of the cuts were masked off by an epoxy coating to avoid rapid disintegration of magnesium alloy inside the corrosion test chamber.

Thirty 3"x 5" ZE41 panels coated with six different types of coatings in quintuplicates were received from TAG. For the purpose of this discussion, the edge of the panel near a hole is considered a top. Each panel had a cadmium-plated steel lock ring installed stud in the upper half, and a cadmium-plated steel stud was inserted into the lock ring. The codes for the coated ZE41 panels are shown in Table 12.

Table 12. Sample matrix for ZE41 panels with Cd-plated steel studs.

Panels Received		Coating	Tested in B117	
ZM	1-5	DOW 17 Anodize	ZM4	ZM5
ZM	7, 8, 13-15	HAE Anodize	ZM14	ZM15
ZM	16-20	DOW7 Chromate	ZM19	ZM20
ZM	24-25	DOW 19 Chromate	ZM24	ZM25
ZM	26-29	Brush Tagnite	ZM28	ZM29
ZM	31-35	TAG8200	ZM34	ZM35

Two panels of each type of coating were placed in the neutral salt fog corrosion chamber (ASTM B117 protocol) alongside the dissected ZE41 helicopter gear parts. The codes for the panels subjected to the B117 salt spray are shown in Table 12 above. The area near the hole of the two DOW17 panels as well as the back of the two Brush Tagnite panels were masked by 3M 764 vinyl tape to prevent salt spray from attacking bare Mg alloy.

Figure 30 shows the inside of the B117 corrosion chamber prior to exposure. B117 is an ASTM standard for conducting salt fog testing of coating for corrosion protection. The chamber is equipped with sprayers that continuously introduce 5% NaCl solution into the space at 35°C. The chamber is designed so that any point in space receives the same amount of salt spray per unit time. The B117 test was conducted for 16 hours, and Figure 31 shows the salt spray chamber after the test. All 12 panels with Cd-plated steel studs showed signs of corrosion in the area around the base of the stud. This junction was affected to various degrees, ranging from severe to mild. Notice the drip lines leading from the joint to the bottom of the panels, and, in some cases, across the entire length of the panel, from top to bottom. These streak lines represent the corrosion products that were left behind as they were washed down by the salt spray. The streak lines are most noticeable on the two panels with chromates, namely DOW7 and DOW19.

Figures 30 through 41 show close-up images of the coated studded panels and ZE41 helicopter gear parts after 16 hours in B117 salt spray chamber.

¹ Mid-America Aviation, Inc., 159 8th Avenue NW, West Fargo, ND 58078

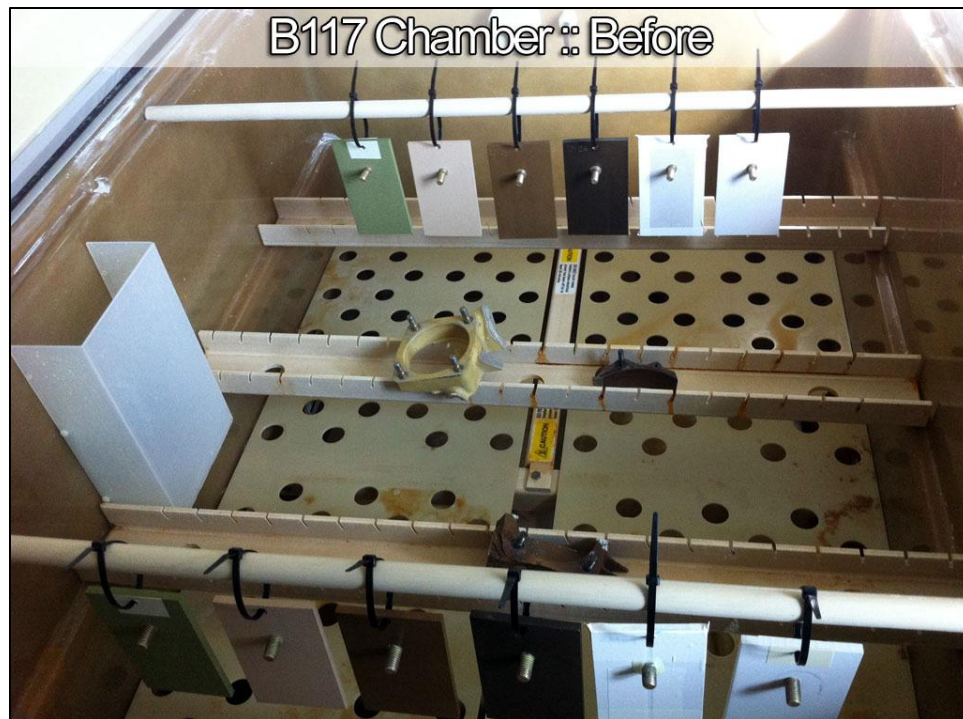


Figure 30. Inside the salt spray chamber before the B117 test.



Figure 31. Inside the salt spray chamber after the B117 test.

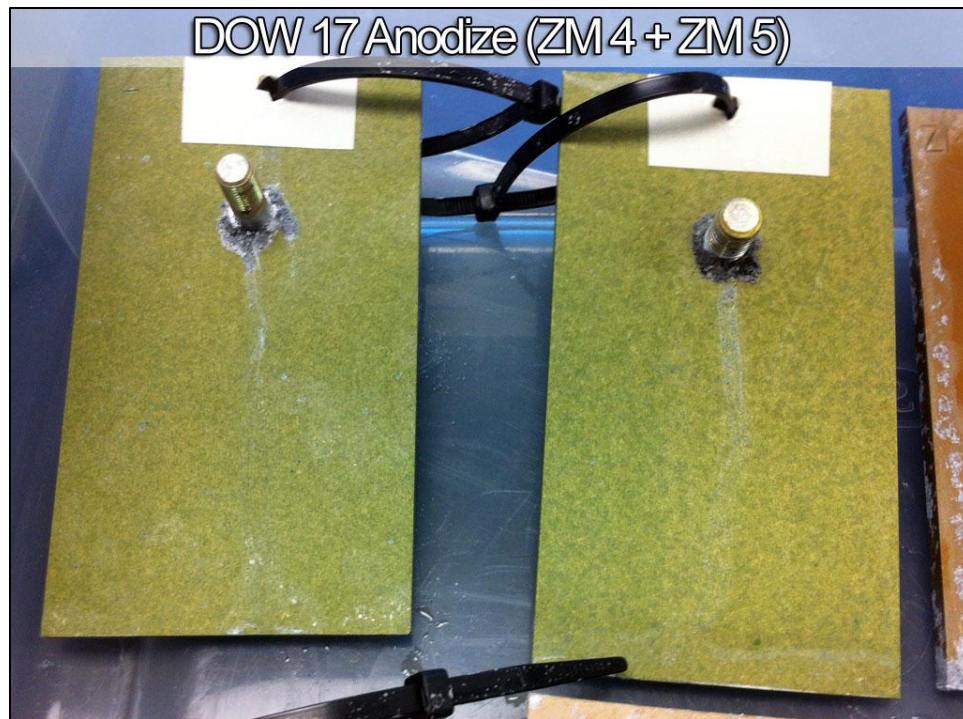


Figure 32. DOW17 Anodize panels after 16 hrs of B117 test.



Figure 33. HAE Anodize panels after 16 hrs of B117 test.



Figure 34. TAG8200 panels after 16 hrs of B117 test.



Figure 35. DOW7 Chromate panels after 16 hrs of B117 test.



Figure 36. DOW19 Chromate panels after 16 hrs of B117 test.

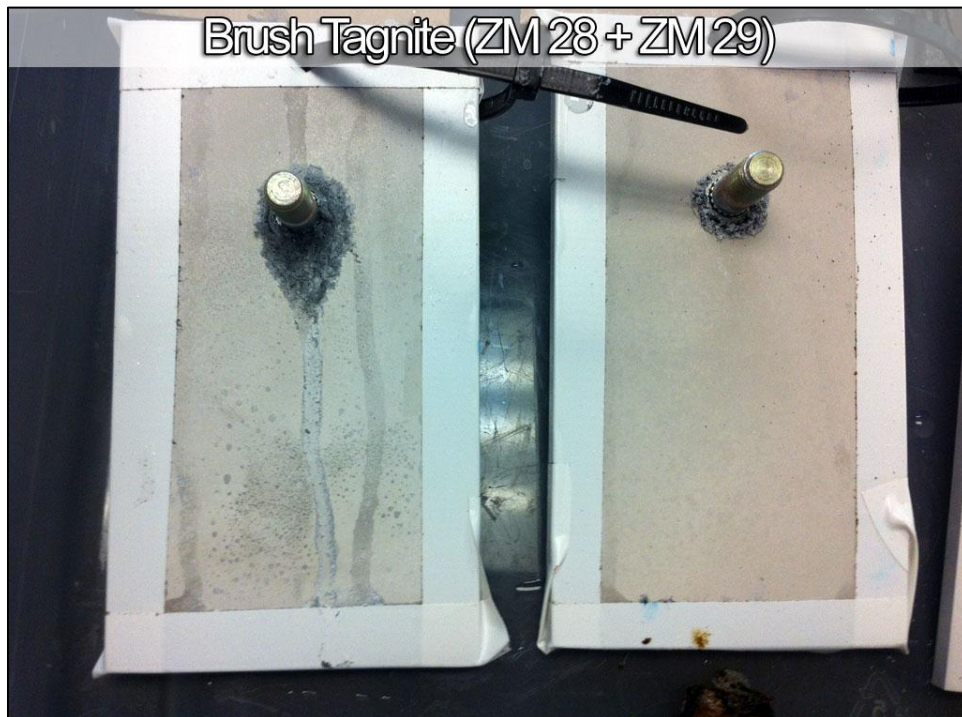


Figure 37. Brush Tagnite panels after 16 hrs of B117 test.

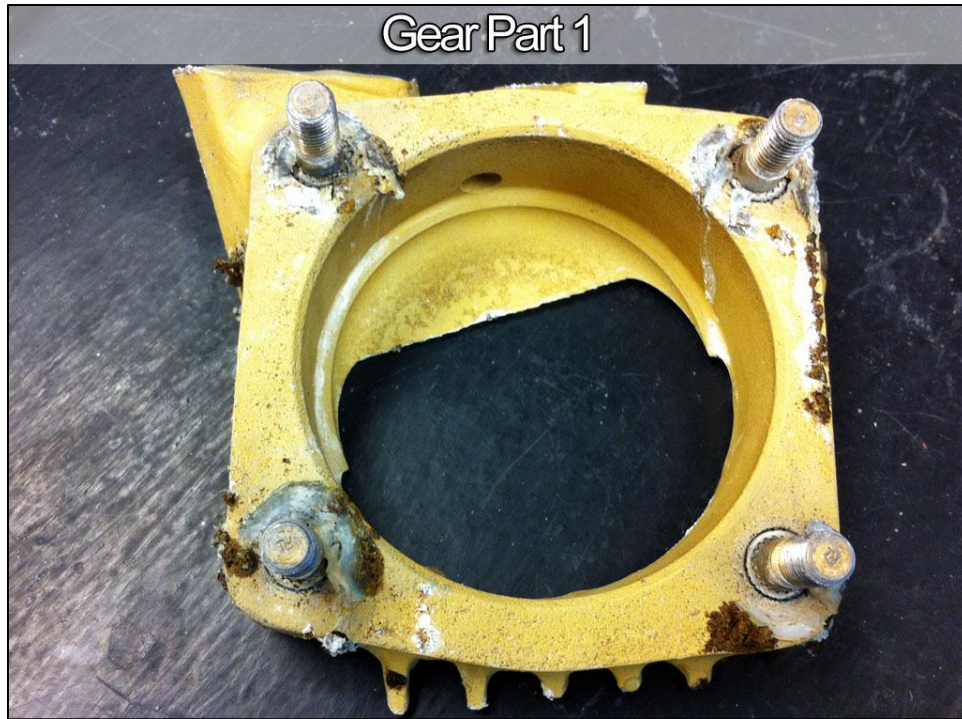


Figure 38. Helicopter gear Part 1 after 16 hrs of B117 test.



Figure 39. Helicopter gear Part 1 after 16 hrs of B117 test, alternate view.



Figure 40. Helicopter gear Part 2 after 16 hrs of B117 test.



Figure 41. Helicopter gear Part 3 after 16 hrs of B117 test.

4. Galvanic corrosion and potentiodynamic scan of six types of Mg alloy ZE41 surface treatment

4.1 Galvanic corrosion

Magnesium alloys are the most electrochemically active structural alloys, and their protection from corrosion is not a trivial matter. The presence of two or more dissimilar materials in direct physical and electrical contact (e.g. Cd-plated steel stud and Mg alloy ZE41) only exacerbates the corrosion problem through the phenomenon called galvanic corrosion. Galvanic Corrosion (GC) results from the direct contact of two dissimilar metals in a corrosive environment. The measure of GC is galvanic current, which is indicative of the kinetics of corrosion reactions. Typically, a lower coupling current between dissimilar metals is desired. Passivation of the metal brought about by surface treatments containing low-solubility chromates achieves lower coupling currents. The hexavalent chromates contained in the currently used surface treatments, while effective, are known carcinogens, and their use is slowly being phased out through environmentally-benign chromate replacement technologies. Correct interpretation of GC results, however, relies on many more factors beyond the absolute value of corrosion current.

Six types of surface treatment for Mg alloy ZE41 were evaluated in a galvanic corrosion experiment. As previously stated, all electrochemical experiments were performed in 1% NaCl solution with a saturated calomel electrode as a reference. Figure 42 shows corrosion potential and corrosion current records for the six scribed surface treatments identified in Table 12, taken over 72 hours of constant immersion in 1% NaCl.

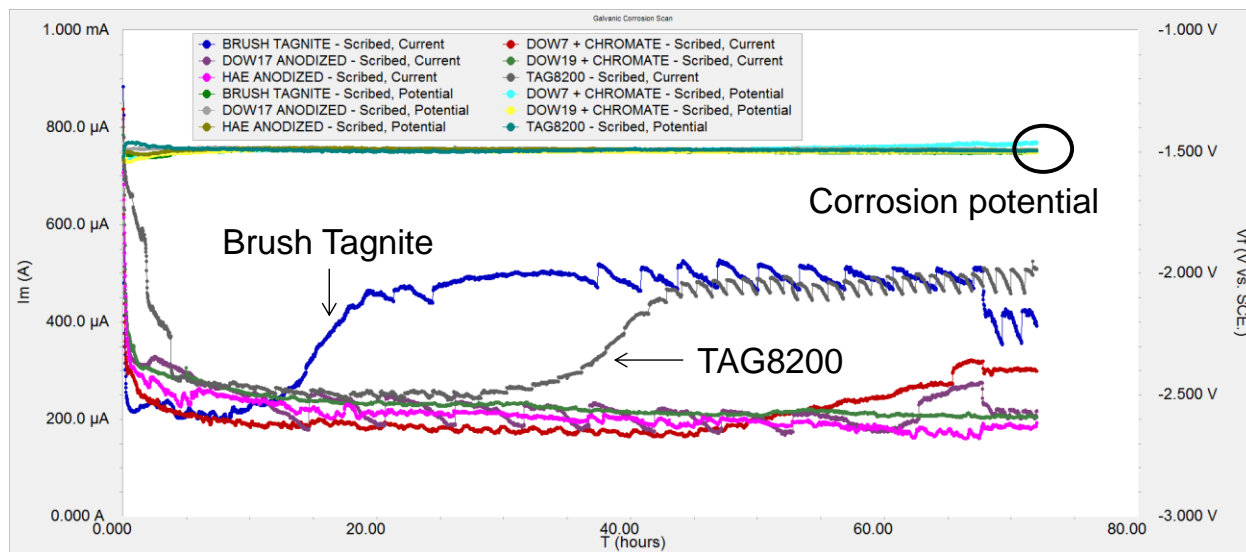


Figure 42. Galvanic corrosion for six types of surface treatments for Mg alloy ZE41.

The corrosion potential records (labeled Vf) in Figure 42 overlap due to fact that the value of E_{corr} is dependent on the underlying corrosion reaction of the metal or metals. During the first 30 mins to an hour, it is possible to differentiate the six surface treatments based on their E_{corr} values, as the presence of the coating, albeit very thin, would alter the corrosion potential. However, as soon as the electrolyte reaches the metal, E_{corr} is dictated by the electrochemical potential of the metal and is independent of the coating deposited on the substrate. Variations in

E_{corr} could further arise due to the formation of corrosion products, but since in the case of ZE41 they are soluble and are free to escape into the solution, corrosion potential is unaffected by the accumulation of corrosion products on the surface.

Galvanic current, I_{corr} (labeled I_m in Figure 42) stabilizes after several hours for all types of coatings. The decrease of the corrosion current is due to the formation of corrosion products in the scribe that impede the flow of charge in the cell. After 12 hrs, the corrosion current for Brush Tagnite increases, indicating that further corrosion of metal is taking place. Similarly, corrosion current for TAG8200 increases after 36 hours, and for DOW7 Chromate and DOW17 Anodize, the I_{corr} increase takes place at the 50-hr mark. While it appears that HAE Anodize and DOW19 Chromate have the lowest corrosion current at the end of the 72-hr GC experiment and thus could be considered best performers in a typical galvanic corrosion experiment, due to the highly reactive nature of Mg alloys, visual observation of the surfaces performed after the test provide additional information about the corrosion protection properties of the surface treatments.

The blue “GC Scribed” labels in Figure 43 correspond to the scribed areas subjected to the galvanic corrosion experiment depicted in Figure 42. We can observe that in the group of Brush Tagnite (labeled as TAG_{Br}) – DOW19 Chromate and DOW7 Chromate, corrosion is confined to the circular area that was exposed to the electrolyte. For DOW19 Chromate, corrosion extends slightly outside the exposure area, and in the case of DOW7, the area almost doubles in size compared to the test area of 1 cm² that was fixed with an electroplating tape. However, the area has an effect on the current density, and since the size of the cathode (Cd-plated steel) is fixed, in order to supply the same amount of electrons to carry out cathodic (reduction) reactions on the surface of the steel, higher currents will be generated from areas with less exposed metal. Higher current density further destroys the coating and the metal faster than lower current density that would be spread over a larger area.

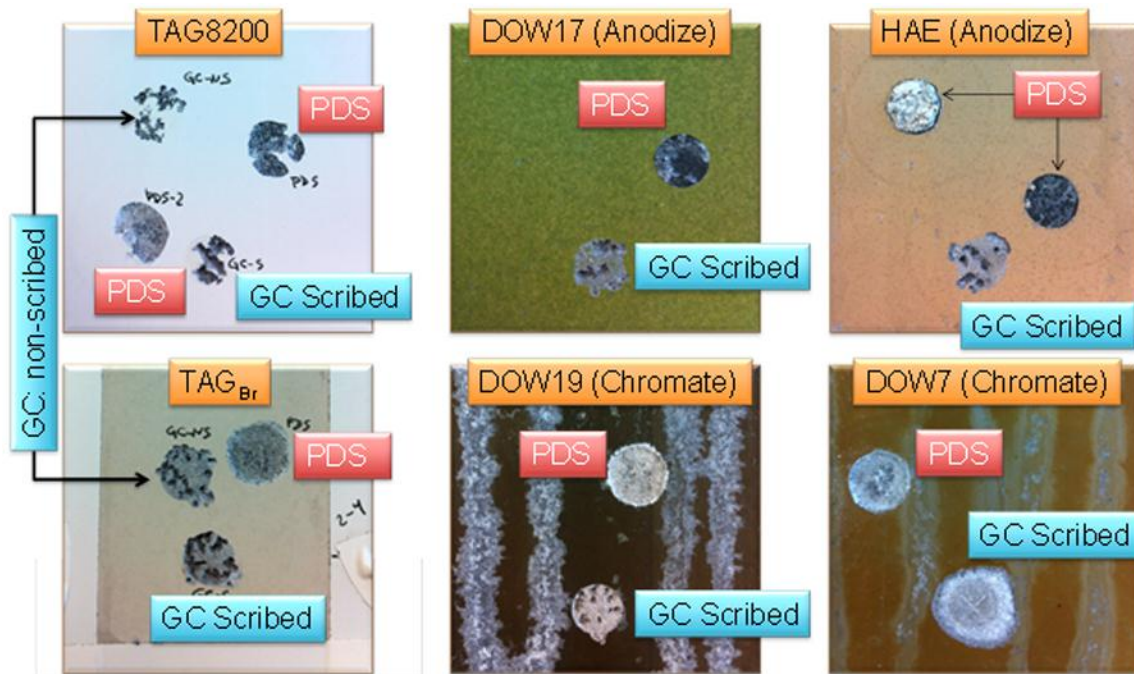


Figure 43. Visual observation of surface treatments on ZE41 after GC and PDS.

For the group of TA8200 – DOW17 Anodize and HAE Anodize, TAG8200 is the only coating that remained uncorroded at the end of the GC experiment. In fact, the corroded scribe can still be observed for TAG8200, while for DOW17 and HAE, the coating over the entire exposure area had disintegrated. In the case of TAG8200, having a more protective coating resulted in increased current densities that caused rapid progression of corrosion into the bulk metal. Table 13 shows the pit depth values for the scribed panels after the GC experiment.

Table 13. Pit depths for scribed areas after galvanic corrosion.

DOW7 Chromate	DOW17 Anodize	DOW19 Chromate	HAE Anodize	Brush Tagnite	TAG8200
8-12 mil	35-55 mil	45-60 mil	45-55 mil	60-80 mil	55-75 mil

Figure 44 depicts GC records for TAG8200 and Brush Tagnite, both scribed and non-scribed. By testing the non-scribed coatings, we are not creating an artificial defect that drives the corrosion density up and contributes to faster degradation of the coating. For the Brush Tagnite, the increase in I_{corr} shifted from 12 hrs for the scribed panel to ~40 hrs for the non-scribed panel. Similarly, non-scribed TAG8200 protects the metal substrate throughout the entire immersion period of 72 hrs.

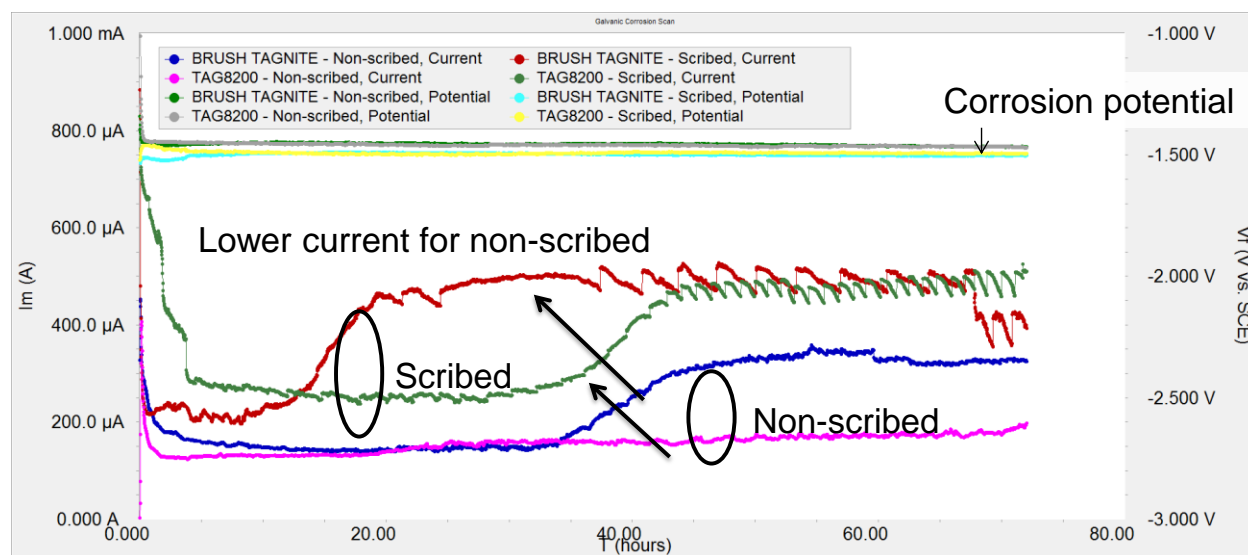


Figure 44. Galvanic corrosion for ZE41 with Brush Tagnite and TAG8200.

Galvanic corrosion experiments clearly indicate that Brush Tagnite and TAG8200 coatings protect well when undamaged. Once damaged and due to corrosion being confined to defect sites, high current densities develop at the defect, and in the absence of active corrosion inhibition, lead for rapid deterioration of the metal. Superior barrier properties of Tagnite coatings lead to corrosion expanding into the metal defect vs. across the surface, as is the case with chromated systems.

4.2 Potentiodynamic scan

The experimental setup for potentiodynamic scan (PDS) is described previously in Chapter 1.3. Figure 45 shows a full potentiodynamic scan for TAG8200, with several features of the technique mentioned in the description of Figure 11 labeled for easy understanding. Of particular interest is the anodic branch of the curve, as it represents the reaction taking place on the anode, namely corrosion of Mg alloy ZE41.

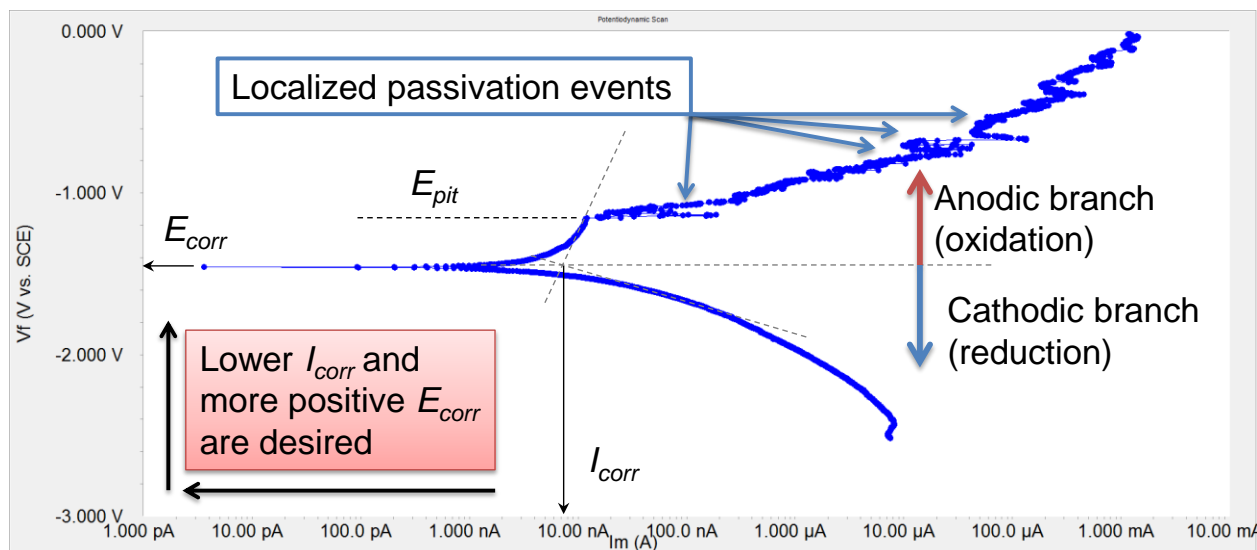


Figure 45. Potentiodynamic scan for ZE41 with TAG8200 in 1% NaCl.

The E_{corr} for TAG8200 is determined to be -1.45 V (vs. SCE), which is close to the E_{oc} value recorded in the galvanic corrosion experiment, at -1.46 V (vs. SCE). The close agreement of the two values is indicative of a stable system. The corrosion current, I_{corr} , is determined by the Tafel analysis and found to be ~ 8 nA. Pitting potential, E_{pit} is observed at -1.18 V (vs. SCE). In PDS experiments, lower current and more positive potential are desired for a protective system.

Potentiodynamic curves for the three different anodization coatings, namely TAG8200, HAE, and DOW17, are shown in Figure 46. It can be clearly seen that TAG800 possesses lower I_{corr} and more positive E_{corr} than either DOW17 or HAE.

The pitting potentials for DOW17 Anodize and HAE Anodize are very close to their respective corrosion potentials, indicating that these coatings have limited to no passivation properties and are less resistant to electrolyte attack than TAG8200, whose E_{pit} is almost 300 mV above E_{corr} . Corrosion currents estimated from PDS curves in Figure 46 are shown below:

$$I_{corr}: \text{TAG8200} (\sim 8 \text{ nA}) < \text{HAE} (\sim 1 \text{ } \mu\text{A}) < \text{DOW17} (30\text{-}40 \text{ mA})$$

Above the pitting potential, the irregularities in the potentiodynamic curve for TAG8200 indicate localized passivation events due to small pits passivating and de-passivating (re-activating) on the surface. No such events are evident for HAE or DOW17, further indicating that HAE and DOW17 are prone to corrosion resulting from global electrolyte attack.

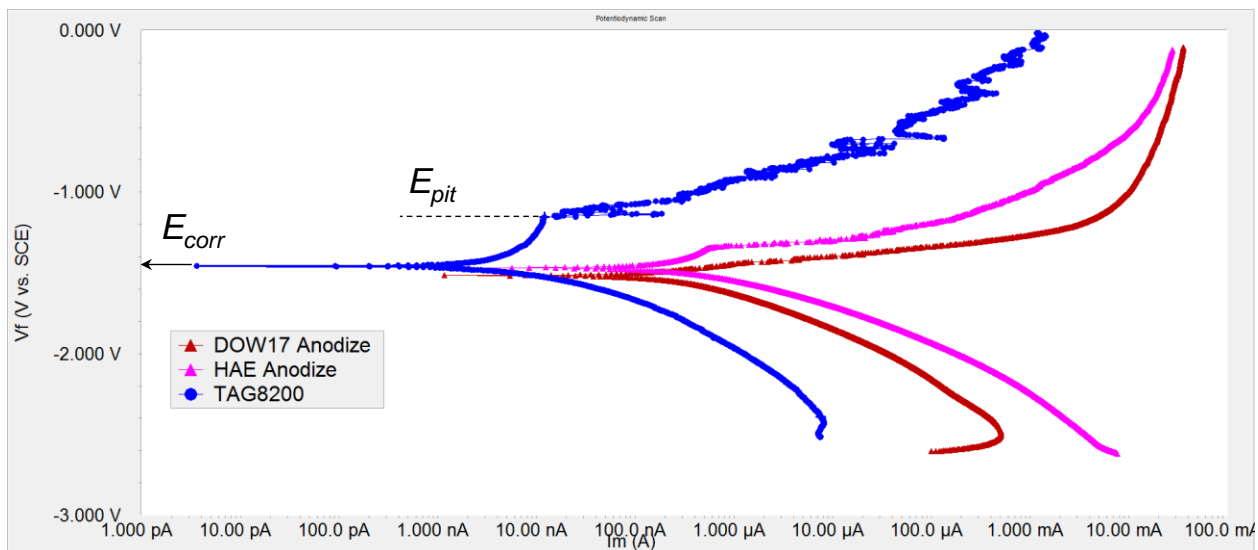


Figure 46. Potentiodynamic scan for anodized coatings TAG8200, HAE, and DOW17.

Figure 47 shows a potentiodynamic curve for Brush Tagnite. The corrosion potential and corrosion current estimated from PDS are $E_{\text{corr}} = -1.58 \text{ V}$ (vs. SCE) and $I_{\text{corr}} \sim 2 \mu\text{A}$. While the corrosion current is significantly higher than that for TAG8200, the pitting potential of Brush Tagnite, E_{pit} , of -1.06 V (vs. SCE) is 520 mV above its corrosion potential, indicating significant passivation power.

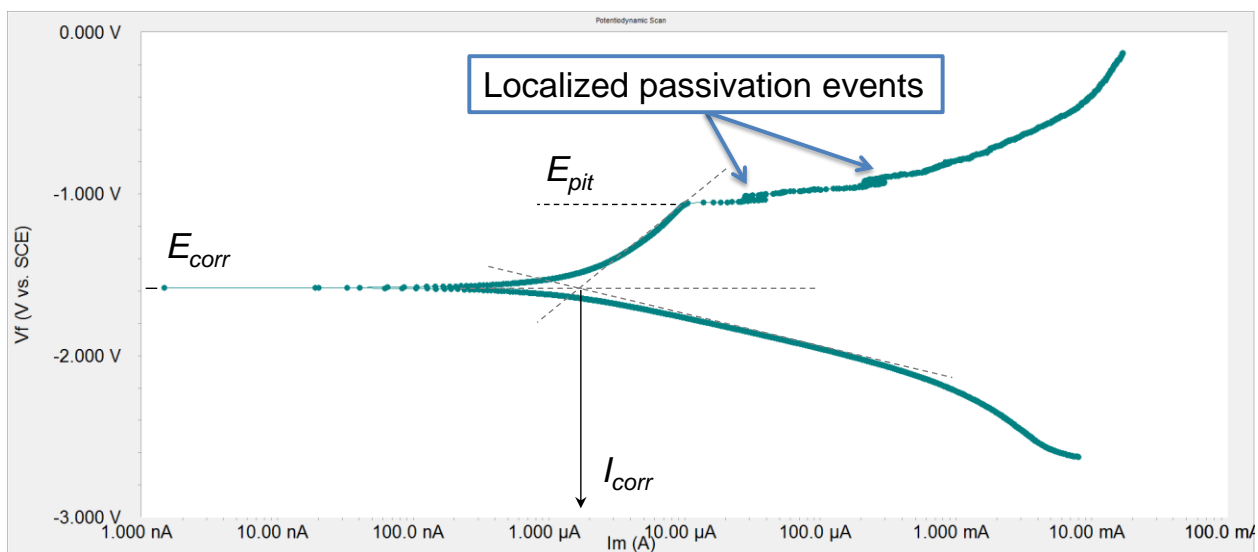


Figure 47. Potentiodynamic scan for ZE41 with Brush Tagnite in 1% NaCl.

Above E_{pit} , several localized passivation events can be observed. These are due to localized passivation and re-activation of active corrosion sites. However, unlike TAG8200, these passivation events do not contribute significantly to the decrease of corrosion current above E_{pit} .

For comparison, potentiodynamic curves for the two chromated coatings, namely DOW7 and DOW19, are shown alongside the PDS curve for Brush Tagnite in Figure 48. It should be pointed out, that while Brush Tagnite records a lower E_{corr} , it is the only coating with a well-defined E_{pit} at -1.06 V (vs. SCE). Additionally, Brush Tagnite has the lowest I_{corr} at $\sim 2 \mu\text{A}$ vs. 30 mA for both DOW7 and DOW19.

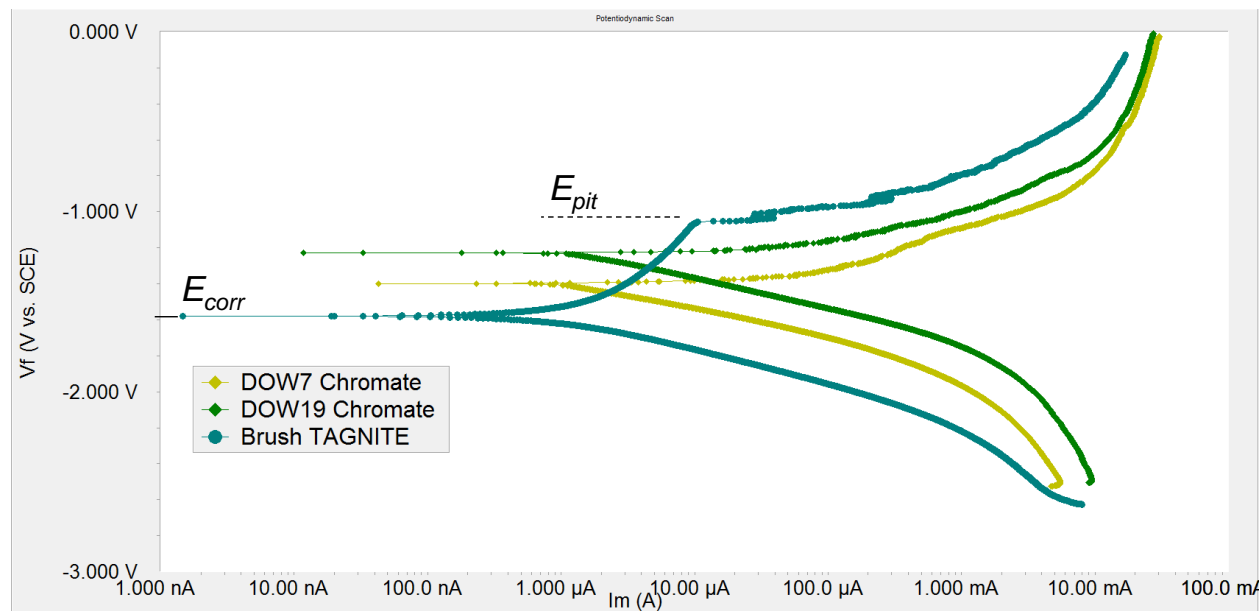


Figure 48. Potentiodynamic scan for Brush Tagnite and chromated coatings DOW7 and DOW19.

The lack of E_{pit} for DOW7 and DOW19 indicates that these coatings are prone to global electrolyte attack, a fact that is consistent with their behavior in the galvanic corrosion experiment.

Potentiodynamic curves for all six coatings are presented for comparison in Figure 49. The localized passivation regions observed for TAG8200 and Brush Tagnite could be brought about by fluorides or silicates incorporated into the coatings during deposition. Chromated (DOW7 and DOW19) and anodized (HAE & DOW17) systems do not show any localized passivation regions.

TAG8200 and Brush Tagnite are the only two coatings with well-defined pitting potentials that are several hundred mV above the respective corrosion potentials. Based on the I_{corr} values, anodize systems can be characterized as better barrier coatings, with TAG8200 being the best in that group.

If we examine test areas in Figure 43 marked with a red label “PDS”, we can clearly observe that TAG8200 is the only coating with some intact regions of coating left after PDS (and GC) experiments, whereas the original coating is completely degraded for all other coatings.

Therefore, as gauged by PDS and GC, TAG8200 affords the best corrosion protective performance. At the same time, application of Brush Tagnite could be considered adequate for short-term protection of Mg alloys.

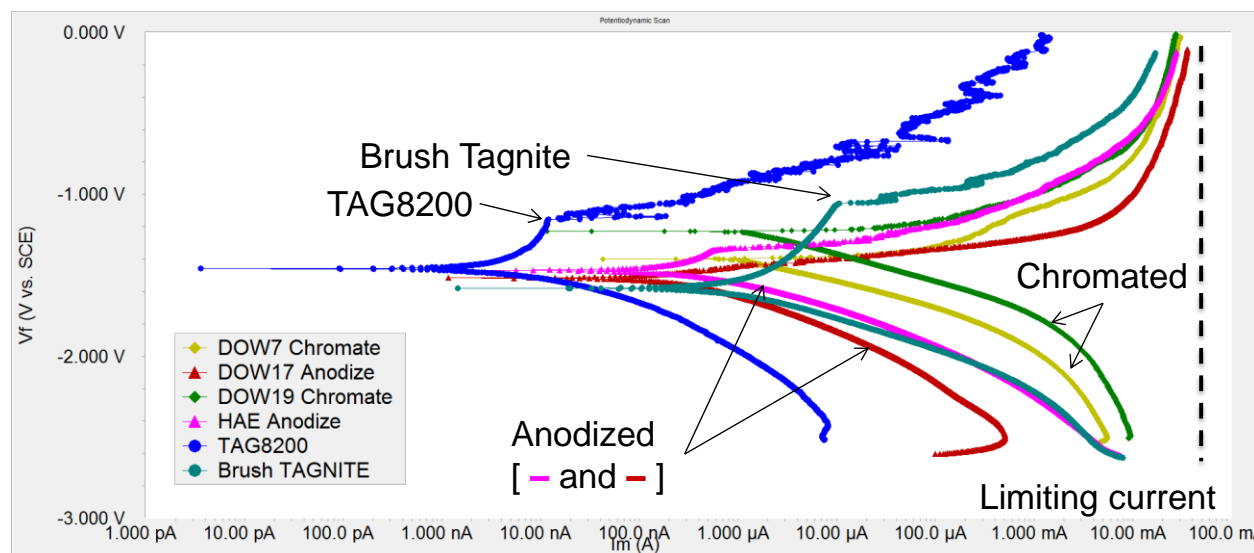


Figure 49. Potentiodynamic scan for Brushed Tagnite, anodized, and chromated coatings.

Superior barrier properties of TAG8200 lead to higher corrosion current densities and to corrosion being confined to the defect site. Conversely, while corrosion inhibition of DOW7 passivates the defect, it does not stop corrosion from expanding outside the defect area across metal surface. The size of the defect is important. Small defects for chromated systems result in quick passivation due to the low solubility of chromates. Chromates are typically used with a layer of primer or topcoat or are incorporated into a primer in order to prevent their leaching out into the electrolyte. For coatings like TAG8200 and Brush Tagnite, which are more protective, their superior barrier properties result in the corrosion attack being localized to the defect itself, creating much higher current densities in a GC experiment, due to the constant demand for current from the cathode, whose area is fixed.

5. Initial inhibitor studies

Superior barrier properties for TAG8200 and Brush Tagnite over their anodized and chromated counterparts result in the corrosion attack being confined to the defect site and putting more stress on the coating in corrosive environment. Potentiodynamic scan and galvanic corrosion results from Chapter 4 suggest that incorporating small amounts of corrosion inhibitor could possibly be effective on TAG8200 and Brush Tagnite to prevent further propagation of corrosion into the metal.

Inhibitors are chemical compounds that react with either a metal surface of the environment that the metal surface is exposed to, giving the surface a certain level of protection. For the metals widely employed in the industry such as iron, copper, zinc and aluminum, adding corrosion inhibitors is an effective and convenient method to decrease the corrosion rate. For magnesium and its alloys, there are very few publications on their corrosion inhibitors, and only few inhibitors such as the fluorides, chromates, and so on are involved. However, fluorides pollute the environment and chromates are known carcinogens; therefore it is necessary to pay attention to developing environmentally friendly corrosion inhibitors for magnesium and its alloys.

CSP has identified several environmentally benign corrosion inhibitors for protection of Mg alloys and have performed preliminary electrochemical tests of two of the inhibitors in various corrosive environments. In this chapter, PDS results for one of the inhibitors, referred to as Inhibitor A, are presented.

Inhibitor A is a sodium salt of an organic acid that is widely used in household products. Its inhibitive potential has been tested in several electrolytes:

- Inhibitor A in deionized water. The electrolyte is the aqueous solution of the inhibitor itself.
- Inhibitor A in 1% sodium chloride (NaCl), for consistency with prior GC and PDS experiments.
- Inhibitor A in 1% sodium sulfate (Na_2SO_4). This electrolyte is less corrosive to Mg alloys and is often used to impart a very mild corrosion attack on a metallic substrate.
- 1% sodium chloride without inhibitor, for comparison.

The severity of corrosive attack brought about by the electrolyte could be ranked in the following order:



Figures 50 and 51 show families of PDS curves for TAG8200 and Brush Tagnite, respectively. When sodium sulfate is used as electrolyte, smallest corrosion currents are produced for both coatings. Additionally, Na_2SO_4 PDS curves are characterized by the absence of a pitting potential. Mg alloy ZE41 does not pit in the presence of this electrolyte, and thus the mode of failure has been altered vs. chloride-containing environment. While Na_2SO_4 is the electrolyte of choice when no degradation of the system is desired, in this particular case, lack of pitting makes Na_2SO_4 unsuitable for simulating testing conditions that mimic real life corrosive environment that almost always contains chloride.

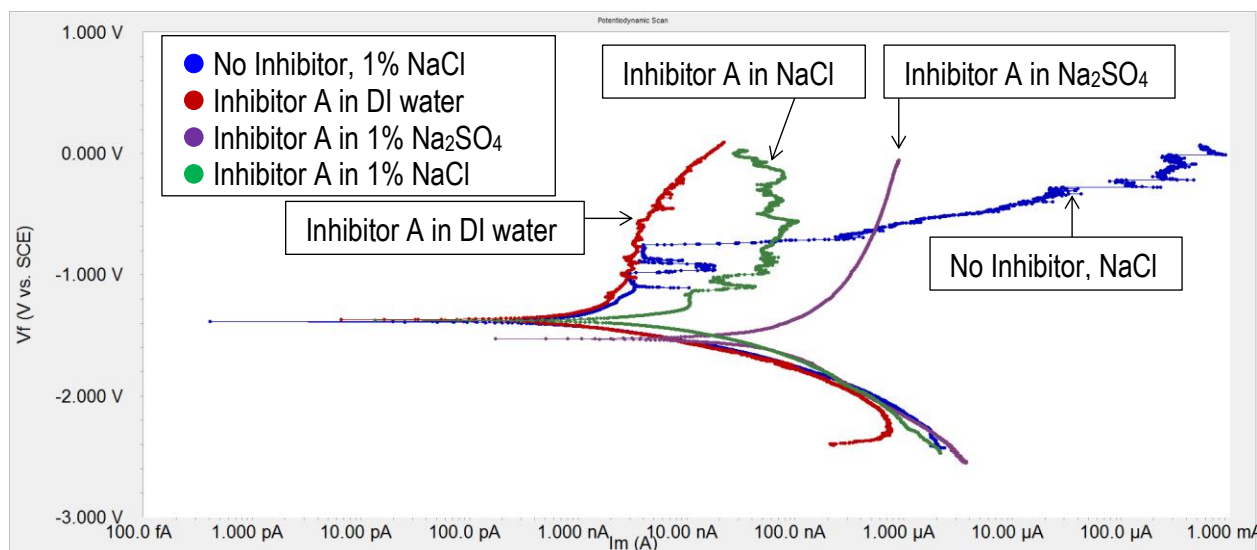


Figure 50. Potentiodynamic scans for ZE41 with TAG8200 and Inhibitor A.

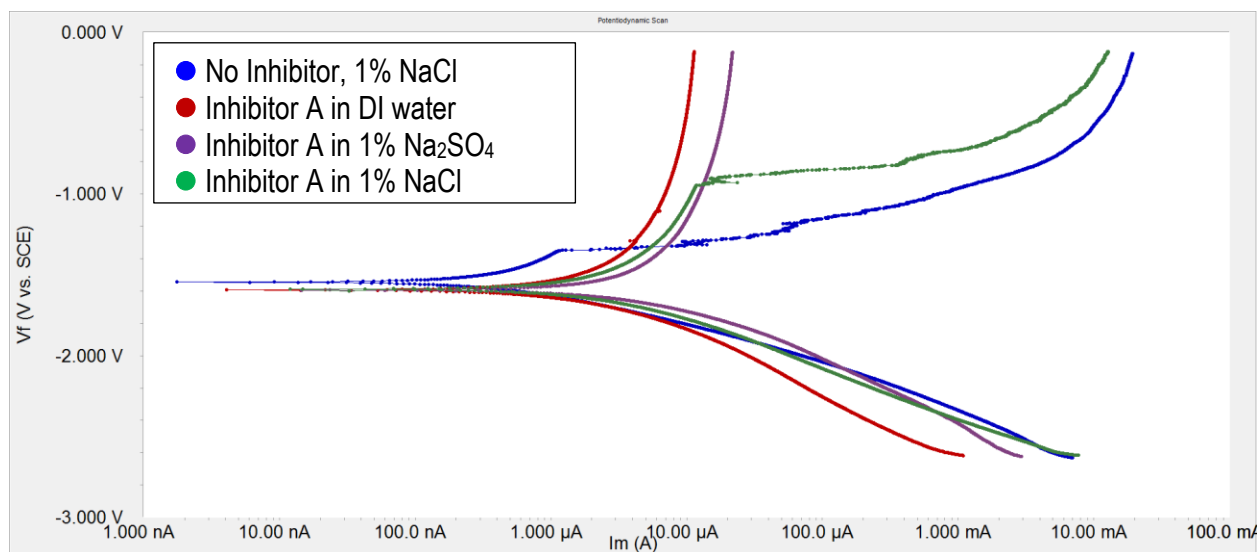


Figure 51. Potentiodynamic scans for ZE41 with Brush Tagnite and Inhibitor A.

PDS results from Figures 50 and 51 show that incorporation of Inhibitor A has a dramatic effect on corrosion current and pitting potential. In the case of TAG8200, corrosion current is greatly reduced above E_{pit} . For Brush Tagnite, E_{pit} is raised by almost 400 mV. Figures 52 and 53 compare PDS curves for TAG8200 and Brush Tagnite, with and without Inhibitor A, with two other coatings within their group: TAG8200 and anodized coatings, Brush Tagnite and chromates.

TAG8200 stands out from the group as having the lowest corrosion current, I_{corr} , and most positive corrosion potential, E_{corr} . The addition of Inhibitor A reduces the current above E_{pit} by almost 5 orders of magnitude (green trace). Similarly, Inhibitor A raises the pitting potential for Brush Tagnite and results in the lowest I_{corr} about E_{pit} . More research is needed in order to optimize the amount of inhibitor, its composition, as well as consider synergistic phenomena that may arise from mixing several inhibitors.

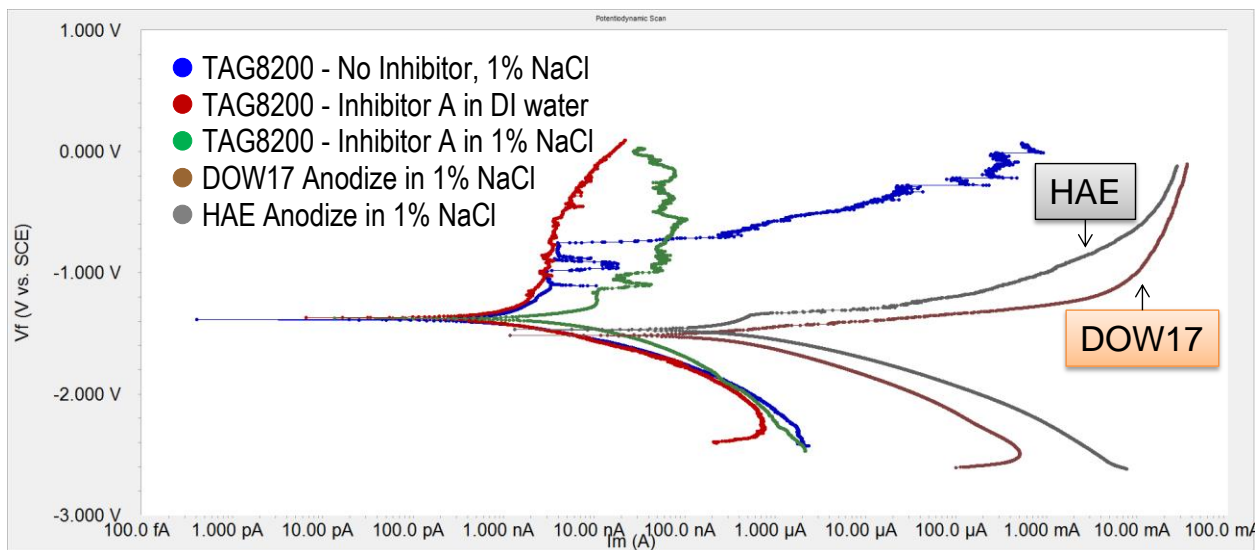


Figure 52. Potentiodynamic scans for ZE41 with TAG8200, HAE, and DOW 17.

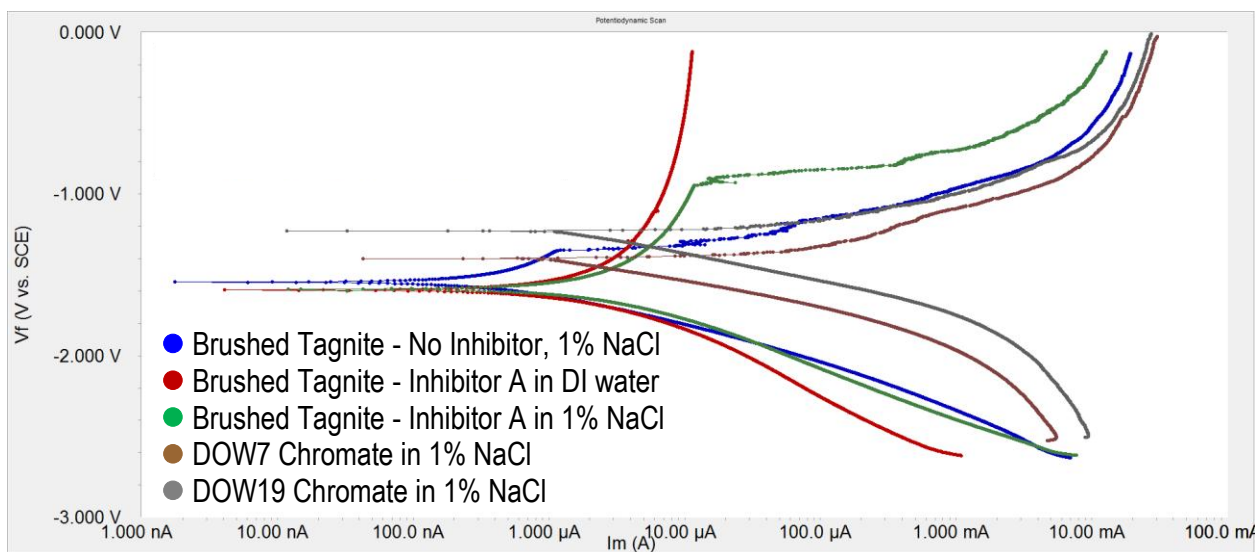


Figure 53. Potentiodynamic scans for ZE41 with Brush Tagnite, DOW7, and DOW19.

Notations and abbreviations

EIS	Electrochemical impedance spectroscopy
PDS	Potentiodynamic scan
GC	Galvanic corrosion
E_{oc} , OCP	Open circuit potential
SCE	Saturated calomel electrode
Z_{mod} , $ Z $	Impedance modulus, $ Z = (Z_{Real}^2 + Z_{Imag}^2)^{1/2}$
Z_{phz}	Impedance phase
$ Z_{lf} $	Low-frequency impedance modulus
I_{corr} , I_m	Corrosion current
E_{corr} , V_f	Corrosion potential
E_{pit}	Pitting potential

NO. OF
COPIES ORGANIZATION

1 DEFENSE TECHNICAL
(PDF) INFORMATION CTR
DTIC OCA

1 DIRECTOR
(PDF) US ARMY RESEARCH LAB
IMAL HRA

1 DIRECTOR
(PDF) US ARMY RESEARCH LAB
RDRL CIO LL

1 GOVT PRINTG OFC
(PDF) A MALHOTRA

ABERDEEN PROVING GROUND

1 RDRL WMM D
(PDF) K CHO

INTENTIONALLY LEFT BLANK.